EXAMINING THE LINK BETWEEN THE DUCTULAR REACTION AND FIBROSIS IN FATTY LIVER DISEASE

by

ALEXANDER BOYD

A thesis submitted to

The University of Birmingham for the degree of

DOCTOR OF MEDICINE

Centre for Liver and Gastrointestinal Research

Institute of Immunology and Immunotherapy

University of Birmingham

March 2024

ABSTRACT

The ductular reaction (DR) is a structural remodelling which takes place within and around the portal tracts in response to liver injury. There is known to be a positive correlation between the magnitude of the DR and the amount of liver fibrosis, particularly within the realm of biliary disease. The propensity of DR cells to directly drive fibrosis has been demonstrated in some murine models of biliary injury, however the degree to which this plays out within the sphere of metabolic dysfunction-associated steatotic liver disease (MASLD), particularly in humans, remains unknown.

Two murine models of MASLD (methionine and choline deficient (MCD) and choline deficient, L-amino acid defined (CDAA) diet) were compared for their ability to induce a DR and fibrosis, and the gene expression profile of DR cells was analysed. An *in vitro* co-culture model was set-up to assess any activating effect on hepatic stellate cells (HSC) following co-culture with biliary epithelial cells (BEC). A protocol was developed to freshly isolate human biliary/DR cells using fluorescence-activated cell sorting from donor and non-alcohol related steatohepatitis (NASH) explant livers and bulk RNA sequencing undertaken to perform transcriptomic analysis.

The CDAA model was shown to better recapitulate some features of human NASH. DR cells from injured mice were shown to upregulate gene expression of platelet derived growth factor beta (Pdgfβ) and connective tissue growth factor (Ctgf), known HSC activating ligands. Immunohistochemical staining was used to demonstrate increased expression of the PDGFβ receptor in both murine and human MASLD, and dual immunofluorescent staining showed co-localisation between DR cells and activated HSC/fibroblasts. Co-culture with alcohol-related liver

disease-derived BEC was shown to activate HSC *in vitro,* whereas co-culture with donor-derived BEC had the opposite effect. Transcriptomic analysis via geneset enrichment of biliary/DR cells from NASH and donor human livers showed differential regulation of pathways including tumour necrosis factor alpha signalling via nuclear factor kappa-light-chain-enhancer of activated B cells, epithelial mesenchymal transition and inflammatory response.

This is the first report directly comparing the gene expression profile of biliary/DR cells in healthy versus NASH human livers. The findings support a potential role of DR cells in activating HSC and driving fibrosis within the realm of human MASLD. This work has helped to streamline protocols for biliary/DR cell isolation to facilitate future single-cell RNA sequencing techniques.

ACKNOWLEDGEMENTS

I would first like to thank my two supervisors, Professor Newsome and Dr Wei-Yu Lu, for their unwavering support throughout the work undertaken for this thesis. It simply would not have been possible without their dedication, insight and, most importantly, patience. Thank you for having faith in me from the start.

Undertaking laboratory work for the first time is daunting, and everyone in the Liver Labs was so helpful and gave me support, guidance and often hands-on help along the way. Particular thanks go to Thin, who went out of her way to guide yet another blundering clinician through new protocols, dedicating significant amounts of her time to ensure my experiments eventually began to work!

My thanks also go to the patients who kindly gave consent for their organs to be available for research.

Completing this thesis was one of the biggest challenges I have faced, coming at the time of a worldwide pandemic and alongside the demands of clinical training. It simply would not have been possible without the love and support of Sally, my wife. My parents, John and Alison, and sister, Imogen, deserve enormous gratitude for helping with childcare so I could write in relative peace.

Finally, thank you to my children, Arthur and Rose. You are my proudest achievement of all.

CONTENTS

LIST OF ABBREVIATIONS

- 2-AAF 2-acetylaminofluorene
- ArLD alcohol-related liver disease
- BEC biliary epithelial cell
- CCl4 carbon tetrachloride
- CDAA choline deficient, L-amino-acid defined
- CDAHFD choline-deficient, L-amino acid-defined, high-fat diet
- CDE choline deficient ethionine supplemented
- CK cytokeratin
- CTGF connective tissue growth factor
- DAPI 4’,6-Diamidine-2’-phenylindole dihydrochloride
- DDC 3,5-diethoxycarbonyl-1,4-dihydrocollidine
- DNL de novo lipogenesis
- DR ductular reaction
- EpCAM epithelial cell adhesion molecule
- FACS fluorescence-activated cell sorting
- FCS fetal calf serum
- FFPE formalin fixed paraffin embedded
- H&E haematoxylin and eosin
- Hep-Par1 hepatocyte specific antigen 1
- HPC hepatic progenitor cell
- HSC hepatic stellate cell
- IHC immunohistochemistry
- IL interleukin
- IMC immune matched control
- MACS magnetic activated cell sorting
- MASLD metabolic dysfunction-associated liver disease
- MCD methionine and choline deficient
- MCP-1 monocyte chemoattractant protein 1
- MELD model for end-stage liver disease
- NASH non alcohol-related steatohepatitis
- NFKB nuclear factor kappa-light-chain-enhancer of activated B cells
- PBS phosphate buffered saline
- PDGFRβ platelet derived growth factor receptor beta subunit
- PDGFβ platelet derived growth factor beta
- QC quality control
- qPCR quantitative polymerase chain reaction
- TGF transforming growth factor
- Th T helper cell
- TNFα tumour necrosis factor alpha

- αSMA alpha smooth muscle actin

LIST OF FIGURES

LIST OF TABLES

1. INTRODUCTION

1.1 Anatomy and function of the liver

Macroscopic anatomy

The liver is the largest internal organ in the human body, usually weighing between 1.2-1.5kg. The liver contains two lobes: the larger right lobe, which also contains the quadrate and caudate lobes, and the left lobe. Further anatomical sub-division separates the liver into eight individual segments[1].

The liver is unique in having a dual supply of blood. The portal vein provides about 75% of the liver's supply, returning venous blood from the gastrointestinal tract. The hepatic artery provides the remaining 25% of blood, originating from the coeliac axis. Venous return from the liver is provided by the right, middle and left hepatic veins which drain into the inferior vena cava[2].

Biliary drainage of the liver is provided by the right and left hepatic ducts which unite to form the common hepatic duct. This joins the cystic duct from the gallbladder to become the common bile duct which enters the second part of the duodenum with the pancreatic duct via the ampulla of Vater[1].

Microscopic anatomy

On a microscopic level, the liver is seen to comprise functional units termed acini. An acinus contains a portal triad - containing a branch of the portal vein, hepatic artery and a bile duct – and a central venule[3]. Between these two structures is an area of hepatocytes and a network of sinusoids, a specialised type of capillary lined by fenestrated endothelium which serves as the

location for the mixing oxygen and nutrient-rich blood from the hepatic artery and portal vein respectively. Blood flows from the sinusoids into a central venule where it drains into the hepatic veins. Kupffer cells, the liver resident macrophage, are found within the sinusoids and play a vital role in surveying for pathogens. Hepatic stellate cells (HSC) are found within the Space of Disse which separates the sinusoidal endothelial cells from the hepatocytes: HSC respond to liver injury by changing to an activated myofibroblast phenotype and produce collagen[4]. A bile canaliculus forms between the surface of hepatocytes and drains bile into the ductule of a portal triad via the Canal of Hering[2].

Three zones are defined via the microscopic distribution between the portal tract and central venule: zone 1 is closest to the portal tract, zone 3 is closest to the central venule and zone 2 is in between[3]. The concept of metabolic zonation describes how hepatocytes within the three zones have different functions, reflecting the difference in oxygen and nutrient delivery relative to the proximity to the portal triad[5]. Zone 3 hepatocytes are more prone to ischemic damage and contain a higher proportion of cytochrome P450 enzymes; they are prone to preferential injury and toxicity due to compounds such as acetaminophen[6].

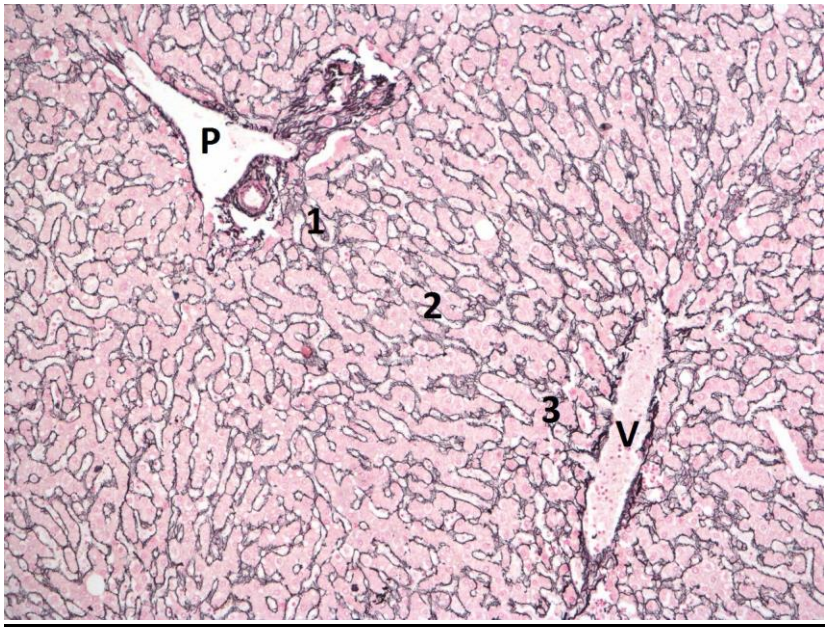

Figure 1 - reticulin stain of a section from a normal liver.
P = portal triad, V = central venule, 1-3 label the zones. Image kindly provided by Dr Owen Cain.

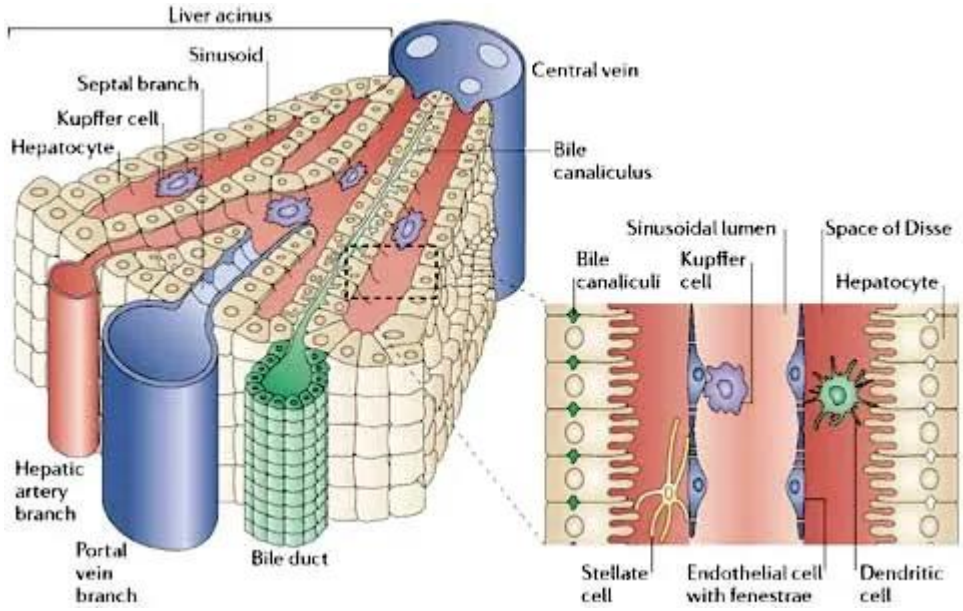

Figure 2: representation of a liver acinus
Diagram showing the 3-dimensional relationship between the portal triad, sinusoids, bile canaliculi and central venule. Taken from Adams et al, 2006

Functions of the liver

The liver has numerous important functions, and currently no artificial devices exist which can adequately take over its actions.

Metabolism

The liver plays a crucial role in carbohydrate metabolism, and is the major glucose store in the body in the form of glycogen. Lipids are also metabolised and re-assembled as lipoproteins which are transported around the body. In addition, the liver absorbs amino acids which are converted to keto-acids and enter the citric acid cycle[2].

Synthesis

The liver produces 10-12g of albumin per day and other important proteins including ferritin, caeruloplasmin, alpha-1-antitrypsin and complements. The liver also synthesises coagulation factors II, V, VII, IX and X in a vitamin-K dependent fashion.

In addition, the liver produces bile acids from cholesterol which are a crucial component of the alkaline bile which is produced to neutralise stomach acid, emulsify fats to aid their digestion and facilitate excretion of waste products[7].

Drug metabolism

Many drugs are metabolised by the liver. Of particular mechanistic importance are the cytochrome P450 enzymes which oxidise or reduce drugs and can be induced or inhibited by multiple factors[8]. The kidneys are the major route of excretion for many drugs and their metabolites, however some drugs are extensively excreted via the biliary system[2].

1.2 Current landscape of liver disease, and role of cell therapies

Liver disease is increasing within the UK[9], and worryingly liver disease is now the third largest cause of premature mortality behind cancer and cardiovascular disease[10]. Whilst a small proportion of liver disease is accounted for by acute liver failure, a rare syndrome of sudden impairment of liver function in people with no previous history of liver disease[11], the majority of morbidity and mortality is accounted for by chronic liver disease. Chronic liver disease is defined by the presence of liver injury or impairment for greater than six months and is usually accompanied by the development of liver fibrosis[12]. The most severe form of liver fibrosis is termed cirrhosis and is defined by the presence of macroscopic or microscopic nodules[13]. Cirrhosis can remain compensated, with no clear clinical evidence of liver failure, or progress to decompensated disease which is associated with clinical evidence of liver failure (for example ascites, jaundice or encephalopathy) and a poorer prognosis[13].

The majority of end-stage liver disease in the UK is caused by alcohol-related liver disease (ArLD) and metabolic dysfunction-associated steatotic liver disease (MASLD), which is a consequence of the metabolic syndrome[10]. Other causes of end-stage liver disease are immune-mediated diseases (for example auto-immune hepatitis, primary biliary cholangitis and primary sclerosing cholangitis), viral diseases (for example chronic hepatitis B and hepatitis C infection) and rarer metabolic causes (for example haemochromatosis, Wilson disease and alpha-1-antitrypsin deficiency).

The only curative treatment for end-stage liver disease is liver transplantation. In the UK, the majority of liver transplants are cadaveric grafts whereby the donor organ is removed either after

brain or cardiac death. There is a shortage of potential organ donors in relation to the number of people in need of a liver transplant[14], and therefore around 11% of patients die whilst on the waiting list[15]. As such, there is a need for alternative therapies to either delay or prevent the need for liver transplantation. Cell therapy is one area which has been extensively investigated in this regard with numerous types of cell trialled: progenitor cells are discussed in a later section due to their close relationship to the ductular reaction (DR), a key focus of my thesis.

*Some content in the following section (until ***) has been paraphrased from an editorial written and published during the course of my degree, please see below*

The role of stem cells in liver injury and repair
Expert review of Gastroenterology and Hepatology
Boyd A, Newsome PN, Lu W
DOI: 10.1080/17474124.2019.1618186

Hepatocyte transplantation has been studied extensively for over twenty years. In humans, it can provide a short-term benefit to children with conditions such as inborn errors of metabolism[16] however a long-term cure has not been demonstrated and challenges remain with regard to the generation of cells and variable rates of engraftment within the liver[17]. Various types of stem cell, which are not dependent on the availability of donor organs for their production, have also been trialled including haematopoietic stem cells, embryonic stem cells and induced pluripotent stem cells. Mesenchymal stromal cells, a multipotent cell without true stem cell properties[18], have also been investigated.

Haematopoietic stem cell therapy was shown to provide no benefit when administered to patients with compensated cirrhosis during the REALISTIC randomised control trial reported in 2018[19]. The cell therapy group showed no improvement in the model for end-stage liver disease (MELD) score

or non-invasive markers of fibrosis, and suffered a greater rate of adverse events in comparison to the control group. Mesenchymal stromal cells are thought to act via an immuno-modulatory action rather than directly restoring liver function[20]. A recent meta-analysis of trials in human subjects suggested a possible short-term improvement in MELD score however there was significant heterogeneity in the evidence-base[21]. Trials are ongoing including a safety and feasibility study of mesenchymal stromal cell therapy in patients with auto-immune hepatitis and primary sclerosing cholangitis in Birmingham.

Embryonic stem cells are mainly used for *in vitro* modelling and have shown promise in animal studies,[22] however have not been studied in humans due to ethical constraints and concerns surrounding the potential for teratoma formation and tumorigenicity. Induced pluripotent stem cells are differentiated cells which are artificially restored to a stem cell phenotype; re-differentiation can then be induced to produce a hepatocyte-like cell. Animal models of transplantation of these hepatocyte-like cells have shown promising results[23]; however hepatocyte-like cells do differ from primary hepatocytes in important ways[24] and human trials have not yet been carried out.

As such, cell therapy cannot yet provide an adequate alternative to liver transplantation which remains the mainstay of treatment, where appropriate, in end-stage liver disease.

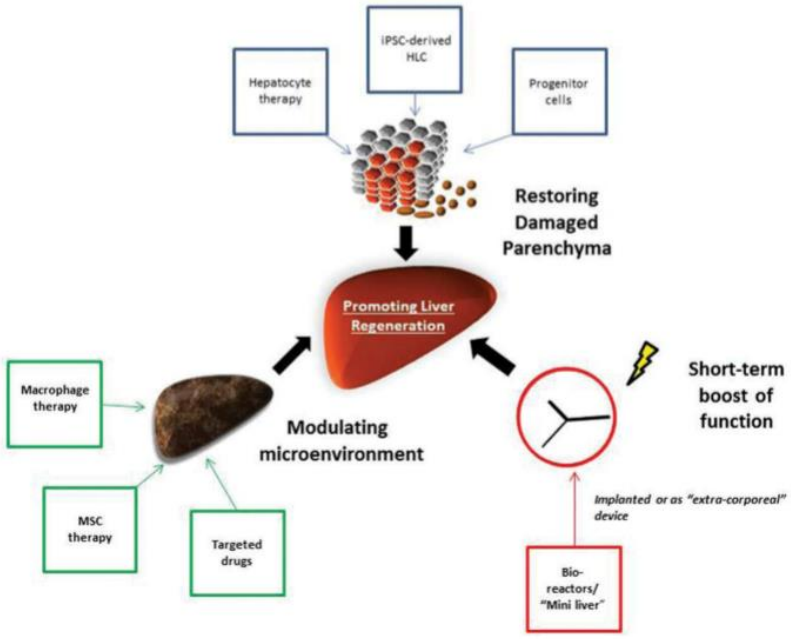

Figure 3: schematic representation of current and anticipated treatments to delay or prevent the need for transplantation in liver disease
From Boyd et al, 2019

***

1.3 MASLD

Epidemiology and classification

MASLD is an important and increasing cause of liver disease in the UK and worldwide[25]. The increase in prevalence reflects the growing burden of obesity, type 2 diabetes and the metabolic syndrome among the general population[26]. Estimates suggest that the prevalence of MASLD within the UK population may be as high as 20-30%[25,27], and 1.5%-6.5% of the population may have the more severe form of the disease, non-alcohol related steatohepatitis (NASH)[25].

MASLD encompasses a spectrum from simple fat deposition within the liver (steatosis) through to inflammation, fibrosis and cirrhosis[28]. Liver biopsy enables an accurate staging of disease and is required for the diagnosis of NASH which is characterised by steatosis with ballooning of hepatocytes and lobular inflammation, with or without fibrosis[29]. The presence of steatosis without ballooning and lobular inflammation would be insufficient for a diagnosis of NASH[28].

The majority of patients with MASLD simply develop steatosis without progression to NASH[30]. These patients are particularly at risk of complications from the metabolic syndrome rather than any liver-specific morbidity or mortality[31,32]. Factors which determine the likelihood of a patient developing NASH, and factors driving fibrosis progression, are not clearly defined but may include polymorphisms in genes controlling lipid metabolism and insulin resistance such as the patatin-like phospholipase domain-containing protein family[28]. Analysis of data from cohorts of MASLD patients with paired liver biopsies shows that risk factors for fibrosis progression vary from study to study, however the presence of type 2 diabetes, obesity and hypertension have all been shown to associate independently with progressive disease[32,33]. It is known that the presence of advanced fibrosis is an important prognostic indicator, as this is associated with the development of end-stage liver disease and an increase in liver-related mortality[34]. Therefore, current non-invasive risk stratification protocols in Primary Care aim to identify patients who may have MASLD with advanced fibrosis, and facilitate their referral to specialist services[35]. Of note, increased liver-specific mortality has also been shown with moderate levels of fibrosis (>F2)[36].

Pathophysiology

Steatosis is defined as the abnormal deposition of fat in more than 5% of hepatocytes[37]. The size of the vesicles in which the fat is stored determines whether the histological pattern of steatosis is

termed micro or macro-vesicular. Steatosis in MASLD is the result of abnormal lipid-handling pathways, reflecting the underlying insulin resistance and obesity found in the majority of such patients[30]. A key step in pathogenesis is the increased delivery and formation of free fatty acids within the liver[38]. The esterification of fatty acids with glycerol is one pathway by which fatty acids are metabolised. This process produces triglycerides, which can be stored in hepatocytes resulting in steatosis.

The increase in free fatty acids within the liver can be caused by dietary intake of fat-rich foods, enhanced breakdown of adipose tissue (lipolysis) and upregulation of de novo lipogenesis (DNL)[38], which is a mechanism of creating fatty acids using acetyl-coA molecules generated during multiple metabolic processes including carbohydrate metabolism[39]. Insulin resistance plays a key role in increasing the rate of adipose tissue lipolysis, leading to an efflux of fatty acids[40], and stimulating transcription factors responsible for controlling the expression of genes underlying DNL[41]. In addition, insulin resistance suppresses the ability of hepatocytes to perform beta-oxidation of fatty acids[42], thus promoting their conversion to triglycerides.

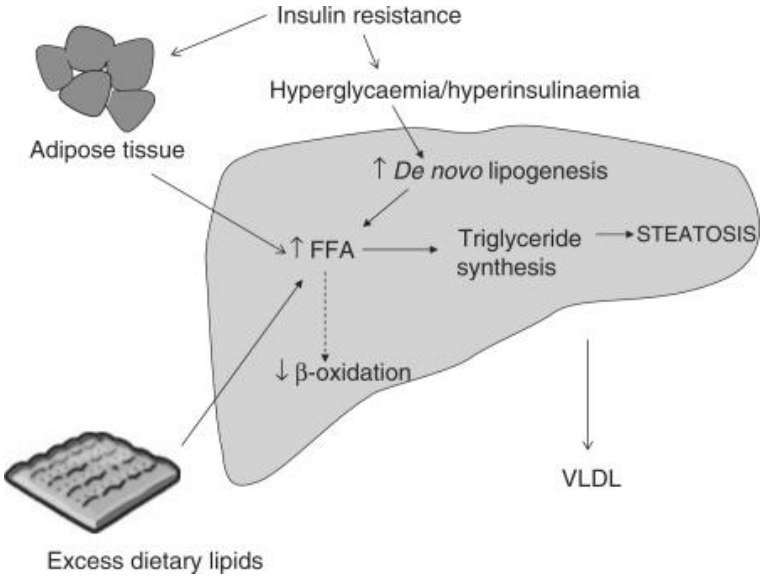

Figure 4: representation of the pathways underlying increased hepatic free fatty acids in patients with metabolic syndrome
From Dowman et al, 2010

NASH is defined in part by the presence of a lobular inflammatory infiltrate[37], which is driven by activation of inflammatory cytokines[38] and hepatocyte injury. Hepatocyte injury is shown histologically as ballooning, often with the presence of intra-cytoplasmic inclusions of twisted cytokeratin filaments termed Mallory-Denk bodies[43].

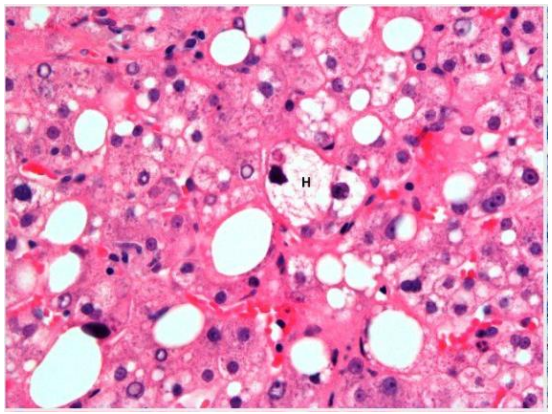

Figure 5: haematoxylin and eosin (H&E) stain showing large droplet steatosis with a ballooned hepatocyte (H) containing a Mallory-Denk body
Image kindly provided by Dr Owen Cain

Steatosis is associated with activation of the nuclear factor kappa-light-chain-enhancer of activated B cells (NFKB) signalling pathway, resulting in increased expression of inflammatory cytokines such as tumour necrosis factor alpha (TNFα) and Interleukin (IL)-6[44]. In addition, the high fatty acid load within the liver results in an increase in mitochondrial beta oxidation. If this pathway is overwhelmed then reactive oxygen species are formed which lead to oxidative stress, damage to mitochondria[45] and further activation of the inflammatory cascade. In addition, gut hyper-permeability and bacterial overgrowth, which are more frequently observed in patients with MASLD[46,47], may lead to increased levels of bacterial lipopolysaccharides within the portal circulation which activate Kupffer cells and promote further hepatic inflammation[48].

The inflammatory cascade has the end-point of activating HSC, which convert to an activated myofibroblast phenotype and produce extra-cellular matrix such as collagen[4]. If this is persistent, progressive collagen deposition leads to fibrosis and eventually cirrhosis.

Treatments

There are currently no licensed treatments for MASLD, with patient lifestyle intervention and clinician management focused on the target of weight loss. Weight loss of >10% has been shown to significantly reduce steatosis, abort NASH and stabilise or even improve fibrosis[49]. Good management of other aspects of the metabolic syndrome – type 2 diabetes, dyslipidaemia and hypertension – is also of paramount importance.

Clinical trials are in advanced phases for numerous therapeutic compounds which target different and often multiple aspects of the pathophysiology simultaneously. For example, glucagon-like-peptide 1 agonists have been shown to promote weight loss and reduce insulin resistance, and are already licensed for the treatment of type 2 diabetes. C-C chemokine receptor 2/5 inhibitors,

peroxisome proliferator-activated receptor α/δ agonists and farnesoid X receptor agonists are proposed to both dampen steatohepatitis and have anti-fibrotic actions[50].

Liver transplantation remains the only curative treatment for end-stage NASH. With a substantial projected increase in the prevalence of NASH over the coming decades, and the shortfall in the number of suitable donor livers available for transplantation[14], an increased understanding of the pathways underlying the development of fibrosis in NASH is of paramount importance with the aim of developing new targeted therapies.

Animal models of NASH

Animal models provide an important tool to study the mechanisms underlying the pathophysiology of MASLD, identify target pathways for potential therapeutics and test compounds directly. Methods used include transgenic strains, for example the *ob/ob* mouse which is leptin deficient and demonstrates hyperphagia, obesity and insulin resistance[51]; and the use of chemicals such as carbon tetrachloride (CCl4) and diethylnitrosamine in combination with dietary manipulation[52]. However, dietary manipulation alone is a straightforward and commonly utilised method of modelling fatty liver disease.

Mice, particularly C57/Bl6 mice which have a natural propensity to develop features of the metabolic syndrome[52], are commonly subjected to dietary manipulation to model MASLD. Murine models of MASLD, however, differ from the human disease phenotype in several important ways[53]. It is particularly difficult to recapitulate moderate or advanced levels of fibrosis, which is a prognostically important disease milestone in human MASLD[34].

High fat diet

The high fat diet simply increases the proportion of total calories in the feed provided by fat. This leads to an excess of free fatty acids delivered to the liver, which promote storage as triglycerides: indeed, steatosis may be microscopically visible by as early as 1-2 weeks[54]. Histological changes of NASH appear after an interval of approximately 12 weeks, and are generally mild[55]. However, mice do mirror the human metabolic syndrome in developing obesity, hyperlipidaemia and insulin resistance[56]. A major problem with the high fat diet is its inability to generate significant fibrosis: even after 12 months the fibrosis induced is only mild[57] and the long timescales involved in the model make it relatively impractical for many researchers.

Methionine and choline deficient (MCD) diet

The MCD diet contains a high sucrose and fat content, and is deficient in methionine and choline; this causes impaired beta-oxidation of fatty acids and reduces production and export of very low density lipoprotein particles[58], compounding the accumulation of free fatty acids. Mice rapidly accumulate triglycerides and develop steatosis, with mild-moderate lobular inflammation, ballooning and increased transaminases after 10 days[59]. However, the model differs significantly from the human disease phenotype in that mice develop marked weight loss and an absence of insulin resistance[60]. In many animal units the weight loss can prove problematic as mice may need to be sacrificed due to welfare concerns after 3-4 weeks of diet: this is generally before the development of any discernible fibrosis[61]. Thus, the MCD recapitulates steatosis and inflammation well, however does not reflect the metabolic syndrome which accompanies human NASH and fibrogenesis is limited.

Choline deficient, L-amino acid defined (CDAA) diet

The CDAA diet is similar to the MCD diet in lacking choline, however the protein is replaced with an equivalent combination of L-amino acids and a high fat content is frequently added. This leads to the rapid development of steatosis, although the appearance of lobular inflammation, ballooning and raised transaminases can take a little longer, perhaps around 4-6 weeks[52]. Animals can develop significant fibrosis which is usually detectable from 6 weeks[62]. Animals do not demonstrate the weight loss of the MCD model, however features of the human metabolic syndrome are not recapitulated[63]. The CDAA diet can therefore model some early stages of human MASLD, but would not capture the important prognostic milestones such as bridging fibrosis and nodule formation.

1.4 HSC and liver fibrosis

HSC biology

HSC were first identified in the 1870s by Kupffer[64], and comprise about 15% of the total cell population of the liver[65]. Resident within the Space of Disse, in normal liver they store droplets of Vitamin A within their cytoplasm[64] and remain in a generally quiescent state. However, in response to liver injury they lose their Vitamin A droplets and adopt an activated phenotype, evolving into a myofibroblast-like cell primed to release collagen fibres[4]. Whilst once thought to represent a relatively homogenous population, recent work using single cell RNA sequencing has demonstrated that there are functionally disparate populations of HSC in different zones of the liver, termed portal vein-associated and central vein-associated HSCs; at least in mouse models of liver injury, these populations may behave differently[66].

HSC secrete an array of cytokines and growth factors, contributing to the inflammatory and fibrogenic response to liver injury via paracrine signalling. Notably, HSC also respond to many of these molecules in an autocrine fashion via expression of membrane receptors[4]. Examples of important secreted factors include transforming growth factor (TGF) alpha and epidermal growth factor, which stimulate hepatocyte proliferation and also promote proliferation of HSC in an autocrine signalling loop[67,68]. HSC also secrete platelet derived growth factor beta (PDGFβ), the most potent HSC mitogen identified to date[69]. Binding of PDGFβ to the membrane PDGFβ receptor (PDGFRβ) instigates an autocrine feedback loop, and interacts with TGFβ signalling pathways[70]. HSC production of TGFβ and connective tissue growth factor (CTGF) is also of importance, both molecules acting via paracrine and autocrine pathways to promote fibrogenesis[71,72].

Furthermore, HSC produce monocyte chemoattractant protein 1 (MCP-1) and platelet activating factor, regulating both macrophage and neutrophil influx to the liver respectively[73,74]. Production of IL-6 has also been demonstrated, suggesting a role in amplifying the acute phase inflammatory response to liver injury[75].

Three stages of HSC activation in response to liver injury have been proposed: initiation, perpetuation and resolution[4]. Initiation happens in response to paracrine signalling from neighbouring cell types including platelets, endothelial cells and hepatocytes, which release cytokines in response to the first stages of liver injury and subsequent inflammation[4]. This results in the earliest detectable changes to HSC phenotype including increased responsiveness to further stimulation[76]. Perpetuation describes the changes which ensure continuing activation of the primed cells[76], and involves changes to different aspects of cell behaviour including proliferation, contractility and chemotaxis[4].

Proliferation of HSC is increased by factors including TGFβ and PDGFβ. A key downstream mediator of TGFβ signalling is the activation of Smads[77], while PDGFβ stimulation results in activation of the extracellular signal-regulated/mitogen activated protein kinase pathway[78]. Increased cell contractility is observed during HSC activation and is thought to be dependent on factors including calcium and nitric oxide signalling[79]. The increased production of alpha smooth muscle actin (αSMA), a cytoskeletal protein and key marker of HSC activation, helps to increase contractile potential[80]. Chemotaxis describes the migration of HSC towards different molecules. Factors shown to attract HSC include PDGFβ[81] and MCP-1[82], among others. Perpetuation of HSC activation has the net effect of increasing collagen and extracellular matrix production.

Resolution refers to deactivation of HSC with the subsequent dampening of the fibrogenic response: this can occur via reversion to a quiescent phenotype, or clearance via apoptosis[4,83].

Given their primary role in liver fibrosis, mechanistic study of HSC biology is likely to remain important. Several human HSC-lines have been generated to facilitate *in vitro* investigation of their biology without the requirement for primary human tissue to directly isolate cells. An example of such is the LX-2 cell line which was generated by spontaneous immortalisation in low serum[84]. Studies have shown close similarities to culture-activated primary HSC[84].

Liver fibrogenesis

Contrary to expectation, the production of collagen and extracellular matrix by HSC is not always a harmful phenomenon, as it also constitutes an important step in the “wound healing” response[85]. Whilst chronic fibrosis can lead to cirrhosis and end-stage liver disease, the short-term fibrosis observed in response to acute liver injury can be seen as a protective step. For example, it has

been shown in mice that collagen deposition protects hepatocytes from toxic insults and decreases the susceptibility of the liver to further damage[86].

The degradation of scar tissue is controlled by numerous mechanisms: a key mediator is the action of matrix metalloproteinases (MMPs), which are zinc-dependent endopeptidases capable of degrading extracellular matrix. MMPs are produced by numerous cell-types including leucocytes, and are upregulated in liver injury[87]. Of course, reversion of activated HSC to a quiescent phenotype will prevent further matrix deposition both directly – via reduced collagen production - and indirectly via the decreased production of tissue-inhibitors of matrix metalloproteinases (TIMPs), a potent inhibitor of MMPs[88].

Macrophages also play an important role in degrading extracellular matrix. It has been recognised that there are different macrophage populations within the liver: the influx of monocyte-derived macrophages during liver injury initially contributes to fibrogenesis, however a phenotypic switch produces a “restorative” macrophage population which is able to promote myofibroblast apoptosis and secrete MMPs, driving scar resolution[89]. In addition, interplay between different T-helper cell (Th) subsets is important, with Th2 cells stimulating fibrogenic pathways to a greater degree than their Th1 counterparts[85].

It can be seen that there are competing mechanisms which control the progression, or regression, of liver fibrosis. Perhaps the chronicity of liver injury – which can last decades in human disease – has the greatest effect in providing a continual stimulus for HSC activation and collagen deposition. However, injury chronicity forms just one part of an important balance also including the action of MMPs, TIMPs and diverse cell populations including macrophages, dendritic cells, T cells and HSC themselves.

Although in human disease liver fibrosis is harder to reverse than in rodent models, perhaps due to the prolonged timescales of fibrogenesis involved, progression even to cirrhosis is not a fixed event. For example, removal of the injury-causing agent, whether that be abstinence from alcohol, weight-loss in NASH or viral suppression in chronic hepatitis B or C, can cause fibrosis regression and even reversal of cirrhosis – a phenomenon not infrequently seen in the clinic.

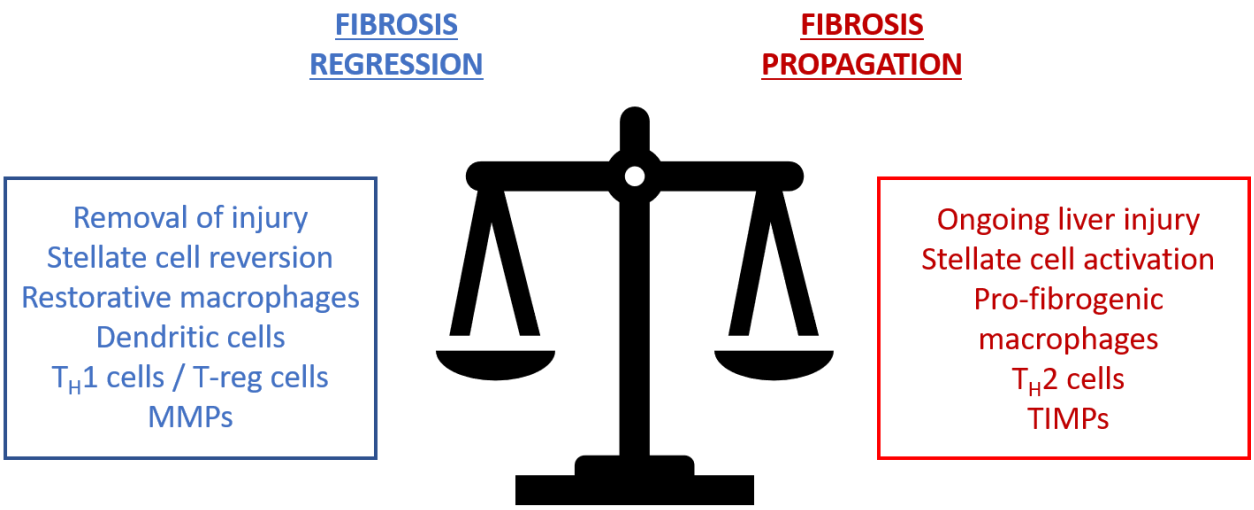

Figure 6: schematic of the different factors controlling the propagation or regression of liver fibrosis.

1.5 Stem cells, liver regeneration and hepatic progenitor cells

*Some content in the following section (until ***) has been paraphrased from an editorial written and published during the course of my degree, please see below*

The role of stem cells in liver injury and repair
Expert review of Gastroenterology and Hepatology
Boyd A, Newsome PN, Lu W
DOI: 10.1080/17474124.2019.1618186

Stem cells

Stem cells are defined by the possession of three general properties: they are unspecialized cells, capable of self-renewal and demonstrate potency - the ability to differentiate into multiple

specialized cell types[90]. There are two broad classes of stem cells: embryonic stem cells and adult stem cells. Embryonic stem cells serve to produce the different cell types required for the development of the foetus including those of endodermal, mesodermal and ectodermal lineage. These cells represent the inner cell mass of the developing blastocyst and are termed pluripotent. Strictly speaking, there are cells with an even higher degree of potency, namely the first few cells formed after division of the zygote, before separation of the trophectoderm. These cells are, by definition, totipotent, capable of producing both embryonic and nonembryonic tissues.

Adult stem cells or somatic stem cells act to maintain cellular turnover in homeostasis (if required) or repair damaged tissue: they are found within the organ in question and are multipotent, capable of differentiation into the specialized cell types of the organ in question. The existence of a true somatic liver stem cell, *per se*, remains controversial[91-94]. Although definitions can vary, there are also tissue-resident cells termed progenitor cells. These also seek to repair tissue, although demonstrate less capacity for self-renewal and generally are less potent than a true somatic stem cell[95].

Liver regeneration

Adult hepatocytes divide very infrequently, with the average lifespan in the region of 200-300 days[96]. This enables the gradual replacement of hepatocytes, and the maintenance of liver function, during homeostatic conditions. However, the liver's ability to regenerate is much greater than this would suggest: following 70% hepatectomy there is a compensatory proliferation of epithelial and stromal cells to support rapid growth and restoration of homeostasis within days[97]. Although the resected lobes do not grow back, there is a compensatory increase in the size of the remaining lobes to restore liver mass without the need for stem cells[96].

Importantly, 70% hepatectomy models do not induce liver injury *per se*, as there is no damage to hepatocytes or significant inflammation. Whereas, in most chronic parenchymal liver disease, there is ongoing damage to hepatocytes alongside a blunted proliferative response. In this setting alternative mechanisms ensue to attempt healing, such as activation and proliferation of hepatic progenitor cells (HPC)[98].

HPC

HPC (also termed oval cells in rodents due to their ovoid nucleus) represent bipotent precursors of hepatocytes and cholangiocytes[99]. Following chronic or massive acute liver injury, HPC are seen to proliferate in association with development of a DR (discussed in detail in following sub-chapter): the cells within the proliferation are seen to adopt a range of morphologies from mature cholangiocyte to mature hepatocyte with indeterminate phenotypes in between, expressing markers in keeping with both hepatocyte (albumin, hepatocyte specific antigen 1 (Hep-Par 1)) and biliary (cytokeratin-19 (CK19)) lineage.

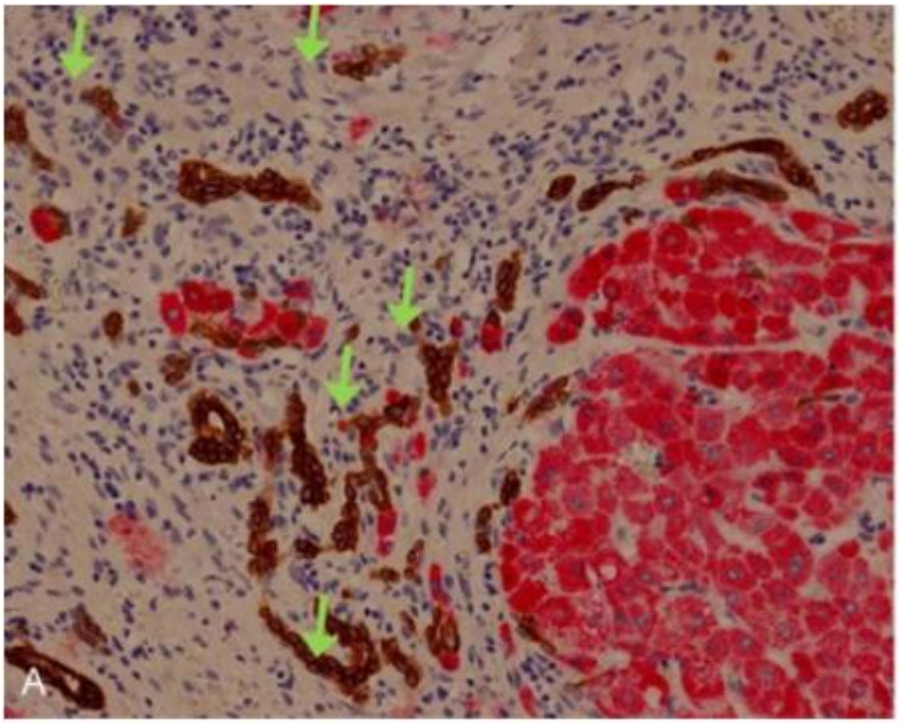

Figure 7: immunohistochemical (IHC) staining of human tissue with biliary cirrhosis
Staining shows cells positive for Hep-Par 1 (red) and CK19 (brown). Arrow show dual-positive cells i.e. concurrent expression of hepatocytic and biliary markers. From Lee et al, 2014

The exact degree to which HPC contribute toward hepatocyte regeneration has been an area of uncertainty. Genetic lineage tracing experiments would suggest a negligible contribution in normal homeostasis, with uninjured hepatocytes undergoing normal replication, but this increased to 3.26% of hepatocytes in different models of liver injury[100]. Other studies would suggest a negligible contribution even in liver injury[93]. However, the models of liver injury in rodents typically take the form of short-term administration of chemicals or partial hepatectomy, neither of which are reflective of the long-term chronic and iterative liver injury involved in humans conditions such as NASH or ArLD, and HPC-mediated repair could be much higher in patients with chronic liver disease.

Direct evidence for liver regeneration via HPC is more difficult to demonstrate in humans, although proliferations of HPC are common in chronic liver injury[101] and epithelial cell adhesion

molecule (EpCAM) positive hepatocytes geographically associate with HPC: moreover these hepatocytes also have a longer telomere length than EpCAM negative hepatocytes suggesting their origin from a stem/progenitor cell compartment[102]. In addition, hepatocytes within regenerating cirrhotic nodules have been shown to share specific mutations with neighbouring HPC[103].

Although HPC have been shown to play a role in regeneration, the origin of these cells remains contested. One long-held school of thought considers HPC to represent or derive from a facultative liver stem cell niche, activated in response to liver injury[104]. An opposing view states that HPC are generated by the de-differentiation of mature hepatocytes. Certainly, *in vitro* work has demonstrated that rat hepatocytes can give rise to a population of cells which resemble HPC when cultured, and that these cells differentiate back into hepatocytes when re-transplanted[105]. However, a murine model of wild-type hepatocyte transplantation in fumarylacetoacetate hydrolase deficient mice, with 3,5-diethoxycarbonyl-1,4-dihydrocollidine (DDC) mediated stimulation of the HPC response, found a negligible proportion of donor-genotype HPC suggesting that hepatocyte de-differentiation was not significant in this model.

It has also been suggested that marrow-derived cells may contribute to the generation of HPC via trans-differentiation. This was demonstrated in a rat model of liver injury caused by the combination of 2-acetylaminofluorene (2-AAF) with 70% partial hepatectomy, with prior sex mismatched bone marrow transplantation and mitotic inhibitor therapy. About 20% of oval cells were found to be of donor genotype, and fusion events were not common[106]. This model, and particularly use of a mitotic inhibitor to suppress native HPC proliferation, is notably

unphysiological and other experiments without the use of mitotic inhibitors have found no evidence of significant contribution of marrow-derived cells to the oval cell population[107].

It is becoming evident that there is plasticity in the liver epithelium. Recent work has shown that hepatocytes can trans-differentiate into biliary epithelial cells (BEC) in response to liver injury, transitioning through a stage of 'atypical ductal cell' (akin to oval cell/HPC)[108]. Further work in this area will likely shed more light on the pathways involved in liver repair and may lead to a paradigm shift in how we view HPC and regeneration in general.

***

1.6 DR and its relationship to liver fibrosis

The DR is a structural remodelling which occurs within and around the portal tracts in response to liver injury[109]. The most striking appearance of the DR is a proliferation of biliary-phenotype cells, however interactions between multiple cell-types are important in influencing the re-modelling that takes place within the DR. The different cell-types associated with the DR have been described as residing within a "niche", and include hepatic progenitor cells (HPC), stromal cells including HSC and inflammatory cells[110]. The presence of micro-vessels within the DR niche is suggestive of a relationship between the DR and angiogenesis[109].

The appearance of a DR has been noted in many aetiologies of liver disease, albeit with contrasting phenotypic appearances in response to different injuries[109]. Despite its common presence in both human and animal models of liver disease, its precise relationship to liver regeneration and fibrosis is incompletely understood.

HPC and DR markers

Within the DR is seen a population of proliferating HPC [111], bipotential cells which can be induced to differentiate *in vitro* into both hepatocytes and biliary cells [99]. HPC have been demonstrated to arise for the Canals of Hering, at the interface of the bile canaliculi and the bile ducts [112]. Hence, the phenotype of cells observed within the DR is diverse, from primitive progenitors to more hepatocyte and biliary-like cells [113]. Moreover, the DR shows a distinct polarity, with hepatocyte-like and biliary-like cells at opposing ends [114].

As expected, there are various markers associated with the DR. As a whole, the epithelial component of the DR has a predominantly biliary phenotype: this results in difficulty in identifying markers which reliably differentiate mature biliary cells from HPC, a useful distinction given that proliferating HPC are implicated in the structural remodelling that takes place within and around the DR. For example, staining with CK19 or EpCAM – commonly used markers to demonstrate the DR – will identify both mature biliary cells and HPC[109,114].

Markers have been proposed which are more specific for HPC, and therefore identify the more "active" components of the DR, however there is often overlap and results are not always recapitulated between different studies. For instance, suggested HPC markers include CD133, forkhead box L1, trophoblast antigen 2, Kruppel-like factor 5 and cystic fibrosis transmembrane conductance regulator[109,115-118]. However, no marker has gained acceptance as a "true" signature of the DR.

The uncertainty surrounding the degree to which HPC contribute to regeneration in homeostasis and liver injury has been previously discussed. However, it is clear that propagation of HPC and appearance of a DR is common occurrence in liver injury. Therefore, it is important to keep in

mind a potential regenerative function of the DR, particularly when considering tools to manipulate or target the DR as a therapeutic strategy.

DR in different liver injuries

A DR can be seen in many causes of chronic liver injury, and in acute severe liver injury such as that caused by hepatic necrosis due to paracetamol toxicity. Perhaps the most well-known pattern of DR occurs in biliary obstruction, whereby a proliferation of small ductules occurs at the periphery of portal tracts; as obstruction becomes chronic this is associated with increasing amounts of mature collagen fibres. Chronic biliary injury due to conditions such as primary biliary cholangitis and primary sclerosing cholangitis can give similar appearances[110].

However, DR are also observed in conditions where the insult is non-biliary, for example viral hepatitis and MASLD, where hepatocellular damage predominates. In the latter condition, a DR usually appears when steatohepatitis develops rather than bland steatosis[109]. The pattern of the DR in NASH has been described as more “invasive” than that observed in biliary diseases, with propagation of the DR cells away from the portal areas and into the lobule[110]. Lobular propagation of the DR has been associated with the formation of new hepato-biliary junctions, suggesting that a potential outcome for the DR is improved biliary drainage and restoration of the bile canaliculi which are damaged in hepatocellular injury[119].

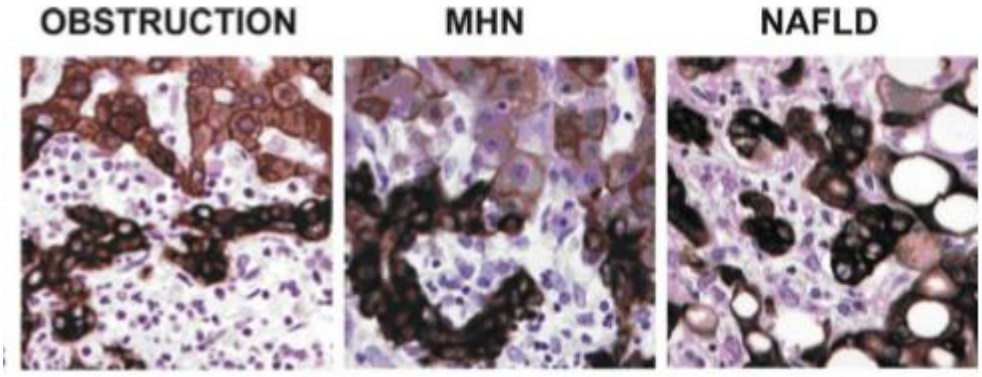

Figure 8: IHC cytokeratin 8/18 staining for the DR in biliary obstruction, massive hepatic necrosis and MASLD.
From Gouw et al, 2011

Relationship between DR, HSC and fibrosis

The magnitude of the DR is known to correlate with the severity of fibrosis in many causes of chronic liver disease[111]. This observation has led to the common view that the DR may directly drive fibrogenesis. However, different explanations are possible, for instance that the DR is an adaptive response to fibrosis, or that the two are driven by separate mechanisms which are stimulated concurrently by liver injury.

Of note, the evidence to date does not resolve this uncertainty. For example, in an analysis of human hepatitis C liver biopsy samples, a strong correlation between the DR and fibrosis was confirmed, however it was noted that a DR was present in 43% of samples where there was no discernible fibrosis[120]. This would imply that the DR can precede fibrosis, and the authors concluded that given the direction of this temporal relationship, the DR is likely to drive portal fibrosis. Conversely, in a murine model of liver injury caused by choline deficient ethionine supplemented (CDE) diet, which is known to stimulate a HPC response, it was shown that deposition of collagen fibres (early fibrosis) occurred four to seven days before the development of any significant CK19 staining[121]. It was hypothesised that a portal collagen framework may be a necessary development for the propagation of the DR away from the portal tracts. A further study used transgenic mice, engineered to produce an abnormal form of collagen-1 that is resistant to degradation by MMPs. When injured with either CCl4 or CDE diet, staining showed a persistence of fibrosis during the recovery phase associated with an attenuated HPC response. The authors concluded that matrix

turnover was a requirement for a robust HPC response, rather than simply the presence of fibrosis[122].

Given the crucial role which HSC play in the development of liver fibrosis, it would seem logical to assume that interactions between the DR and HSC are important, considering the close association between the DR and fibrosis. Previous work has shown that the oval cell/HPC compartment in injured rodent and human liver tissue is surrounded by a niche of cells including HSC, macrophages and endothelial cells[123]. Interestingly, this was a common finding among different models of injury including partial hepatectomy/2-AAF and CDE diet in rodents, and chronic hepatitis B and C in human tissue.

Particularly in biliary models of liver injury, it is clear that, once established, cells within the DR produce growth factors and pro-fibrogenic factors which are able to activate HSC, the main scar-forming cell within the liver. For example, in a bile duct ligation murine model, molecules shown to be produced by bile duct segments included PDGFβ, a potent HSC mitogen[124], and indeed the bile duct segments were able to induce chemotaxis of HSC *in vitro* using a Transwell assay[125]. Another growth factor implicated in fibrogenesis, CTGF, has also been shown to co-localise with the DR via a combination of IHC and fluorescent *in-situ* hybridisation in a murine bile duct ligation model, but interestingly not in an acute CCl4 induced injury[126].

Notably, evidence exists to imply that some DR populations are able to have the opposite effect and reduce HSC activation: DR cells expressing the marker leucine-rich repeat-containing g-protein-coupled receptor 5 (LGR-5) were shown to be upregulated in response to liver injury, and reduced myofibroblast activation during *in vitro* co-culture as assessed by quantitative polymerase chain reaction (qPCR) for fibrosis-associated genes[127].

In addition to the paracrine signalling from DR cells to HSC described above[125], evidence also exists for reciprocal signalling from macrophages and HSC to DR cells[128], co-ordinating the activation of pathways including Wnt and Notch which are proposed to control the differentiative fate of HPC. In addition, HSC have been identified as the source of growth differentiation factor 11 which is able to increase the proportion of LGR-5 positive DR cells, although the mechanism for this remains uncertain[127]. This evidence of reciprocal paracrine signalling between HPC and neighbouring cells highlights the complexity of cellular interactions within the DR niche.

RNA sequencing of the DR has confirmed that many signalling pathways are active on a transcriptomic level, controlling factors such as inflammation and recruitment of immune cells. For example, bulk RNA sequencing of the DR in human patients with alcohol related liver disease has shown activation of pathways including Wnt, PDGFβ, TNFα and IL-17[115]. Single-cell RNA sequencing offers the ability to cluster individual cells within the DR into groups based on their activation profiles, and identify markers to define novel DR sup-populations. Whist single-cell RNA sequencing has not yet been carried out on a pure population such as the DR in humans, this approach has given new insights to the fibrotic niche in cirrhosis, for example re-defining subsets of “scar-associated” macrophages and mesenchymal cells based on transcriptomic profile[129].

Given the intricacy of the DR cell niche in terms of different cell-types and the signalling pathways involved, it is not surprising that the relationship between the DR and fibrosis is complicated. Turnover of matrix may occur early in liver injury, and it is possible that the DR is activated in response to this early fibrosis. The DR could perhaps also induce adjacent matrix deposition both to aid the initial “wound healing” response and to enable propagation of HPC to promote regeneration.

Perhaps in response to chronic injury and continual activation of the DR, this DR-driven fibrosis becomes unchecked and deleterious.

Whilst much of the work described above has been carried out in biliary models of liver injury, MASLD has a large unmet need and the degree to which the DR influences fibrosis in this condition is poorly defined. Attempting to further refine this complicated relationship could open the way to new therapeutic targets.

Inducing and modulating the DR

Multiple methods exist to induce a DR in animal models. Perhaps the most effective methods combine a large stimulus for hepatocyte regeneration, such as partial hepatectomy, with mitotic inhibitors to prevent replication of mature hepatocytes and stimulate activation of a HPC response and DR. Whilst highly effective in inducing a large DR, such methods are notably un-physiological. Biliary injury models, such as bile duct ligation or DDC diet, induce a robust and prolonged DR, assuming the injury is maintained. Of course, a sustained DR will also develop gradually in response to chronic hepatocellular injury such as that induced by CDAA diet (as a model of human NASH). Interestingly, the strain of mouse can also have an effect on the magnitude of the DR: for example, BALB/c mice, which have a dampened Th1 response, were shown to develop an attenuated DR on exposure to CDE diet, in comparison to C57/Bl6 animals[130].

To further shed light on the relationship between the DR and fibrosis, it would be useful to modulate the DR – with the ability to both stimulate and attenuate it – and assess the downstream effects on regeneration and fibrosis. Several potential ways of doing this have been described.

One such method used a transgenic model whereby conditional deletion of murine double minute 2 was achieved under the control of a CK19 promoter during DDC diet, inducing senescence in cells

expressing CK19 i.e. biliary cells. The ability to activate the *Cre* with intra-peritoneal tamoxifen allowed the deletion to be activated in a controlled fashion, and could be instigated at different stages of liver injury. The induction of biliary senescence was shown to attenuate the DR: this was associated with greater fibrosis and impaired regeneration[131]. The Notch inhibitor dibenzazepine, administered intra-peritoneally, has also been shown to attenuate the DR following injury caused by DDC diet. This was associated with reduced numbers of HPC, however any effect on fibrosis was not reported[132]. A further method used blockade of the TWEAK pathway via a neutralising antibody in fibrotic mice (due to previous CCl4 treatment), following partial hepatectomy. There was significant attenuation of the DR in association with reduced oval cell proliferation, in addition to reduced expression of fibrosis-related genes by qPCR and increased hepatocyte proliferation[133].

The models described above all constitute relatively "blunt" tools to modulate the DR, and it is possible that the administration of treatments such as neutralising antibodies could have effects on other cell-types and therefore confound aspects of the analysis. To further understand the complex relationship between the DR, fibrosis and regeneration, a possible approach would be to use transgenic methods to directly modulate expression of molecules from the DR itself.

1.7 Aims and hypothesis

Three main observations were made in deciding the aims and hypotheses for this piece of work. Firstly, the causality between the development of a DR and fibrosis is unknown including within the sphere of MASLD. Secondly, MASLD comprises a large proportion of cases of advanced liver disease worldwide and understanding mechanisms underpinning fibrosis progression is important to try to identify therapeutic targets. Thirdly, HSC are crucial in the development of fibrosis and thus interactions between DR cells and HSC could be of mechanistic significance in MASLD.

Of note, from herein, isolated DR cells are denoted *biliary/DR cells*. This is to acknowledge that isolation of a pure DR population is not possible based on any currently known cell markers (and of course donor livers should not contain DR cells); the term BEC has been reserved for cultured cells.

Principal aims:

1) Investigate murine models of MASLD for their ability to induce a DR and fibrosis
2) Compare murine findings to human MASLD using multiple disease stages
3) Investigate potential cellular interactions between biliary/DR cells and HSC using both *in vit*ro and *in vivo* methods
4) Isolate human biliary/DR cells from NASH cirrhosis and donor livers: perform bulk RNA sequencing to characterise any difference in transcriptomic profile

Hypothesis:

Biliary/DR cells in advanced stages of MASLD represent a fibrogenic phenotype, activating neighbouring HSC to promote the propagation of fibrosis.

2. METHODS

2.1 Acquisition of human liver tissue

Human liver tissue was obtained from the Queen Elizabeth Hospital, Birmingham with approval of the Local Research Ethics Committee and previous informed written consent from the patients. The tissue comprised transplant hepatectomy specimens, or donor livers which were deemed unsuitable for transplantation.

2.2 Processing of human liver tissue

Livers were stored on ice until they were taken to the laboratory. Processing was usually within 6 hours for transplant hepatectomy specimens which were explanted during working hours; for out-of-hours explants and for donor livers the processing was usually undertaken the following working day. As part of the standard laboratory processing, slices of liver tissue were cut by an expert pathologist following exclusion of tumour or alternative/incidental pathology. $1cm^3$ chunks of liver were either snap-frozen in liquid nitrogen and stored at -80C, and small tissue sections were stored in formalin. The formalin-fixed tissue could be embedded in paraffin blocks and cut into slides at a later time, as detailed below, to enable histological analysis.

For the purposes of this project, one slice of liver (either NASH explant or donor) was stored at 4C in DMEM (Gibco) until it could be further processed, within six hours. The slice was trimmed of any surrounding connective tissue and either used fresh for experiments, or cut into tiny chunks using two scalpels. Ten Cryovials were then each filled with approximately one gram of tissue and 750µL of Cellbanker 2 (Amsbio) was added to the vials which were then stored at -80C until future use.

2.3 Mice

Keratin-19 tomato mice on a C57Bl/6 background were bred and maintained under specific pathogen-free conditions at the Biomedical Services Unit at the University of Birmingham. Mice were housed up to four individuals per cage with access to food and water *ad libitum* and a twelve hour light/dark cycle. Male mice between 12-16 weeks of age were used for experiments.

2.4 Instigation of liver injury – MCD diet

Six mice were provided with *ad libitum* access to MCD diet (MP Biomedicals) which was reconstituted and stored according to manufacturer's instructions. Mice were weighed and underwent a welfare check on a daily basis. Three mice were culled after 13 days with a further three culled 26 days after diet instigation.

2.5 Instigation of liver injury – CDAA diet

Eight mice were provided with *ad libitum* access to CDAA diet (ssniff) which was reconstituted and stored according to manufacturer's instructions. Mice were weighed on a twice-weekly basis and underwent a daily welfare check. After three weeks, four mice were culled. The remaining four mice were then weighed weekly and culled at 6 weeks after diet instigation.

2.6 Control mice

Four mice were provided with the standard chow of the Biomedical Services Unit at the University of Birmingham for the duration of the experiments to serve as controls.

2.7 Dissection and collection of liver tissue

Mice were humanely killed via cervical dislocation. The peritoneum was opened and the liver flushed via the inferior vena cava with ice cold phosphate buffered saline (PBS); the portal vein was subsequently transected and a further flush administered until the liver turned pale. The liver and spleen were carefully dissected, fatty/connective tissue were trimmed away and the gallbladder removed.

The left lobe of the liver and the spleen were immediately placed in 10% formalin (Sigma). A small piece of the right lobe was snap-frozen using dry ice and stored at -20C for future processing of frozen sections. The remaining liver tissue was stored in ice cold PBS for subsequent digestion.

2.8 Processing of tissues for histology

The left lobe of the liver was transferred from 10% formalin into a cassette and stored in buffered formalin solution. At a later point, the cassettes were placed into increasing concentrations of ethanol (70%, 95% and 100%) for thirty minutes before being placed in Histoclear for a further thirty minutes. Embedding of the cassette in paraffin was then undertaken using a Histostar embedding station (Thermo Scientific).

Tissue sections 5µm thick were cut using a microtome and placed onto microscope slides (X-tra adhesive, Leica).

2.9 Staining of formalin fixed paraffin embedded (FFPE) sections: de-paraffinisation, antigen retrieval and blocking

Tissue sections were de-paraffinized by washing slides in xylene (3 x three minutes) followed by washes in graded ethanol solutions (3 x three minutes) and subsequently distilled water (2 x three minutes). Antigen unmasking was then performed by heating the sections for 15 minutes on full power in a 800W microwave immersed in pre-warmed solution (990mls distilled water with 10ml high pH antigen-unmasking solution (Vector Labs)). Cooling was undertaken using gentle running distilled water for five minutes.

Sections were then carefully dried, a wax ring was applied to mask off the area of tissue and PBS applied to prevent the tissue from drying out. Blocking of endogenous peroxidases was carried out by applying peroxidase-blocking solution (Dako) for 15 minutes. Sections were rinsed for five minutes in PBS/0.1% Tween-20. Blocking was undertaken using 10X casein buffer (Vector Labs) diluted 1:10, for 20 minutes. This was tapped off but the sections were not rinsed.

2.10 Staining of frozen tissue sections: thawing and blocking

Frozen tissue sections were left to thaw for thirty minutes at room temperature. Following this, a wax ring was applied to mask off the area of tissue and PBS applied to prevent the tissue from drying out. Blocking was undertaken using 10X casein buffer (Vector Labs) diluted 1:10, for 20 minutes. This was tapped off but the sections were not rinsed.

2.11 IHC

Primary antibody or immune-matched control (at the appropriate dilution with PBS, see Table 1) was added to the sections with gentle rocking for either one hour (at room temperature) or overnight (4C). Sections were rinsed for five minutes in PBS/0.1% Tween-20 and then incubated

with a peroxidase-conjugated secondary antibody raised against the species of the primary antibody (Vector Labs) for 30 minutes at room temperature. Sections were rinsed in PBS/0.1% Tween-20 for five minutes. Staining was visualised using Immpact DAB (Vector Labs), made up according to manufacturer's instructions, for 90 seconds followed by a further rinse in PBS. Counter-staining was achieved using filtered Mayer's haematoxylin for 30 seconds followed by a rinse in warm tap water for two minutes. Dehydration and clearing were undertaken via washes in graded ethanol solutions (3 x three minutes) and xylene (3 x three minutes) before mounting in DPX (Sigma).

2.12 Immunofluorescence

Primary antibody or immune-matched control (IMC) (at the appropriate dilution with PBS) was added to the sections with gentle rocking for either one hour (at room temperature) or overnight (4C). Sections were rinsed for five minutes in PBS/Tween and then incubated with fluorescently-labelled secondary antibodies to the host species of the primary antibody/IMC and 1µg/ml 4',6-Diamidine-2'-phenylindole dihydrochloride (DAPI) for 30 minutes at room temperature. Concentrations of secondary antibodies used are listed in Table 1. Following a further rinse in PBS, slides were mounted in Immu-mount (Thermo Fisher).

2.13 Fibrosis staining

Picrosirius Red staining was undertaken using a pre-prepared kit of reagents (Abcam). Sections were de-paraffinized by washing in xylene (3 x three minutes), graded ethanol solutions (3 x three minutes) and distilled water (2 x three minutes). Sections were carefully dried and a wax ring applied to mask off the area of tissue. Reagents were applied to the sections as per the manufacturer's

instructions, followed by dehydration and clearing via washing in graded ethanol solutions (3 x three minutes) and xylene (3 x three minutes) before mounting in DPX (Sigma).

2.14 Antibodies

Primary / secondary	**Producer + catalogue number**	**Target**	**Host / clonality**	**Conjugate**	**Conc. used**	**Application (IHC / IF)**
Primary	Abcam *ab32570*	PDGFRβ	Rabbit Monoclonal	Unconjugated	1:200	IHC IF
Primary	Abcam *ab124964*	αSMA	Rabbit Monoclonal	Unconjugated	1:200	IHC
Primary	DSHB *TROMA-III*	CK19	Rat Monoclonal	Unconjugated	1:200	IF
Primary	Thermo Fisher *PA5-99172*	Pan-cytokeratin	Rabbit Polyclonal	Unconjugated	1:200	IHC IF
Primary	Abcam *ab69506*	PDGFRβ	Mouse monoclonal	Unconjugated	1:200	IF
Primary	Abcam *ab7817*	αSMA	Mouse monoclonal	Unconjugated	1:200	IF

Secondary	Vector Labs *MP-7401*	Rabbit IgG	Horse	HRP	Stock	IHC
Secondary	Vector Labs *MP-7444*	Rat IgG	Goat	HRP	Stock	IHC
Secondary	Thermo Fisher *A-21428*	Rabbit IgG	Goat	AF 555	1:500	IF
Secondary	Thermo Fisher *A-11006*	Rat IgG	Goat	AF 488	1:500	IF
Secondary	Abcam *ab150114*	Mouse IgG	Goat	AF 555	1:500	IF
Secondary	BioLegend *406404*	Rabbit IgG	Donkey	AF 488	1:500	IF
IMC (Mouse IgG-1)	Abcam *ab91353*				1:200	IF
IMC (Mouse IgG-2a)	Abcam *ab18415*				1:200	IF
IMC (Rabbit IgG EPR25A)	Abcam *ab172730*				1:200	IHC IF

IMC (Rat IgG-2a)	Thermo Fisher *02-9688*				1:200	IF

Table 1: unconjugated primary antibodies, secondary antibodies and IMC used for IHC and immunofluorescence

Host species	**Target species**	**Target antibody**	**Fluorophore**	**Producer + catalogue no.**	**Conc.**
Mouse	Human	CD45	BV711	BD Biosciences *564357*	1:200
Mouse	Human	CD31	BV421	BD Biosciences *564089*	1:200
Mouse	Human	EpCAM	APC	BD Biosciences *566842*	1:200
Rat	Mouse	CD45	BV785	BioLegend *103149*	1:200
Rat	Mouse	CD31	AF488	BioLegend *102414*	1:200
Rat	Mouse	EpCAM	APC	BioLegend *118214*	1:200

Table 2: conjugated fluorescence-activated cell sorting (FACS) antibodies used for murine and human experiments

2.15 Primers for qPCR

Gene of interest	**Species**	**Taqman (Thermo Fisher) Assay ID**
Pdgfβ	Mouse	Mm00440677_m1
Ctgf	Mouse	Mm01192933_g1
Gapdh (housekeeping)	Mouse	Mm99999915_g1
PDGFβ	Human	Hs00966522_m1
CTGF	Human	Hs00170014_m1
PDGFRβ	Human	Hs01019589
ACTA2	Human	Hs00426835_g1
GAPDH (housekeeping)	Human	Hs02786624_g1

Table 3: gene expression assays used for qPCR

2.16 Visualisation of slides

Slides were scanned and viewed using a Zeiss Axio Slide Scanner. To quantify areas of staining, six random fields of view at x20 magnification were captured and the *ImageJ* software was used to calculate the area stained, using the same threshold intensity throughout all slides within the experimental group. The median area stained (of the six random fields per slide) was plotted using the *Prism* software.

The immunofluorescence slides were visualised using a Zeiss AX10 microscope. Fluorescence intensity thresholds were set using slides stained with IMC in place of the primary antibody.

2.17 Biliary cell isolation – digestion (murine tissue)

Approximately half of the dissected liver was chopped into tiny pieces using a combination of scissors and scalpel blade in a petri dish. This was collected in ice-cold wash media (DMEM (Gibco) with 1% fetal calf serum (FCS) and 1% penicillin/streptomycin) before being inverted five times and centrifuged at 100g for one minute. The supernatant was aspirated and the wash was repeated two times. The pellet was then re-suspended in digest media (wash media with 0.05mg/ml dispase and 0.05mg/ml collagenase) at 10 minutes and placed in a water-bath at 37C before being centrifuged at 120g for four minutes. The supernatant was aspirated and the pellet re-suspended in 25ms digest media, before the tube was placed on its side in a shaking incubator for 90 minutes at 200 rpm and 37C. The tube contents were mixed via pipetting up and down using a 10ml serological pipette, before being centrifuged at 120g for four minutes. The pellet was then re-suspended in 20mls digest media and the tube placed on its side in a shaking incubator for 30 minutes at 150 rpm and 37C.

The contents were centrifuged at 120g for four minutes, and the pellet re-suspended in pre-warmed 7xTrypLE (3:7 v/v mix of 1XTrypLE and 10XTrypLE (Thermo Fisher)) before being placed in a water-bath for 10 minutes at 37C. The tube contents were mixed by pipetting up and down using a 10ml serological pipette for 1 minute. 30mls of ice-cold was media was added to the tube to stop the reaction, before being centrifuged at 320g for five minutes. The supernatant was aspirated and the pellet re-suspended in 3mls of wash media, before being filtered through a 40µL cell strainer. Light pressure was applied using the plunger from a 2ml syringe and 3mls PBS added to the strainer to wash off any trapped cells. The strained contents were then centrifuged at 320g for 5 minutes. The

supernatant was discarded and the pellet re-suspended in 1000µL PBS before proceeding to staining/FACS.

2.18 Biliary cell isolation – human tissue

Approximately 5g of liver was chopped into tiny pieces using a combination of scissors and scalpel blade in a petri dish. This was collected in ice-cold wash media (DMEM (Gibco) with 1% fetal calf serum and 1% penicillin/streptomycin) before being inverted five times and centrifuged at 100g for one minute. The supernatant was aspirated and the wash was repeated. The pellet was then re-suspended in pre-warmed digest media (wash media with addition of enzymes: Collagenase V (Sigma) 0.8mg/ml, Collagenase D (Roche) 0.625mg/ml, Dispase (Gibco) 1mg/ml, DNase 1 (Roche) 30 µg/ml) and incubated at 37C in a shaking incubator at 150rpm for 30 minutes. 100mls of cold wash media was then added to terminate the digestion and the cell suspension passed through a 40µm strainer with light pressure from a 10ml syringe plunger and a further rinse of the filter with wash media.

The suspension was then centrifuged for 10 minutes at 320g, the supernatant was discarded and the pellet re-suspended in 50ml of PBS before centrifuging again for 10 minutes at 320g. The pellet was then re-suspended in 80µL of magnetic activated cell sorting (MACS) buffer (Miltenyi) before proceeding to different MACS steps (EpCAM enrichment +/- CD45 depletion +/- dead cell depletion) according to the manufacturer's instructions. Briefly, 20 µL of the relevant microbeads were added to the sample followed by incubation for 15 mins at 4C. The sample was then washed with 1ml of buffer and centrifuged at 300g for 10 minutes. The supernatant was aspirated and the pellet suspended in 500µL of buffer. Magnetic separation was then carried out using the relevant column

and magnetic stand. Following the last MACS step, the sample was centrifuged at 320g for 10 minutes, the supernatant discarded and the pellet re-suspended in PBS before proceeding to FACS.

2.19 Biliary cell isolation – FACS of murine and human cells

A small volume of biliary cell suspension was taken from each sample to give a final volume of 300µL. 50µL of the mix was pipetted into four wells of a 96-well plate (single stain controls) and 100µL into a further well (unstained control). The remainder of the samples were transferred to individual 1.5ml Eppendorfs and centrifuged at 500g for 3 minutes to pellet the cells. The pellet was then re-suspended in 100µL live/dead stain (*Zombie NIR* (BioLegend, *BD 423106*), diluted 1:200 in PBS only) and transferred to wells in the 96-well plate. 50µL of live/dead stain was added to one of the control wells and mixed by pipetting. 50µL of FACS buffer (PBS with 2% fetal calf serum) was then added to the remaining control wells. The plate was then incubated for 30 minutes in the dark at 4C before being centrifuged at 400g for four minutes and the supernatant discarded.

The individual sample pellets were re-suspended in 100µL antibody mix (CD45, CD31, EpCAM (all at 1:200 dilution in FACS bufer)). 50µL individual antibody, or FACS buffer, was used to re-suspend cells in the control wells before incubating for 45 minutes in the dark at 4C. The plate was then centrifuged at 400g for four minutes to pellet the cells, and the supernatant discarded. The cell pellets were then re-suspended in FACS buffer before being transferred to FACS tubes. Cells were analysed using a Flow Cytometer with compensation achieved using the single-stain controls. The live, CD45 negative, CD31 negative, EpCAM positive population (denoted hereon as *EpCAM+*) was sorted directly into Eppendorfs containing PBS before being centrifuged at 2000g for five minutes to pellet the cells. The pellet was then re-suspended in 350µL RLT buffer (Quiagen) and stored at -80C.

2.20 RNA extraction - cells

Cells suspended in RLT buffer were Vortexed vigorously for thirty seconds and then aspirated ten times using a needle and syringe to achieve lysis. RNA extraction was performed using either a RNeasy Mini or RNeasy Micro kit (Quiagen), according to manufacturer instructions. RNA was stored in nuclease-free water at -80C until further use.

2.21 RNA extraction – tissues

For human explant/donor liver tissue, samples which had been previously snap-frozen in liquid nitrogen and stored at -80C were removed and put on dry ice. Approximately 50mg of frozen tissue was shaved from each sample and placed in 1000µL QIAzol in a 2ml flat-bottomed Eppendorf. A TissueRuptor (Quiagen) was used for thirty seconds to lyse the tissue.

200µL of chloroform was then added to each sample which were Vortexed vigorously for thirty seconds and placed on the bench-top at room temperature for five minutes. Centrifugation was then performed for fifteen minutes at 10,000g at room temperature. Following this step, phase separation occurs with a lower phenolchloroform phase, an interphase, and an upper aqueous phase which exclusively contains the RNA. The aqueous phase was carefully pipetted out and added to an Eppendorf with an equal volume of 70% ethanol before proceeding with column RNA extraction using the RNEasy Mini kit (Quiagen).

2.22 Reverse transcription

RNA concentration and purity was checked using a Nanophotometer. cDNA synthesis was performed using Superscript II Reverse Transcriptase (Invitrogen) according to manufacturer

instructions. For all experiments except the sorted murine biliary cells, 1000µg of RNA was used for reverse transcription. Due to the lower RNA yields achieved using sorted cells, 50ng of RNA was used for reverse transcription in these experiments. In brief, RNA was added to a micro-PCR tube (Thermo Fisher) with nuclease-free water then added to a total volume of 10µL. 1µL of 10mM dNTP mix (Thermo Fisher) and 1µL random primers (Promega) were added and the sample heated at 65C for five minutes before quick-chilling on ice. Following brief centrifugation, 4µL 5xfirst-strand buffer (Invitrogen), 2µL 0.1M DTT (Invitrogen) and 1µL RNaseOUT 40units/µL (Invitrogen, *used if starting volume of RNA </= 50ng)* were added and the samples incubated for 2 minutes at 25C before quick-chilling on ice. Following brief centrifugation, 1µL of Superscript II Reverse Transcriptase (Invitrogen) was added and the sample mixed by pipetting gently. The sample was heated at 25C for ten minutes then 42C for fifty minutes and then 70C for fifteen minutes to inactivate the reaction. The cDNA was stored at -20C until further use.

2.23 Quantitative PCR

A 10µL reaction volume was used in either 96 or 384 well PCR plates (Thermo Fisher), comprising 5µL Taqman Mastermix (Invitrogen), 4µL nuclease-free water, 0.5µL of FAM-labelled gene-specific probes (Invitrogen) and 0.5µL of undiluted cDNA. Samples were run in triplicate with a housekeeping gene and a nuclease-free water control in place of cDNA. The plate was subjected to qPCR using a Applied Biosystems 7900HT Fast Real-Time PCR System (Life Technologies Ltd). Differential expression levels were calculated using the 2^{-ddCT} method.

2.24 RNA sequencing

Cells suspended in RLT buffer were transferred from -80C storage and shipped directly to Lexogen on dry ice. QC was carried out as per Lexogen's internal protocols. In brief, samples were characterized by UV-Vis spectrophotometry (Nanodrop2000c, Thermo Fisher) and RNA integrity was assessed on a Fragment Analyzer System using the DNF-471 RNA Kit (15 nt) (Agilent). Individual libraries were quality controlled on a Fragment Analyzer device (Agilent), using the HS-DNA assay, and then pooled for sequencing. The sequencing-ready pool was quantified using a Qubit dsDNA HS assay (Thermo Fisher) and quality controlled on a Fragment Analyzer device (Agilent), using the HS-DNA assay.

Following QC, 3' mRNA sequencing was performed using Lexogen's QuantSeq FWD with UDI technology.

2.25 Cell culture

All cell culture work and media preparation was carried out in a Class II biological safety cabinet using aseptic technique. Cells were maintained at 37C in a 5% CO_2 humidified incubator. Media was changed three times per week. When cells reached a confluent monolayer, media was removed. TryPLE (used for cell-lines) or trypsin/EDTA (used for primary cells) was added to flasks to dissociate cells. Media was then replaced and the cell suspension transferred to a 15ml tube which underwent centrifugation at 2000g for five minutes. The cell pellet was re-suspended in media and seeded into flasks, noting the passage number. In general, cell-lines were split quite liberally (e.g. 1:5) at each passage whereas primary cells were split more conservatively (e.g. 1:2). Counting was performed by diluting a fraction of the re-suspended cell pellet 1:5 with tryptan blue (Abcam). The number of

live cells was then counted using a hemocytometer via the formula (average no. live cells per grid x $5x10^4$ cells/ml.

2.26 Culture of BEC

BEC were extracted from wedges of human livers by a senior researcher via immuno-magnetic bead extraction following mechanical and enzymatic dissociation. Cells were seeded into 25cm^2 flasks coated with type I rat-tail collagen, with 5ml BEC culture media. The BEC culture media constituents are detailed below, and have previously been optimised in our laboratory. Cells were passaged when confluence was achieved and re-seeded into 75cm^2 flasks. Cells were used for the co-culture experiment at P4.

Prior to commencing co-culture experiments, media was removed from one flask of BEC and replaced with HSC media. 6 hours later, microscopy showed no sign of any significant change or injury to the BEC, as assessed by a senior member of the group. The media was then replaced with standard BEC media.

2.27 Culture of human HSC

Human HSC at P4 (originally supplied to laboratory frozen at P1, Sciencell HHSteC #5300) were thawed from liquid nitrogen storage and seeded into a 75cm^2 flask with 10ml HSC media (DMEM (Gibco) with 10% FCS and 1% penicillin-streptomycin). Cells were incubated for 48 hours at which point they were confluent. Media was removed and replaced with media containing only 1% FCS for 24 hours before use in the co-culture experiment.

2.28 Co-culture of BEC with HSC

Sterile forceps were used to transfer 0.6µm cell culture inserts into sterile plastic boxes. The underside of the inserts was then coated with 500µL type 1 rat tail collagen and incubated for one hour at 37C. The inserts were then washed with sterile PBS. BEC were dissociated from a 75cm^2 flask and 250,000 cells were seeded onto each relevant insert, which were incubated for one hour to allow the BEC to adhere. Following this, the inserts were gently washed in sterile PBS to remove non-adherent BEC and the cell culture inserts were carefully flipped and placed into different wells of a 6-well cell culture plate containing 1500µL of HSC culture medium. These were then incubated overnight at 37C.

The following day, HSC were dissociated from a 75cm^2 flask and 250,000 cells were seeded into the upper chamber of each relevant insert. The media on the underside of the cell culture insert was carefully removed. Media was then added to the upper and lower chamber of each insert. The plates and cell culture inserts were then incubated for 48 hours at 37C.

To remove the HSC, 500µL sterile PBS was added to the upper side of the relevant cell culture inserts and a cell scraper was used to gently remove the cells. A further 500µL of PBS was added and the cell suspension aspirated into an Eppendorf (one Eppendorf per well). To remove the BECs the cell culture inserts were carefully removed, flipped over and placed into a new 6-well cell culture plate. 500µL of sterile PBS was added to the upper-side of the inserts and a cell-scraper used to carefully remove the cells. A further 500µL of PBS was then used to wash the cells off the insert into the well. The cell suspension was then aspirated into an Eppendorf.

Eppendorfs containing cell suspensions were then centrifuged at 2000g for five minutes at 4C to pellet the cells. 350µL RLT buffer (Quiagen) was used to re-suspend the pellets and stored at -80C.

2.29 Experimental plan for co-culture of BEC with HSC

Number of well	BEC present	HSC present
1,2,3,4	Y	N
5,6,7,8 +/- 9*	Y	Y
10,11,12,13 +-/ 14*	N	Y

*Due to available numbers of cells, either 4 or 5 wells were used for the co-culture and HSC mono-culture groups

2.30 Experimental plan for co-culture of BEC with HSC, with blocking antibody

Number of well	BEC present	HSC present	Blocking antibody/IMC present
1,2,3,4	Y	N	N
5,6,7,8	Y	Y	Blocking Ab
9,10,11,12	Y	Y	IMC
13,14,15,16*	N	Y	IMC

*****Technical failure meant cells from one well of this group could not be analysed

2.31 Staining of BEC

The condition media was removed from a T25 flask of confluent BEC and the flask rinsed with sterile PBS before 2ml ice-cold methanol was added and the flask stored at -20C for ten minutes to fix and permeabilise the cells. The methanol was discarded and the flask rinsed twice with PBS. 2ml casein was then added to the flask which was stored at room temperature for 20 minutes. The flask was

then rinsed with PBS before addition of the primary antibody (CK19 1:200 dilution or IMC) and incubation for one hour at room temperature. Following two rinses with PBS, the secondary antibody was added to the flask along with DAPI (1 µg/ml). Following incubation for 30 minutes at room temperature in the dark, the secondary antibody was washed off and the cells visualised immediately using a Zeiss AX10 fluorescent microscope.

2.32 Constituents of BEC media (500mls)

DMEM (Gibco) / Hanks F12 (ThermoFisher) 50/50 v/v mix (to ~ 442 mls)

Human serum (Sigma) 50 ml

Penicillin/streptomycin (Merck) 2 ml

Epidermal growth factor (20 µL, 100 µg/ml)

Insulin 248µL

Hydrocortisone (2 ml, 2µg/ml)

Cholera toxin (2 ml, 1 µg/ml)

Tri-iodo-thyronine 2ml

Hepatocyte growth factor (20 µL, 100 µg)

3. RESULTS

3.1 Comparison of DR, fibrosis and HSC activation in two murine models of MASLD

3.1.1 Introduction

Murine models are readily used to induce a DR either by activation of the HPC response such as that provided by partial hepatectomy combined with mitotic inhibition of hepatocytes, or via direct biliary injury such as bile duct ligation or DDC diet. However, a DR is commonly found in association with human MASLD and is known to correlate with disease severity as determined by fibrosis. Therefore, the ability of murine MASLD models to induce a DR is an important factor in the ability to study the DR *in vivo*. Whilst biliary models have shown evidence of interaction between and activation of HSC by nearby DR cells, the degree to which this occurs in MASLD is not known. Given the positive correlation of DR and fibrosis in human MASLD, the DR/HSC axis could be of importance in disease progression.

3.1.2 Aims

1. To compare the MCD and CDAA dietary murine models of NASH in terms of weight change, steatosis and inflammation

2. To compare the models for DR generation, HSC activation and fibrosis at early and late timepoints

3. To isolate biliary/DR cells from injured and uninjured mice and compare gene expression of known HSC activating markers Pdgfβ and Ctgf

3.1.3 Results

Keratin-19 *tomato* mice on a C57Bl/6 background were used for all experiments. Six were given *ad libitum* access to MCD diet: three were culled at day 13 (early timepoint) and three were culled at day 26 (late timepoint). Eight mice were given *ad libitum* access to CDAA diet: four were culled at 3 weeks (early timepoint) and four were culled at 6 weeks (late timepoint). Four mice served as controls and were given standard chow. Mice were weighed immediately before culling.

Both the MCD and CDAA model caused significant weight loss in comparison to the control animals. The combined MCD and CDAA cohorts were also statistically different from each other (*** p=0.0007, comparison not shown on Figure).

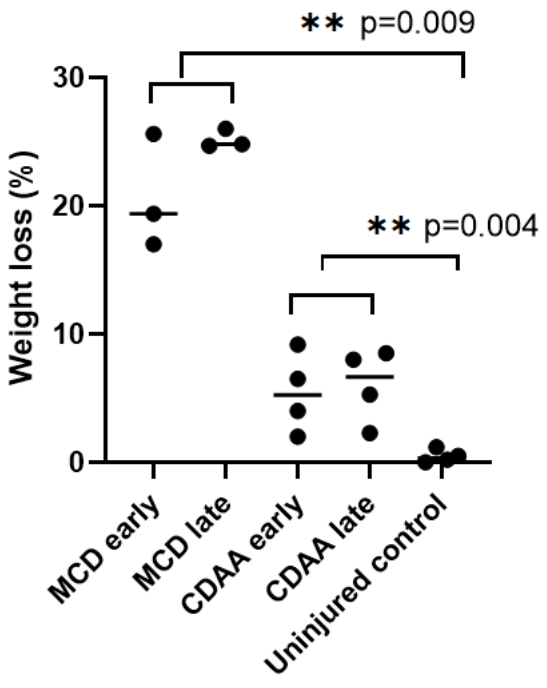

Figure 9: Quantification of weight loss in the CDAA and MCD model of fatty liver disease compared to healthy controls

Mice were weighed shortly before culling at the early timepoint (MCD day 13 (N=3), CDAA week 3 (N=4)), late timepoint (MCD day 26 (N=3), CDAA week 6 (N=4)) or at week 6 for the control animals (N=4). The percentage weight loss for each cohort is shown as individual points with a median bar. Median weight loss was 19.4% (range 17.0% - 25.6%) in the MCD late timepoint mice compared to controls and 6.7% (range 2.3% - 8.5%) in the CDAA late timepoint mice compared to controls. MCD and CDAA animals were grouped (combining early and late timepoints for each model) to permit statistical comparison with the control group using a Mann-Whitney-U test.

To confirm the development of steatosis in the MASLD injury models, H&E staining was carried out on liver tissue from MCD, CDAA and uninjured mice. The presence of severe macrovesicular steatosis is clearly shown in the injured animals, with no evident steatosis in the uninjured animals.

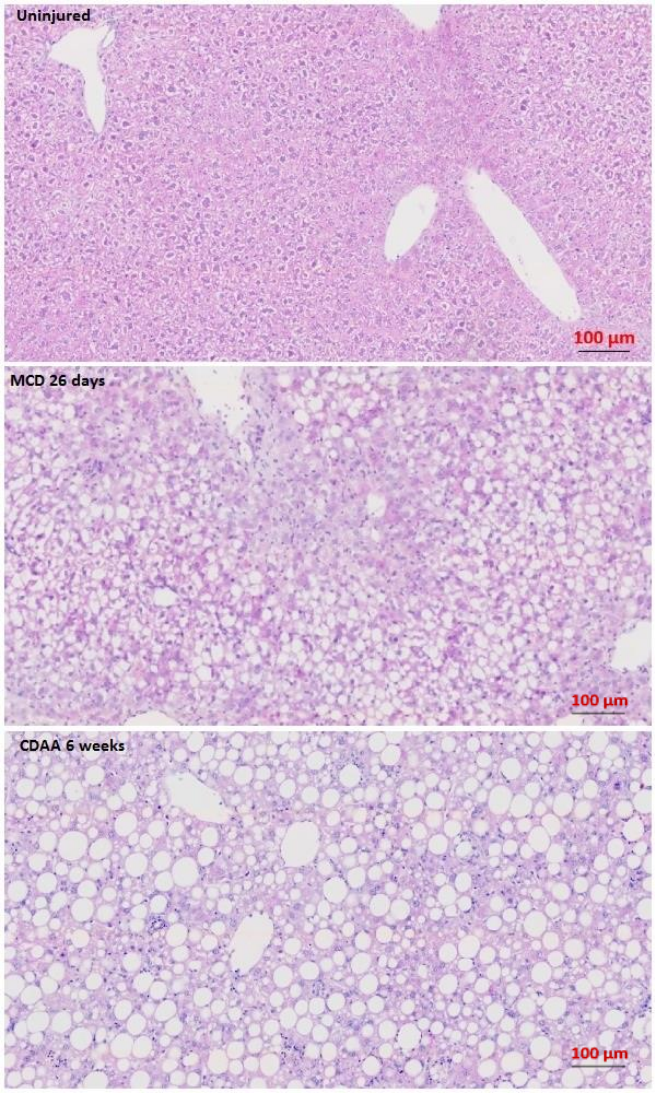

Figure 10: H&E staining on representative liver sections from late timepoint MCD, late timepoint CDAA and uninjured mice

H&E staining was carried out as per manufacturer's instructions. The Figure shows representative sections from uninjured, late timepoint MCD and late timepoint CDAA mice.

To evaluate the presence of steatohepatitis in the MASLD injury models, one H&E section per animal was given to a Histopathologist who was blinded to the animal's treatment group. The Histopathologist evaluated the NAS score for each animal. The data show that steatohepatitis (as evidenced by increased NAS score) is apparent by the early timepoint of both the MCD and CDAA models.

Case no	**S**	**LI**	**B**	**Total**
MCD early 1	3	2	1	6
MCD early 2	3	3	2	8
MCD early 3	3	2	1	6
MCD late 1	3	2	2	7
MCD late 2	3	3	2	8
MCD late 3	3	2	2	7
CDAA early 1	3	2	2	7
CDAA early 2	3	3	2	8
CDAA early 3	3	3	2	8
CDAA early 4	3	2	2	7
CDAA late 1	3	2	0	5
CDAA late 2	3	2	1	6
CDAA late 3	3	3	1	7

CDAA late 4	3	3	0	6
Uninjured 1	0	1	0	1
Uninjured 2	0	0	0	0
Uninjured 3	0	0	0	0

Table 4: total NAS score for injured MCD and CDAA mice in comparison to uninjured controls
The total NAS score is provided alongside the breakdown for steatosis (S), liver inflammation (LI) and ballooning (B).

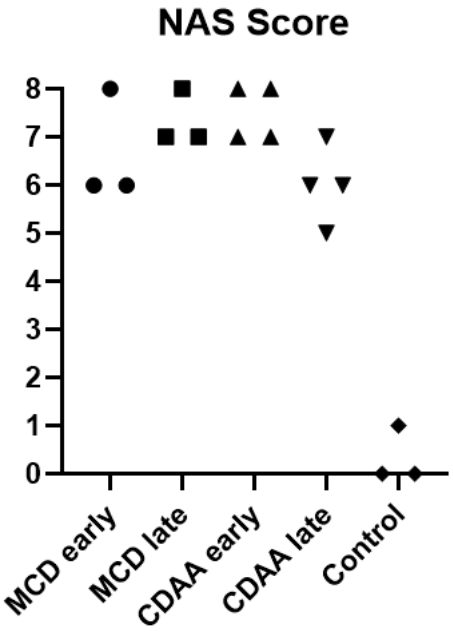

Figure 11: comparison of the NAS score for MCD and CDAA mice, at early and late timepoints, in comparison to uninjured controls
Following review of representative liver sections from MCD, CDAA and uninjured mice by an independent and blinded Histopathologist, NAS scores were obtained which are presented as individual values. Early and late timepoints are shown from MCD (early (N=3) late (N=3)) and CDAA (early (N=4) late (N=4)) animals, in addition to controls (N=3).

To evaluate for the presence of a DR in the MASLD injury models, IHC staining was performed on liver sections from MCD, CDAA and uninjured mice using a pan-cytokeratin primary antibody. The

staining shows evolution of a mild DR by the late timepoint of the MCD and CDAA model. In contrast, in uninjured mice the staining highlights normal bile ducts.

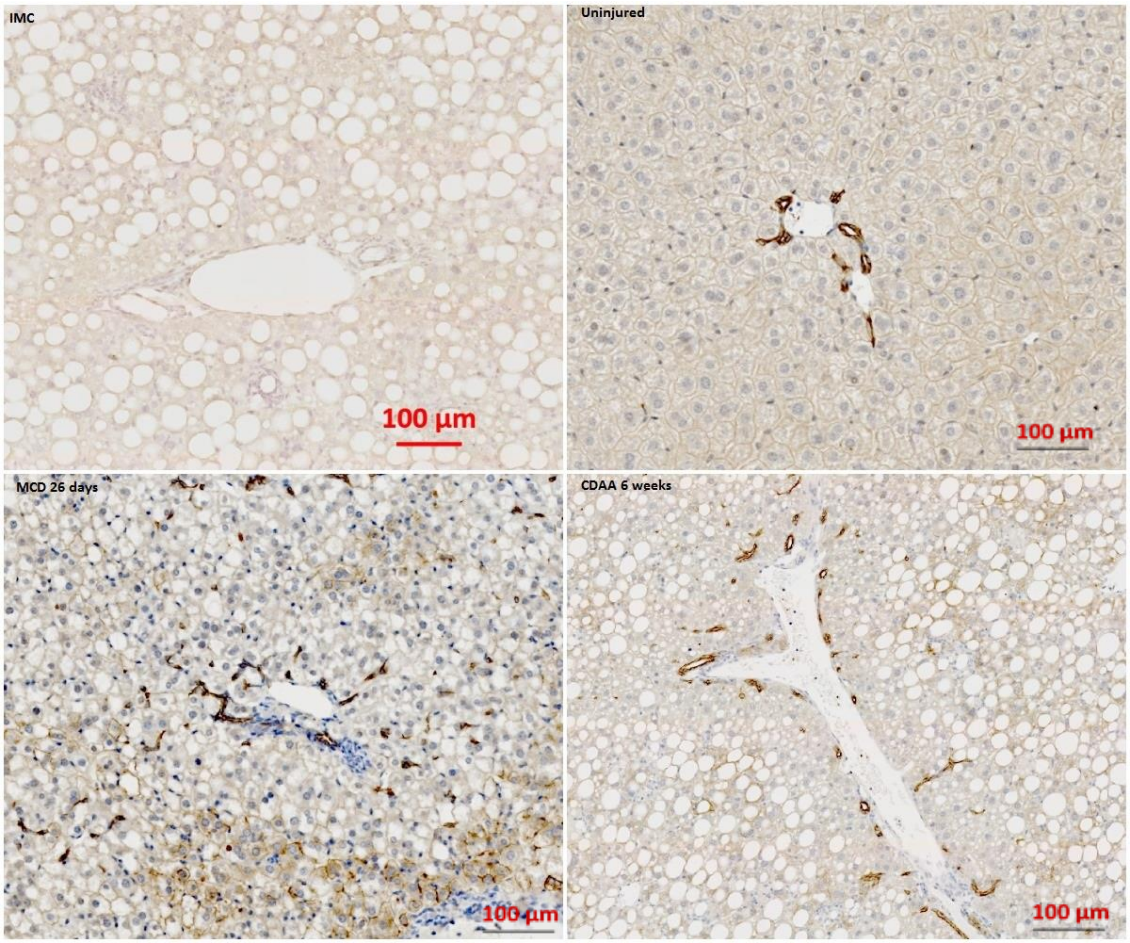

Figure 12: DR staining in MCD, CDAA and uninjured mice
IHC staining for the DR was performed using a pan-cytokeratin primary antibody (1:200) with a peroxidase-conjugated secondary antibody and DAB visualisation. Representative sections are shown from late timepoint MCD, late timepoint CDAA and uninjured mice. Representative image of IMC provided as a negative control.

DR staining was also undertaken at the early timepoint in the MCD and CDAA model, to demonstrate the evolution of the DR throughout the model. The staining shows that a DR is only mild in both the MCD and CDAA model, and is more evident in both models at the late timepoint compared to the early timepoint

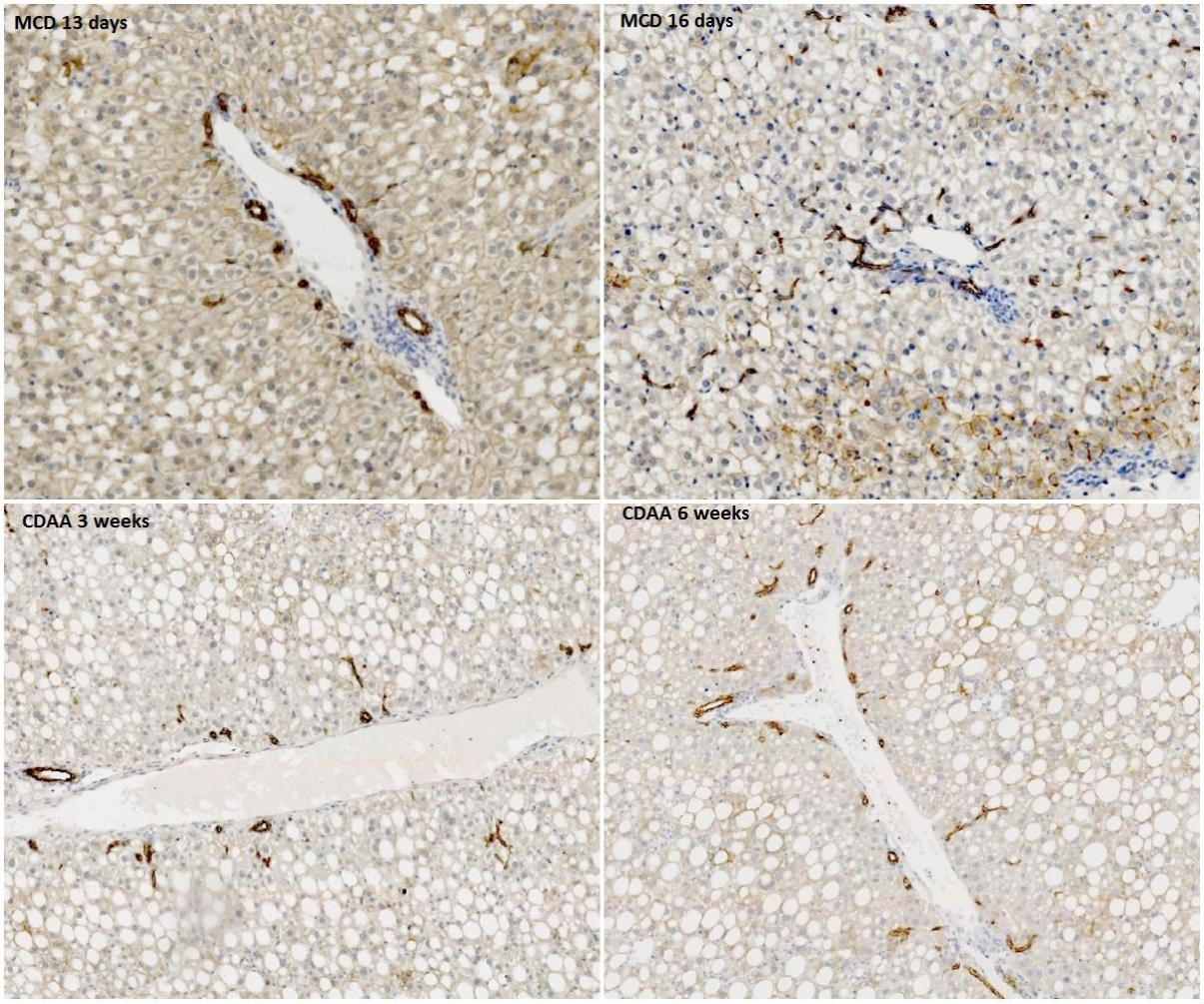

Figure 13: DR staining at the early and late timepoints of the MCD and CDAA model
IHC staining for the DR was performed using a pan-cytokeratin primary antibody (1:200) with a peroxidase-conjugated secondary antibody and DAB visualisation. Representative sections are shown from MCD and CDAA mice (early and late timepoints).

Quantification of DR staining was undertaken using the ImageJ software, as described earlier. The MCD and CDAA model both led to increased DR staining in comparison to control mice. There was

no difference in staining between the grouped MCD and CDAA animals (p=ns, comparison not shown on Figure).

This quantified staining shows that a DR is apparent by the early timepoint of both MCD and CDAA models, and does not appear to develop progressively between the early and late timepoints, as assessed by this method.

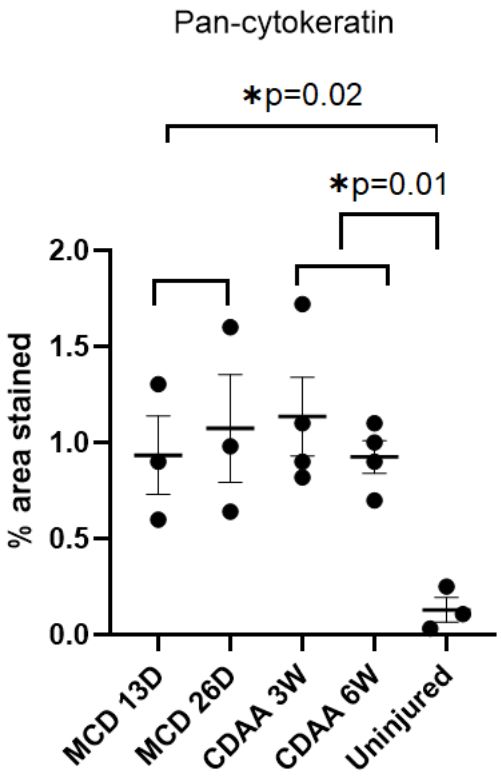

Figure 14: quantification of DR staining using pan-cytokeratin IHC in the MCD and CDAA models in comparison to uninjured controls
Using the ImageJ software, the percentage area stained was calculated for six random fields of view per slide per animal maintaining the same staining intensity threshold across the groups. The median value was plotted for each animal per group and each group is shown with median bar and IQR. Groups shown are MCD early timepoint (N=3), MCD late timepoint (N=3), CDAA early timepoint (N=4), CDAA late timepoint (N=4) and uninjured controls (N=3). Early and late timepoints for the MCD and CDAA animals were grouped to enable statistical comparison of the quantified staining using a Mann-Whitney-U test.

To evaluate the presence of fibrosis in the MASLD injury models, staining was undertaken using a Picrosirius red kit. The staining shows the development of mild fibrosis in the CDAA late timepoint mice, with barely discernible fibrosis in the late timepoint MCD mice. In uninjured mice, collagen fibres are visualised purely within the central vein.

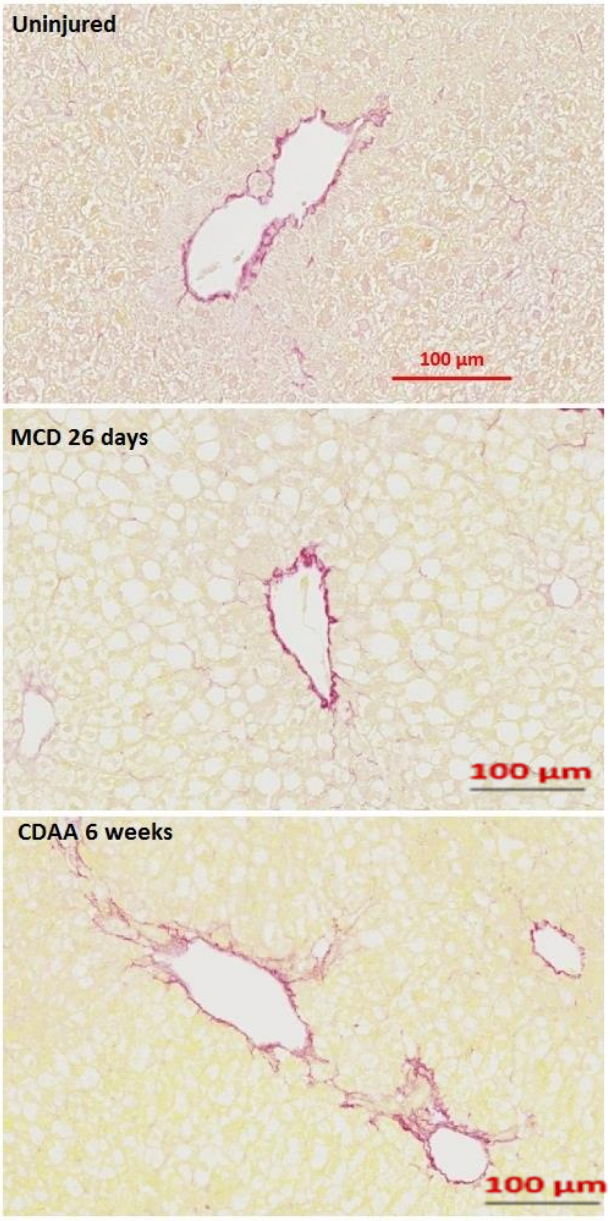

Figure 15: fibrosis staining in MCD, CDAA and uninjured mice
Fibrosis staining was performed using a *Picrosirius red* kit, as per manufacturer's instructions. Representative sections are shown from late timepoint MCD, late timepoint CDAA and uninjured mice.

Fibrosis staining was also undertaken at the early timepoint in the MCD and CDAA model, to demonstrate the evolution of fibrosis during the model. The staining shows that there is progressive mild fibrosis throughout the CDAA model, with barely discernible fibrosis in the MCD mice.

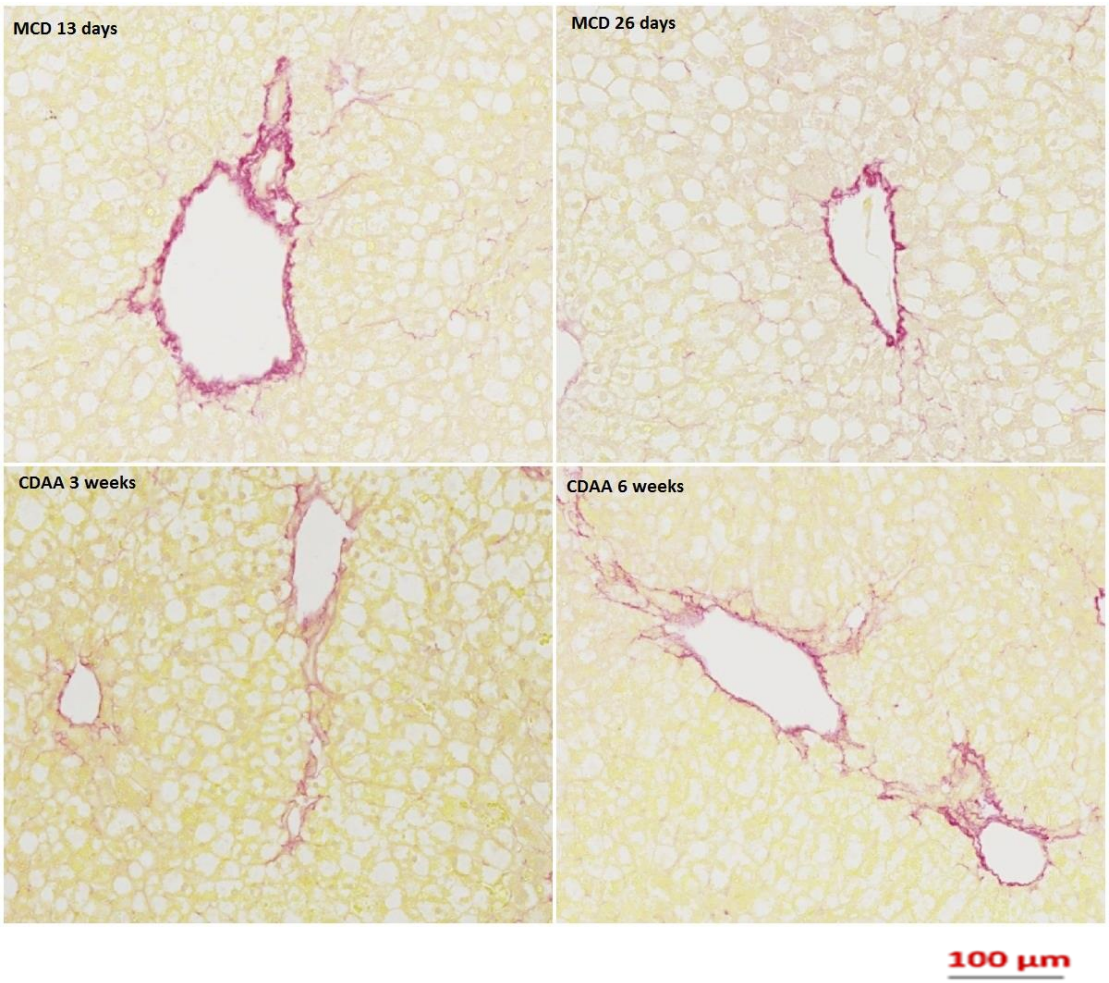

Figure 16: fibrosis staining at the early and late timepoints of the MCD and CDAA model
Fibrosis staining was performed using a *Picrosirius red* kit, as per manufacturer's instructions. Representative sections are shown from MCD and CDAA mice (early and late timepoints).

Quantification of fibrosis staining was undertaken using the *ImageJ* software, as described earlier. The MCD and CDAA model both led to increased fibrosis staining in comparison to control mice. There was no difference in fibrosis staining between the grouped MCD and CDAA animals (p=ns, comparison not shown on Figure).

This quantified staining shows that fibrosis is apparent by the early timepoint of both the MCD and CDAA models. Progressive fibrosis then appears to develop by the late timepoint of the CDAA model, occurring to a much lesser degree in the MCD model.

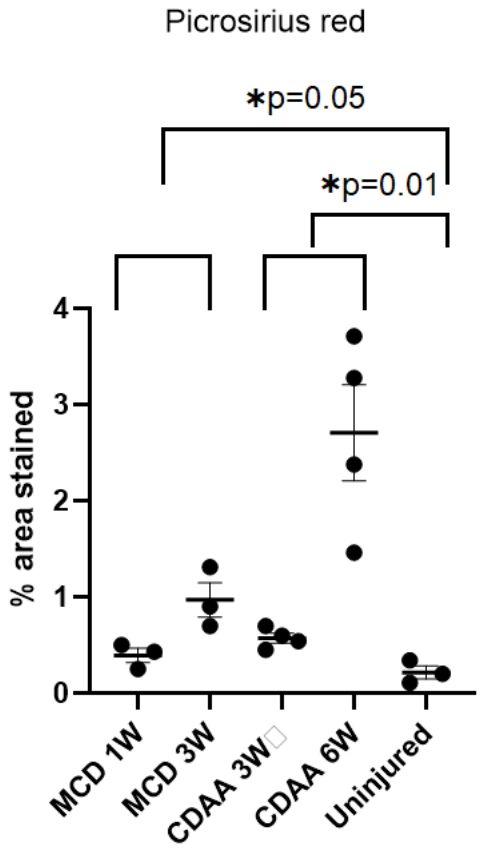

Figure 17: quantification of fibrosis staining using *Picrosirius red* in the MCD and CDAA models in comparison to uninjured controls

Using the ImageJ software, the percentage area stained was calculated for six random fields of view per slide per animal maintaining the same staining intensity threshold across the groups. The median value was plotted for each animal per group and each group is shown with median bar and IQR. Groups shown are MCD early timepoint (N=3), MCD late timepoint (N=3), CDAA early timepoint (N=4), CDAA late timepoint (N=4) and uninjured controls (N=3). Early and late timepoints for the MCD and CDAA animals were grouped to enable statistical comparison of the quantified staining using a Mann-Whitney-U test.

A liver digest protocol was carried out as described earlier, using liver tissue from late timepoint MCD, early timepoint CDAA and uninjured mice. The resulting cell suspension was analysed using FACS with the EpCAM+ gating strategy described above and the target cells were directly sorted. The FACS plot below is representative from an injured early timepoint CDAA mouse.

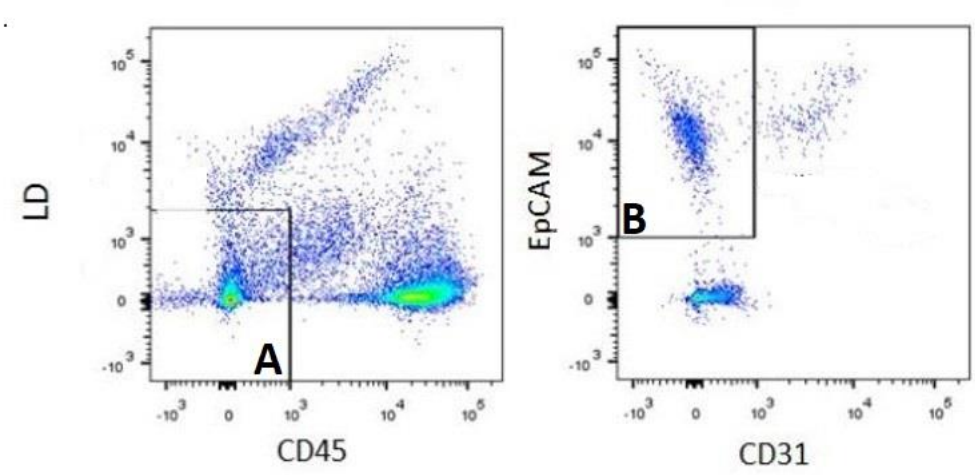

Figure 18: gating strategy for the sorting of biliary/DR cells from MCD, CDAA and uninjured mice following liver digest
Following liver digest and staining using FACS antibodies, the EpCAM+ gating strategy sorted cells directly into ice-cold PBS which were spun down using a centrifuge. The pellet was then re-suspended in RLT buffer and used for downstream qPCR experiments. At least 25,000 cells were isolated per mouse (range 27,000 – 110,000).
Box A shows the live/CD45 negative fraction – these cells were then gated with CD31 (negative) and EpCAM (positive) to identify the target population for sorting in Box B. Fluorescence thresholds for gating were determined using the unstained control. LD = live/dead stain.

The biliary/DR cells isolated from early timepoint CDAA, late timepoint MCD and uninjured livers underwent RNA extraction and reverse transcription, as described earlier. qPCR was used to determine the gene expression of two known HSC activating ligands, Pdgfβ and Ctgf.

Upregulation of Ctgf gene expression occurs in biliary/DR cells isolated from late timepoint MCD livers, in comparison to uninjured controls. There was no difference in the gene expression of Pdgfβ.

By contrast, upregulation of Pdgfβ gene expression occurs in biliary/DR cells isolated from early timepoint CDAA livers, in comparison to uninjured controls. There was no difference in the gene expression of Ctgf.

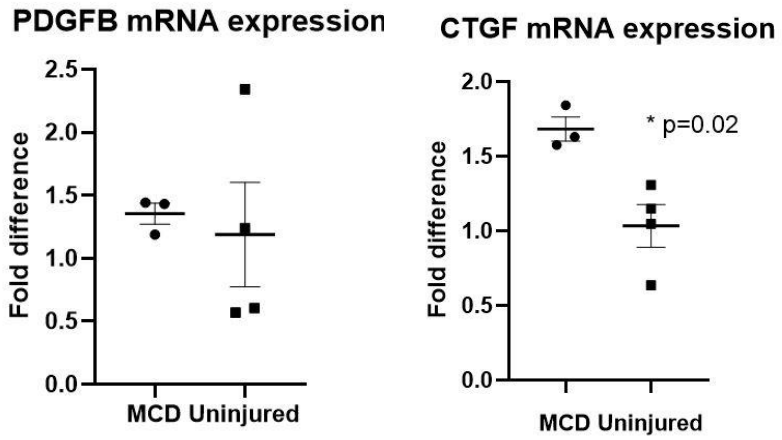

Figure 19: gene expression of Pdgfβ and Ctgf in biliary/DR cells sorted from late timepoint MCD livers in comparison to uninjured controls

The EpCAM+ gating strategy was used to directly sort biliary/DR cells from late timepoint MCD (N=3) and uninjured control (N=4) liver tissue. Following RNA extraction and reverse transcription, qPCR was used to quantify the gene expression of Pdgfβ and Ctgf. Samples were run in triplicate with the gene of interest and a housekeeping gene (Gapdh). The average Ct value was taken for each triplicate and ΔCt calculated for the gene of interest vs the housekeeping gene. ΔΔCt was then calculated using the mean ΔCt value for the control group. $2^{-\Delta\Delta Ct}$ generated the expression fold difference which is plotted above for each sample per group with median bar and IQR. A Mann-Whitney-U test was used to compare the groups.

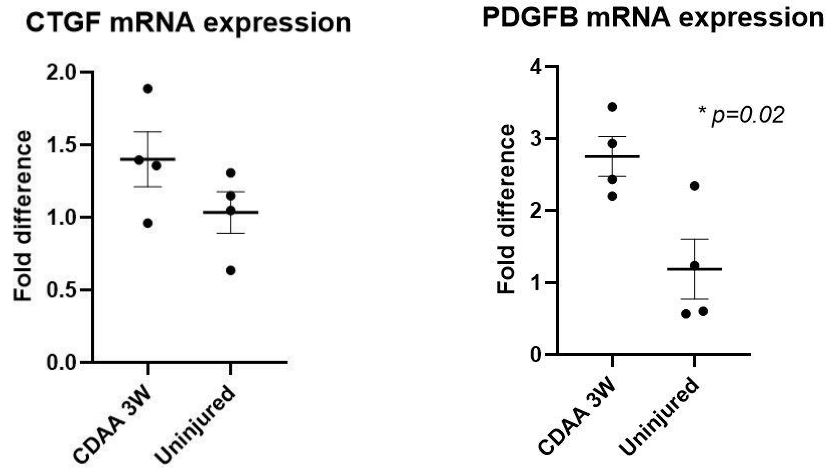

Figure 20: gene expression of Pdgfβ and Ctgf in biliary/DR cells sorted from early timepoint CDAA livers in comparison to uninjured controls

The EpCAM+ gating strategy was used to directly sort biliary/DR cells from early timepoint* CDAA (N=4) and uninjured control (N=4) liver tissue. Following RNA extraction and reverse transcription, qPCR was used to quantify the gene expression of Pdgfβ and Ctgf. Samples were run in triplicate with the gene of interest and a housekeeping gene (Gapdh). The average Ct value was taken for each triplicate and ΔCt calculated for the gene of interest vs the housekeeping gene. ΔΔCt was then calculated using the mean ΔCt value for the control group. $2^{\wedge -\Delta\Delta Ct}$ generated the expression fold difference which is plotted above. A Mann-Whitney-U test was used to compare the groups.
*It was not possible to sort DR cells from late timepoint CDAA livers due to restrictions as a result of the Covid pandemic

Following identification of PDGFβ as a target of interest in potential DR/HSC interaction, IHC staining for its receptor PDGFRβ was performed on liver sections from MCD, CDAA and uninjured mice using a polyclonal primary antibody. The staining shows pronounced PDGFRβ expression throughout the lobule in MCD and CDAA mice. By contrast, in uninjured control mice the staining primarily demonstrates vessels.

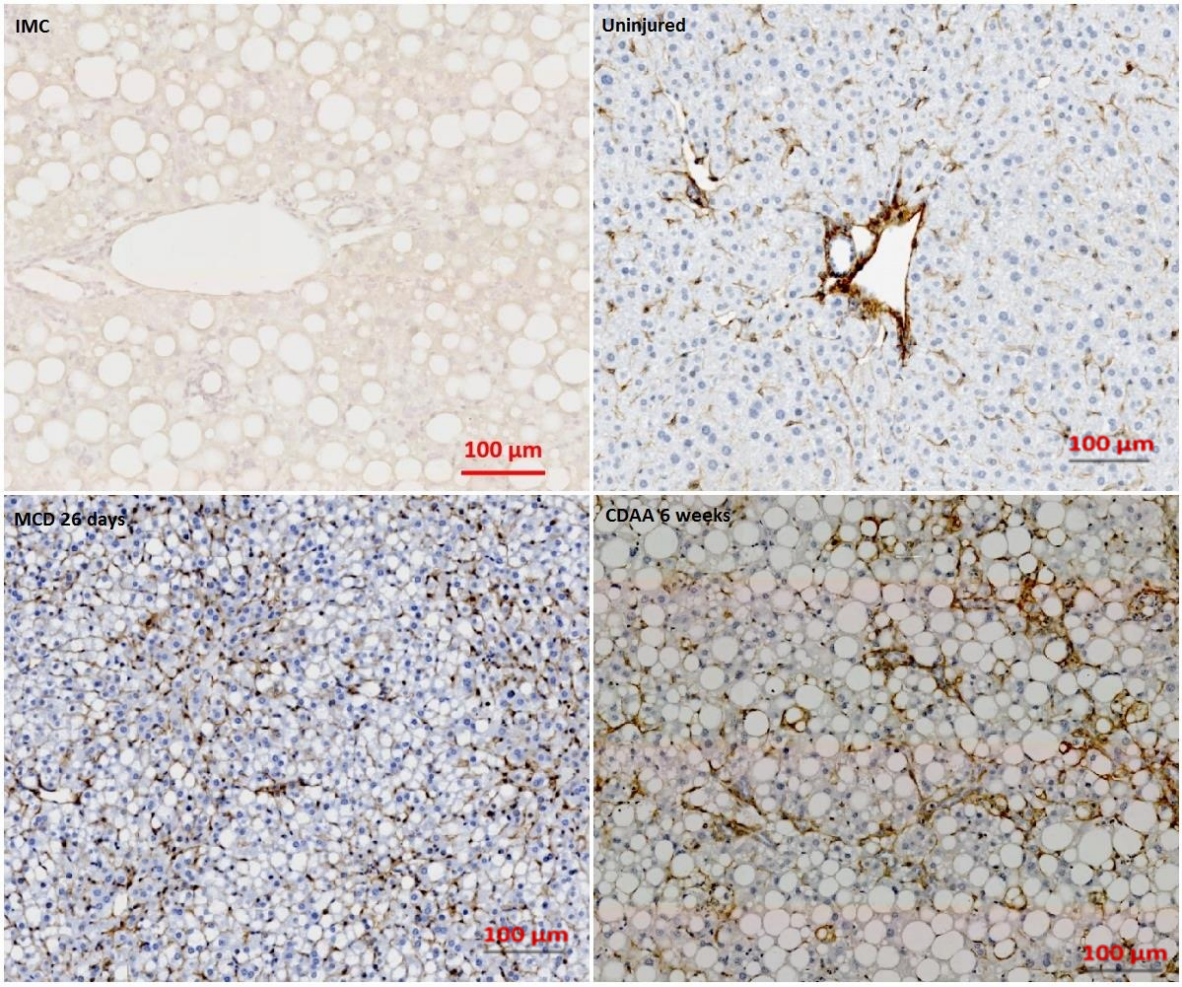

Figure 21: PDGFRβ staining in MCD, CDAA and uninjured mice
IHC staining for PDGFRβ was performed using a polyclonal primary antibody (1:200) with a peroxidase-conjugated secondary antibody and DAB visualisation. Representative sections are shown from late timepoint MCD, late timepoint CDAA and uninjured mice. Representative image of IMC provided as a negative control.

Quantification of PDGFRβ staining was undertaken using the ImageJ software, as described earlier. The MCD and CDAA model both led to increased PDGFRβ staining in comparison to control mice. There was no difference in staining between the grouped MCD and CDAA animals (p=ns, comparison not shown on Figure).

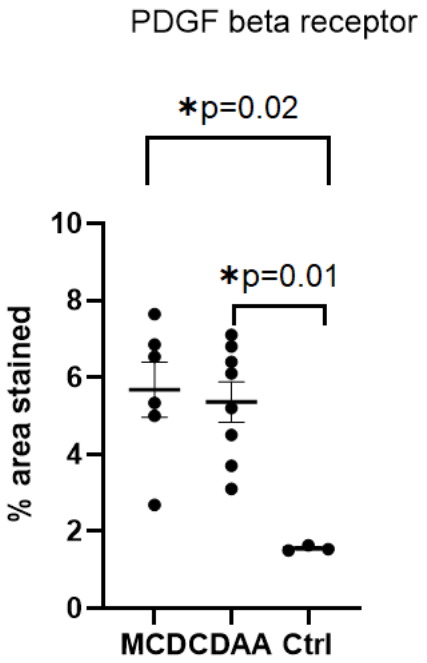

Figure 22: quantification of PDGFRβ staining using IHC in the MCD and CDAA models in comparison to uninjured controls

Using the *ImageJ* software, the percentage area stained was calculated for six random fields of view per slide per animal maintaining the same staining intensity threshold across the groups. The median value was plotted for each animal per group and each group is shown with mean bar and SEM. Groups shown are combined MCD early and late timepoints (N=6), combined CDAA early and late timepoints (N=8) and uninjured controls (N=3). Statistical comparison was performed using a Mann-Whitney-U test.

Following identification of PDGFβ as a target of interest in potential DR/HSC interaction using FACS and qPCR, and having shown that PDGFRβ is expressed more avidly in murine NASH models using IHC, dual immunofluorescent staining was undertaken to show co-localisation between DR cells and PDGFRβ+ cells, the latter known to include activated HSC and fibroblasts.

CK19 is seen highlighting bile ducts in normal portal tracts in the uninjured liver, with PDGFRβ staining confined mostly to portal tracts and central veins. By contrast, in the MCD liver, CK19

staining shows a mild DR and PDGFRβ staining is increased. The white arrows show example areas of co-localisation between DR and PDGRβ+ cells.

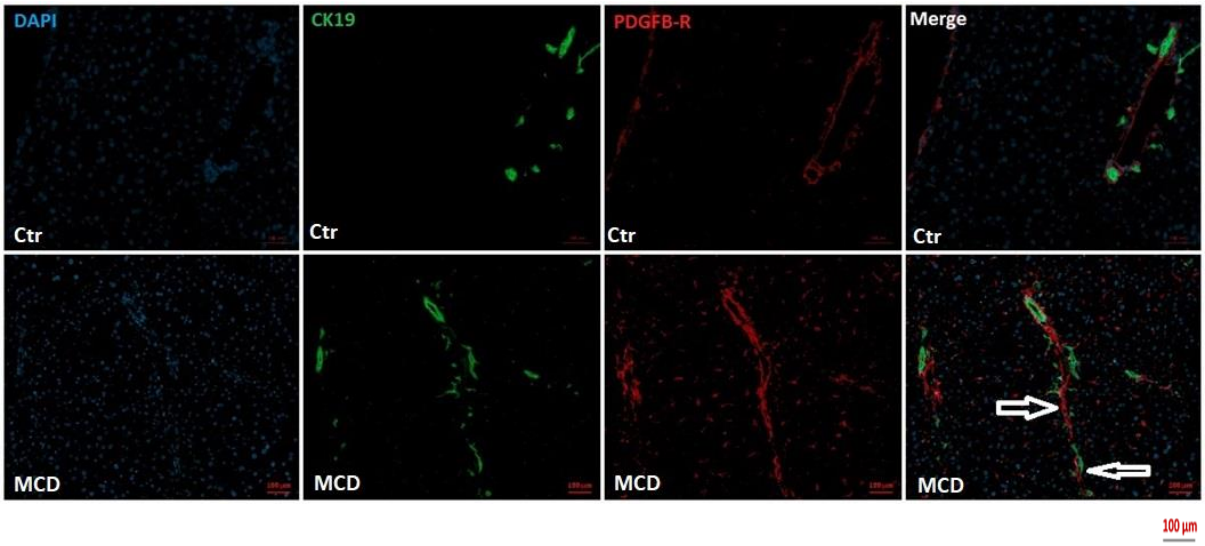

Figure 23: dual immunofluorescent staining for the DR and PDGFRβ in late timepoint MCD livers versus uninjured controls
Representative sections are shown in the panel above for late timepoint MCD livers and uninjured controls. Dual immunofluorescent staining was undertaken using primary antibodies for CK19 (1:200) and PDGFRβ (1:200) with different fluorescent-conjugated secondary antibodies (CK19 = green, PDGFRβ = red). Nuclear staining was undertaken with DAPI (purple).

3.2 Characterisation of human MASLD with regard to DR, HSC activation and fibrosis

3.2.1 Introduction

It is known that a DR often accompanies NASH in human disease, and that the magnitude of the DR often correlates with the degree of fibrosis. Following on from the murine work, showing that MASLD models do induce a DR but only very mild fibrosis, it was decided to investigate the presence/absence of a DR across the spectrum of human MASLD, encompassing different degrees of fibrosis. Access to tissue from the liver transplant program allowed a range of disease stages to

be studied: non-fatty livers with no fibrosis (such as that provided by “discarded” donor livers), donor livers with steatosis and end-stage explants with NASH cirrhosis. In addition, approval was given to access liver biopsies from patients with NASH and advanced (F3, bridging) fibrosis, representing a clinically important stage of the disease where both progression and improvement are possible.

The presence of NASH is associated with hepatocyte injury (ballooning) and inflammation, both of which drive cytokine release and the release of HSC activating factors, causing a phenotypic switch in HSC to a fibrogenic form. Thus, it was decided to investigate HSC activation in the different stages of NASH, including potential interactions with DR cells.

3.2.2 Aims

1. Compare DR, fibrosis and HSC activation across the spectrum of human MASLD

2. Assess the gene expression of PDGFβ and CTGF, found to be of potential importance in DR cells in murine NASH, at a whole-liver level

3. Assess for co-localisation of activated HSC and DR cells in human NASH

3.2.3 Results

FFPE slides of liver tissue were prepared from human livers as described earlier. In the case of NASH with fibrosis, these were liver biopsy specimens received from the BioBank in the form of FFPE slides. IHC staining for the DR was performed using a pan-cytokeratin primary antibody.

The staining shows that a DR – with progression of pan-cytokeratin+ cells away from the portal tracts and into the lobule - is seen modestly in the NASH with fibrosis liver and robustly in the

NASH cirrhosis liver. In normal and fatty donor, ductules are predominantly confined to the portal tracts.

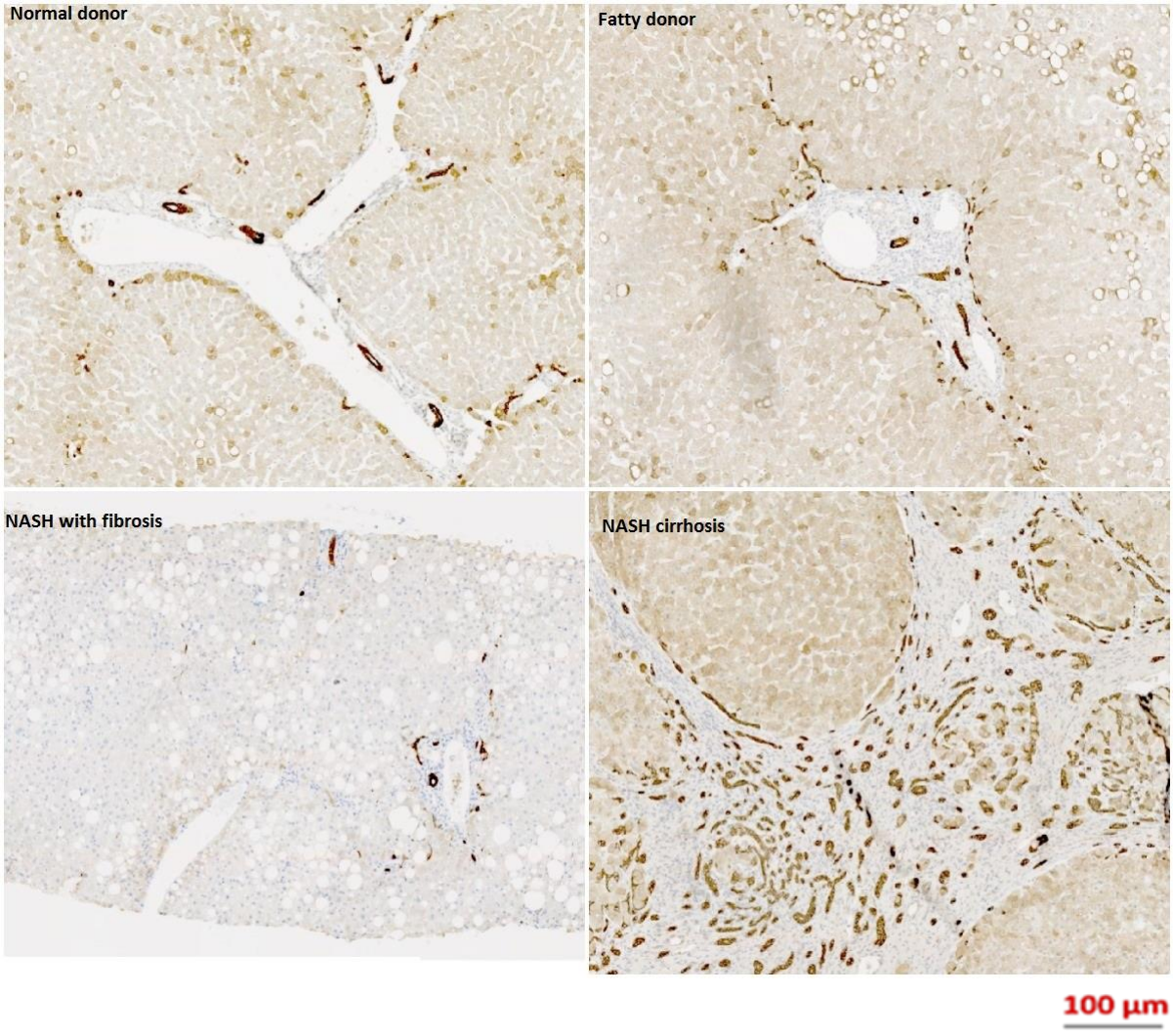

Figure 24: DR staining in normal donor, fatty donor, NASH with fibrosis and NASH cirrhosis human livers
IHC staining for the DR was performed using a pan-cytokeratin primary antibody (1:200) with a peroxidase-conjugated secondary antibody and DAB visualisation. Representative sections are shown from normal donor, fatty donor, NASH with fibrosis and end-stage NASH cirrhosis tissue

Quantification of DR staining was undertaken using the ImageJ software, as described earlier. It is confirmed quantitatively that a robust DR is present in NASH cirrhosis livers in comparison to

normal donors. The comparison between NASH with fibrosis and normal donor did not reach statistical significance (p=ns, comparison not shown on Figure), although qualitatively a mild DR is present in this group.

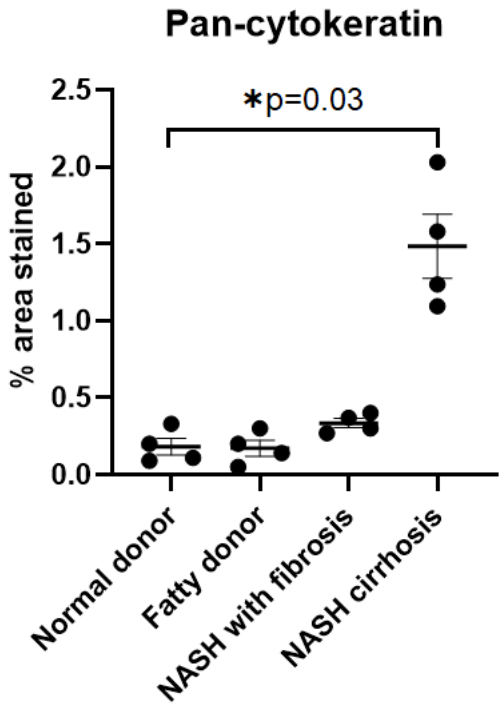

Figure 25: quantification of DR using pan-cytokeratin staining in different stages of human MASLD
Using the ImageJ software, the percentage area stained was calculated for six random fields of view per slide per patient, maintaining the same staining intensity threshold across the groups. The median value was plotted for each patient per group and each group is shown with median bar and IQR. Groups shown are normal donor (N=4), fatty donor (N=4), NASH with fibrosis (N=4) and NASH cirrhosis (N=4). Statistical comparison was performed using a Mann-Whitney-U test.

To confirm that my staining protocol for fibrosis confirmed expected results, staining was performed using a *Picrosirius red* kit on normal donor, fatty donor, NASH with fibrosis and NASH cirrhosis livers.

The staining shows no detectable fibrosis in the normal and fatty donor tissue, with collagen fibres highlighted only around the central veins and portal tracts. In contrast, bridging fibrosis is readily evident in the NASH with fibrosis liver. In the cirrhotic liver, a thick scan is seen demarcating a nodule.

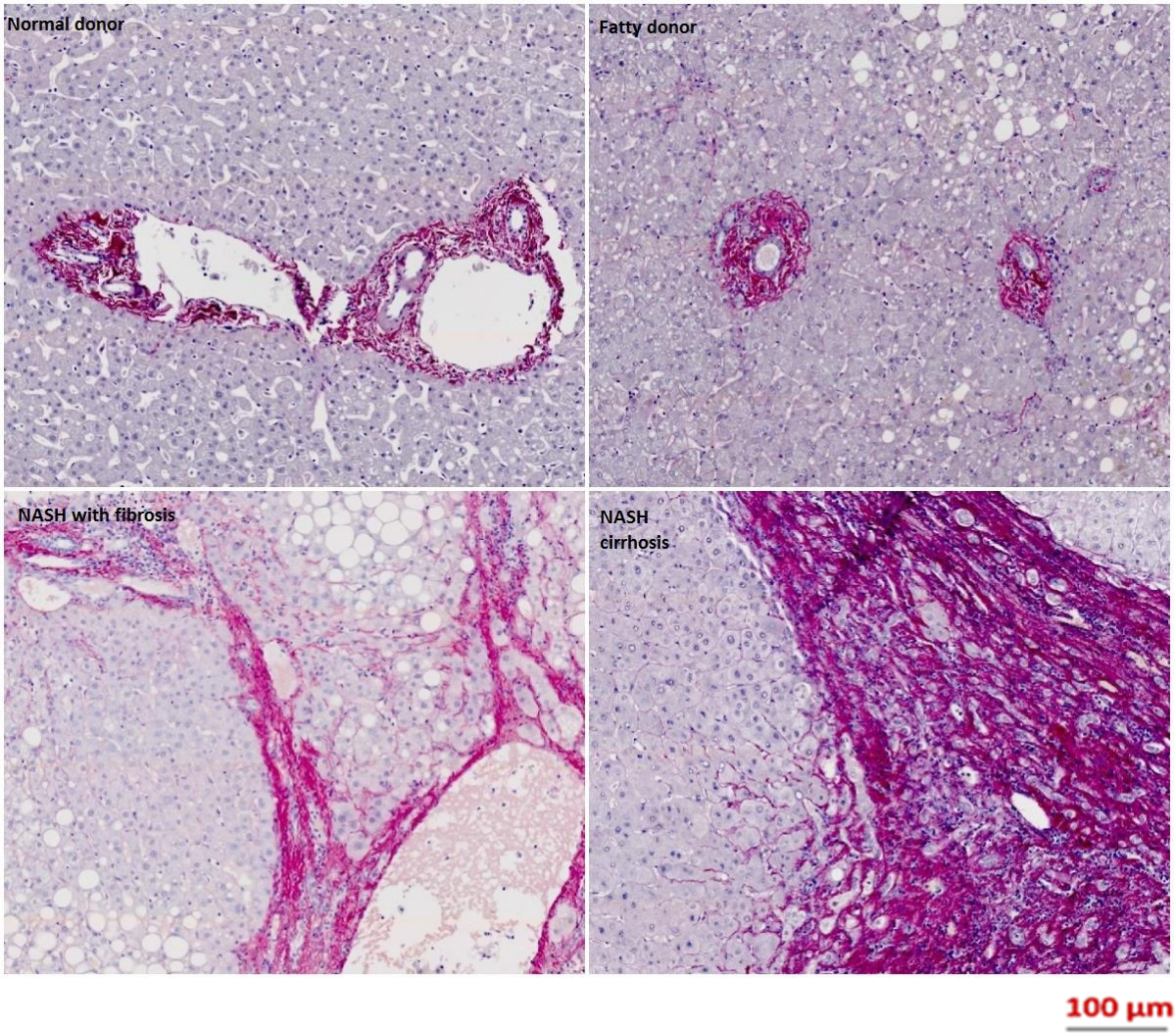

Figure 26: fibrosis staining in normal donor, fatty donor, NASH with fibrosis and NASH cirrhosis human livers
Fibrosis staining was performed using a *Picrosirius red* kit, according to manufacturer's instructions. Representative sections are shown from normal donor, fatty donor, NASH with fibrosis and end-stage NASH cirrhosis tissue.

Quantification of fibrosis was undertaken using the *ImageJ* software, as described earlier.

The staining, as expected, shows increased fibrosis in the NASH cirrhosis livers in comparison to normal donor livers. The comparison between NASH with fibrosis and normal donor did not reach statistical significance (p=ns, comparison not shown on Figure), despite bridging fibrosis being present in this group.

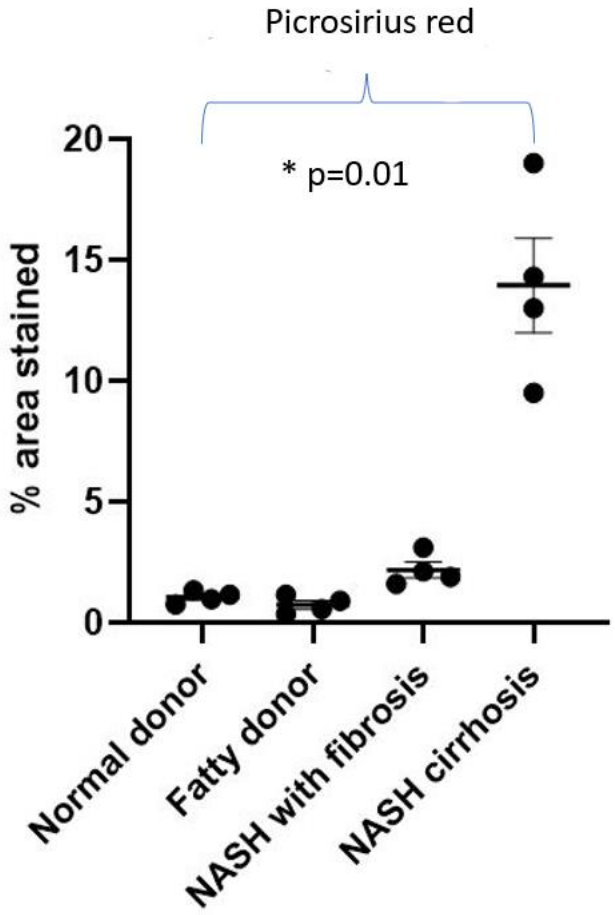

Figure 27: quantification of fibrosis using *Picrosirius red* staining in different stages of human MASLD
Using the *ImageJ* software, the percentage area stained was calculated for six random fields of view per slide per patient, maintaining the same staining intensity threshold across the groups. The median value was plotted for each patient per group and each group is shown with median bar and IQR. Groups shown are normal donor (N=4), fatty donor (N=4), NASH with fibrosis (N=4) and NASH cirrhosis (N=4). Statistical comparison was performed using a Mann-Whitney-U test.

To assess for the presence of activated HSC/fibroblasts, IHC staining was performed using an αSMA primary antibody on normal donor, fatty donor, NASH with fibrosis and NASH cirrhosis livers. The staining shows αSMA positivity only around the portal tracts and central veins in donor and fatty donor tissue, as expected. By contrast, in NASH with fibrosis and cirrhotic liver, αSMA staining is readily demonstrated mirroring the fibrotic bands/scar.

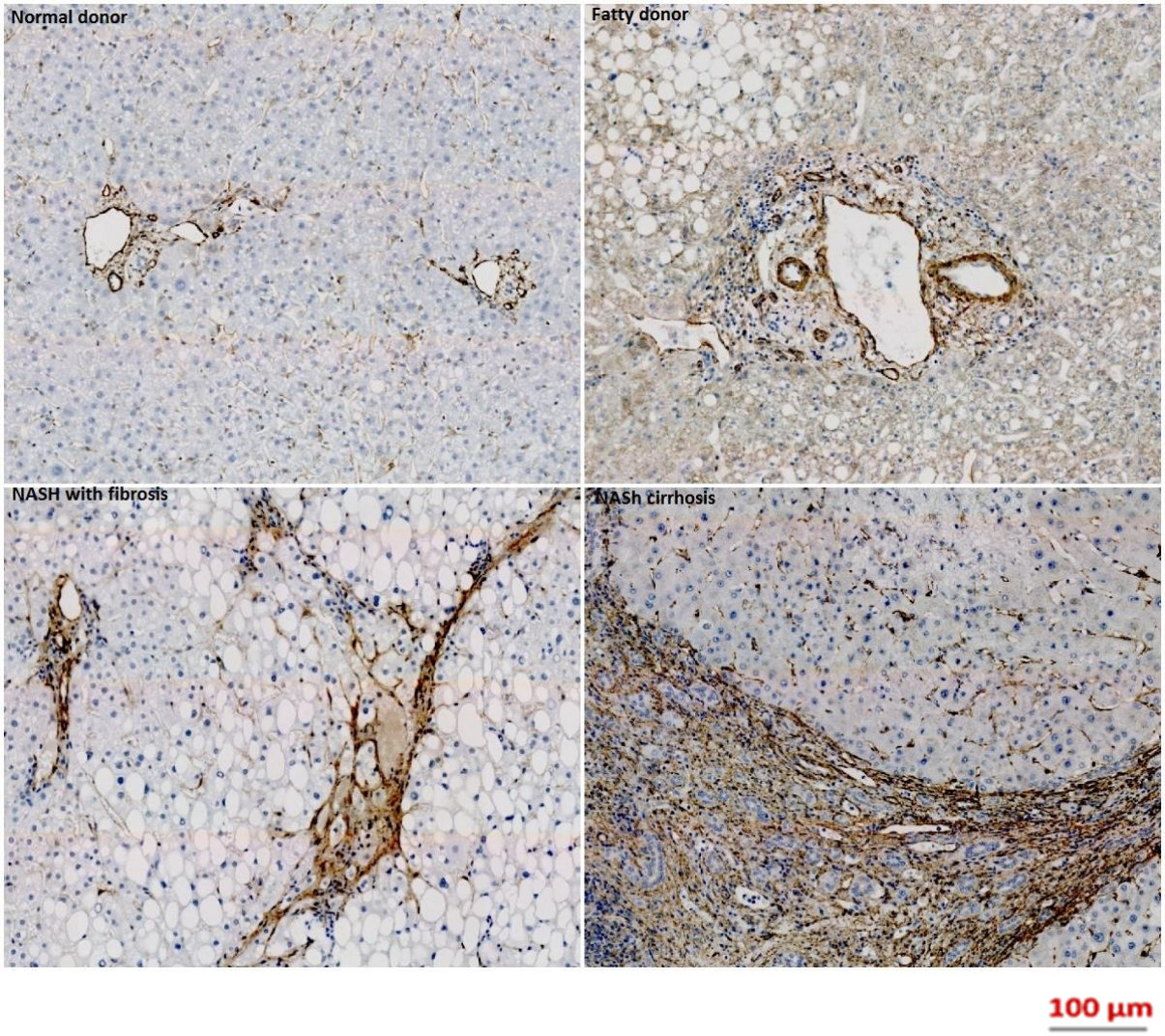

Figure 28: αSMA staining in normal donor, fatty donor, NASH with fibrosis and NASH cirrhosis human livers
IHC staining for αSMA was performed using a primary antibody (1:200) with a peroxidase-conjugated secondary antibody and DAB visualisation. Representative sections are shown from normal donor, fatty donor, NASH with fibrosis and end-stage NASH cirrhosis tissue.

Quantification of αSMA staining was undertaken using the ImageJ software, as described earlier. The staining confirms quantitatively increased αSMA expression in the NASH cirrhosis and NASH with fibrosis livers in comparison to normal donor livers.

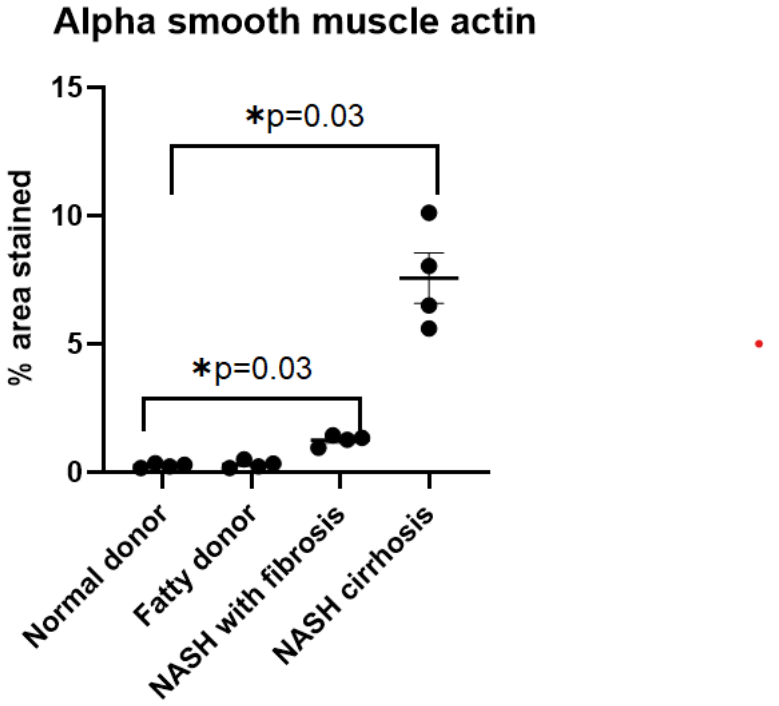

Figure 29: quantification of αSMA staining in different stages of human MASLD
Using the *ImageJ* software, the percentage area stained was calculated for six random fields of view per slide per patient, maintaining the same staining intensity threshold across the groups. The median value was plotted for each patient per group and each group is shown with median bar and IQR. Groups shown are normal donor (N=4), fatty donor (N=4), NASH with fibrosis (N=4) and NASH cirrhosis (N=4). Statistical comparison was performed using a Mann-Whitney-U test.

As PDGFβ, its receptor PDGFRβ, and CTGF were found to be of potential importance in DR/HSC interaction in murine models of NASH, whole liver gene expression of these markers in human livers (normal donor and NASH cirrhosis) was investigated using qPCR.

The qPCR data show increased gene expression of PDGFβ, CTGF and PDGFRβ in NASH cirrhosis compared to normal donor, at a whole-liver level.

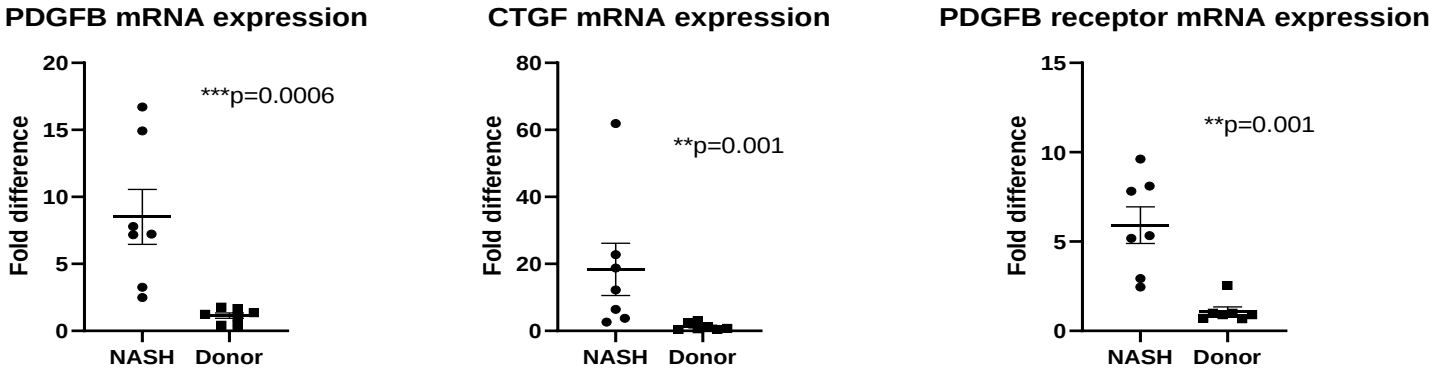

Figure 30: whole liver qPCR for PDGFβ, CTGF and PDGFRβ in NASH cirrhosis versus normal donor livers
An RNA extraction protocol from snap-frozen liver tissue was utilised, as described previously, using NASH cirrhosis (N=7) and normal donor (N=7) livers. Following reverse transcription, qPCR was used to quantify the gene expression of PDGFβ, CTGF and PDGFRβ. Samples were run in triplicate with the gene of interest and a housekeeping gene (GAPDH). The average Ct value was taken for each triplicate and ΔCt calculated for the gene of interest vs the housekeeping gene. ΔΔCt was then calculated using the mean ΔCt value for the control group. $2^{-\Delta\Delta Ct}$ generated the expression fold difference which is plotted above for each sample per group, with mean bar and SEM. A Mann-Whitney-U test was used to compare the groups.

To confirm the murine findings of increased PDGFRβ expression in fatty liver injury, IHC staining for PDGFRβ+ cells was performed using a monoclonal primary antibody in normal donor, fatty donor, NASH with fibrosis and NASH cirrhosis livers.

The staining shows that expression of PDGFRβ is confined to the central vein and portal tracts in normal and fatty donor liver tissue. By contrast, in NASH with fibrosis and NASH cirrhosis liver, marked expression is seen throughout the lobule.

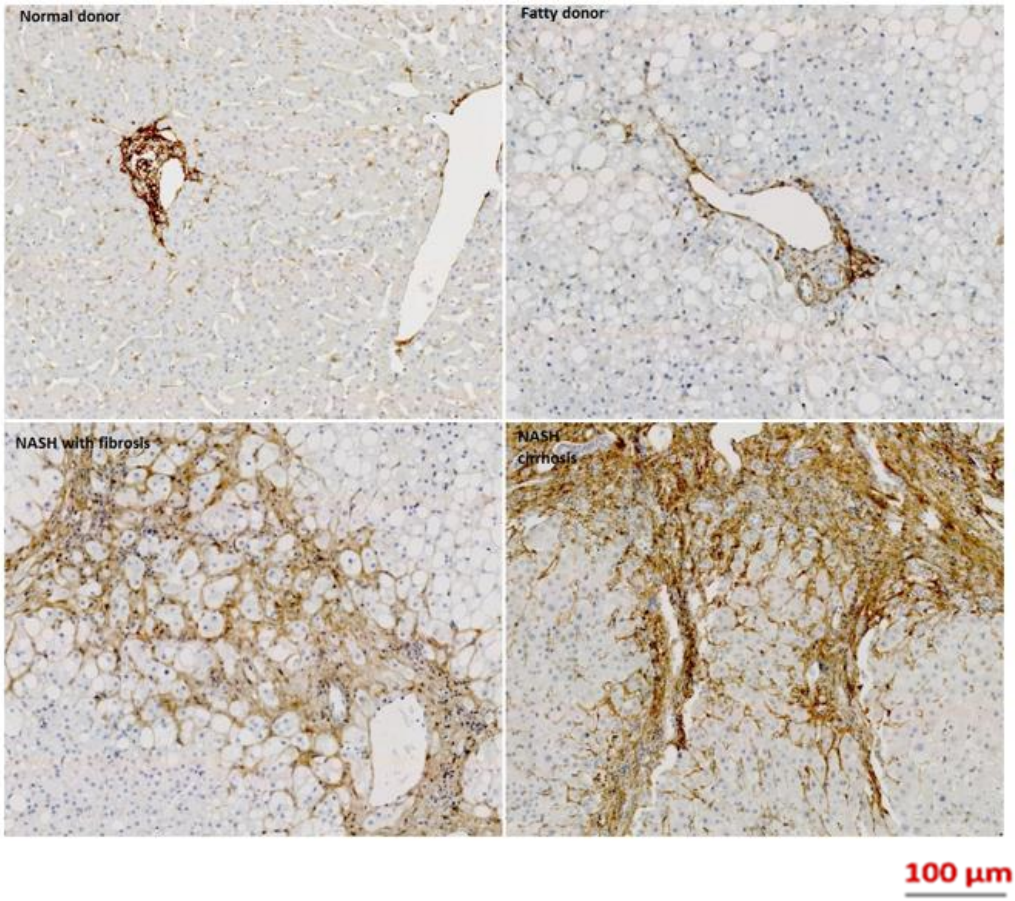

Figure 31: PDGFRβ staining in normal donor, fatty donor, NASH with fibrosis and NASH cirrhosis human livers
IHC staining for PDGFRβ was performed using a primary antibody (1:200) with a peroxidase-conjugated secondary antibody and DAB visualisation. Representative sections are shown from normal donor, fatty donor, NASH with fibrosis and end-stage NASH cirrhosis tissue

Quantification of PDGFRβ staining was undertaken using the ImageJ software, as described earlier. The staining confirms quantitatively increased PDGFRβ expression in the NASH cirrhosis and NASH with fibrosis livers in comparison to normal donor livers.

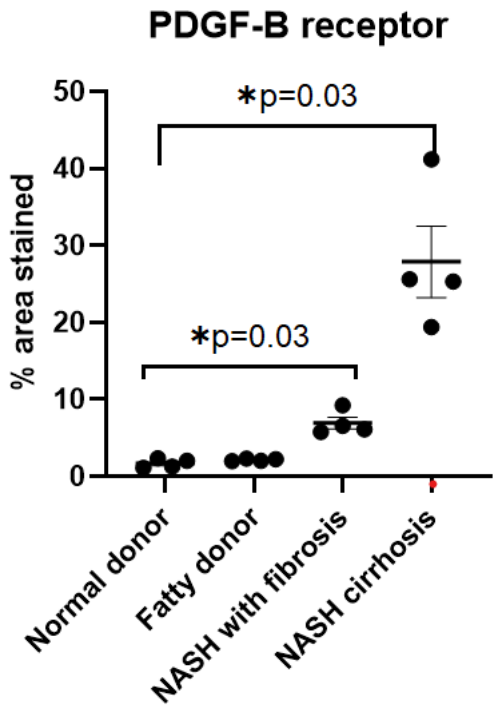

Figure 32: quantification of PDGFRβ staining in different stages of human MASLD
Using the *ImageJ* software, the percentage area stained was calculated for six random fields of view per slide per patient, maintaining the same staining intensity threshold across the groups. The median value was plotted for each patient per group and each group is shown with median bar and IQR. Groups shown are normal donor (N=4), fatty donor (N=4), NASH with fibrosis (N=4) and NASH cirrhosis (N=4). Statistical comparison was performed using a Mann-Whitney-U test.

To confirm the pattern seen in the murine MCD model, dual immunofluorescent staining was undertaken to assess for co-localisation between DR cells (expressing pan-cytokeratin) and αSMA+ cells (activated HSC/fibroblasts) in normal donor, NASH with fibrosis and NASH cirrhosis livers.

The upper panels show pan-cytokeratin and αSMA predominantly confined to portal tracts in donor livers. In NASH with fibrosis there are areas of proximity between pan-cytokeratin positive DR cells and αSMA positive cells (white arrows). In NASH cirrhosis there is a marked proliferation of ductules among the fibrotic tissue which is rich in αSMA.

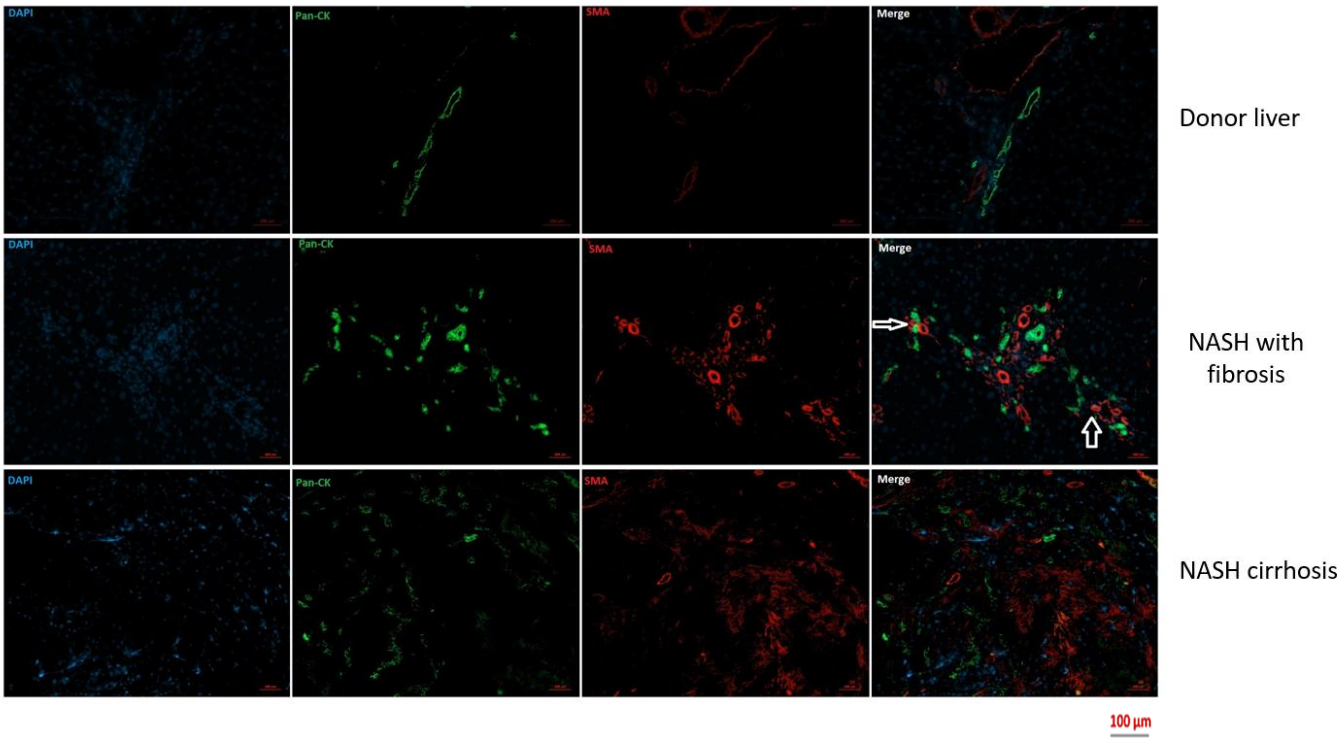

Figure 33: dual immunofluorescent staining for the DR and αSMA in donor, NASH with fibrosis and NASH cirrhosis livers

Representative sections are shown in the panel above for donor, NASH with fibrosis and NASH cirrhosis livers. Dual immunofluorescent staining was undertaken using primary antibodies for pan-cytokeratin (1:200) and αSMA (1:200) with different fluorescent-conjugated secondary antibodies (pan-cytokeratin = green, αSMA = red). Nuclear staining was undertaken with DAPI (purple).

Dual immunofluorescent staining was also undertaken to assess for co-localisation between DR cells (expressing pan-cytokeratin) with PDGFRβ+ cells (activated HSC/fibroblasts).

The upper panels show pan-cytokeratin and PDGFRβ staining predominantly confined to portal tracts in donor liver. In NASH with fibrosis, there are areas of co-localisation between DR cells (expressing pan-cytokeratin) and PDGFRβ+ cells (white arrows). In NASH cirrhosis liver, there is a nodule surrounded by PDGFRβ-rich fibrotic tissue containing a proliferation of ductules.

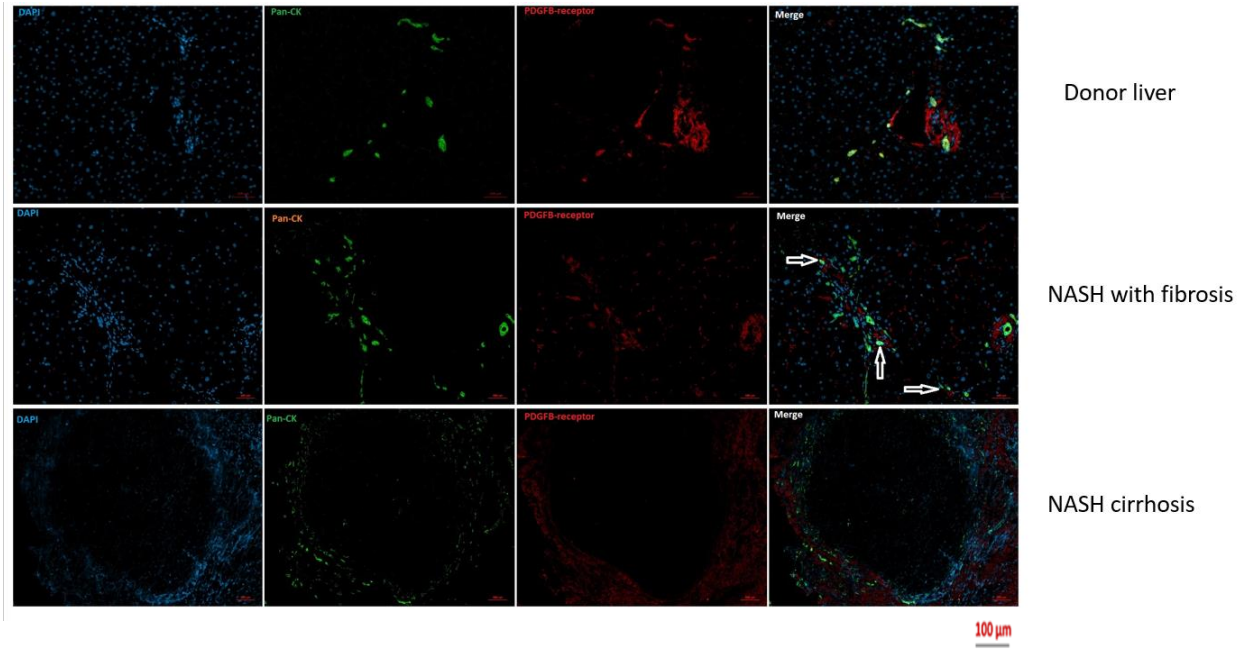

Figure 34: dual immunofluorescent staining for the DR and PDGFRβ in donor, NASH with fibrosis and NASH cirrhosis livers

Representative sections are shown in the panel above for donor, NASH with fibrosis and NASH cirrhosis livers. Dual immunofluorescent staining was undertaken using primary antibodies for pan-cytokeratin (1:200) and PDGFRβ (1:200) with different fluorescent-conjugated secondary antibodies (pan-cytokeratin = green, PDGFRβ = red). Nuclear staining was undertaken with DAPI (purple).

3.3 Assessing the interactions between DR cells and HSC *in vitro*

3.3.1 Introduction

It has been shown above that a progressive DR is associated with the increased activation of HSC, in both murine and human MASLD. Moreover, there is co-localisation between DR cells and activated HSC, and murine DR cells have been shown to upregulate gene expression of the HSC activating ligands Pdgfβ and Ctgf. It has been proposed that interactions between DR cells and HSC may be of importance in driving fibrosis. Thus, it was decided to investigate any effect *in vitro,* and to try to elucidate mechanism.

BEC were used as a surrogate DR cell for experiments. BEC were isolated from donor livers unsuitable for transplantation (donor BEC), and from diseased explant livers from transplant recipients. BEC were freshly isolated and then used at either passage 3 or 4 for experiments. BEC derived from NASH livers were not available, therefore BEC derived from ArLD explants were used as the "injured" phenotype. HSC were used from vials frozen at -80C; these were thawed and then seeded into flasks for at least one passage, before being used at either passage 4 or 5.

It was decided to use a co-culture set-up to monitor the interaction between BEC and HSC. *Transwell* inserts with a 0.6µm pore size were used to enable close cell contact across the membrane, and signalling with soluble mediators, but without allowing migration across the membrane. This allowed the cells to be harvested separately at the end of each co-culture experiment. BEC derived from donor and ArLD were co-cultured separately with HSC, to assess if BEC phenotype had an effect on the interaction with HSC.

3.3.2 Aims

1. Examine the effect of co-culture on HSC in terms of activation markers, using co-culture with donor and ArLD derived BEC

2. Use a blocking antibody to try to modulate any effects seen

3.3.3 Results

In order to perform co-culture experiments, both HSC and BEC needed to be grown in the same media. It was decided to use the "simpler" media – HSC media (DMEM with 10% FCS) – for the experiments. To show that culture with HSC media, rather than specialised BEC media, did not fundamentally alter the phenotype of the BEC, BEC were grown in both normal and HSC media for

48 hours, before fixing the cells and staining with a CK19 primary antibody. The staining shows that CK19 expression is maintained on BEC grown in a simple HSC cell-culture media for 48 hours.

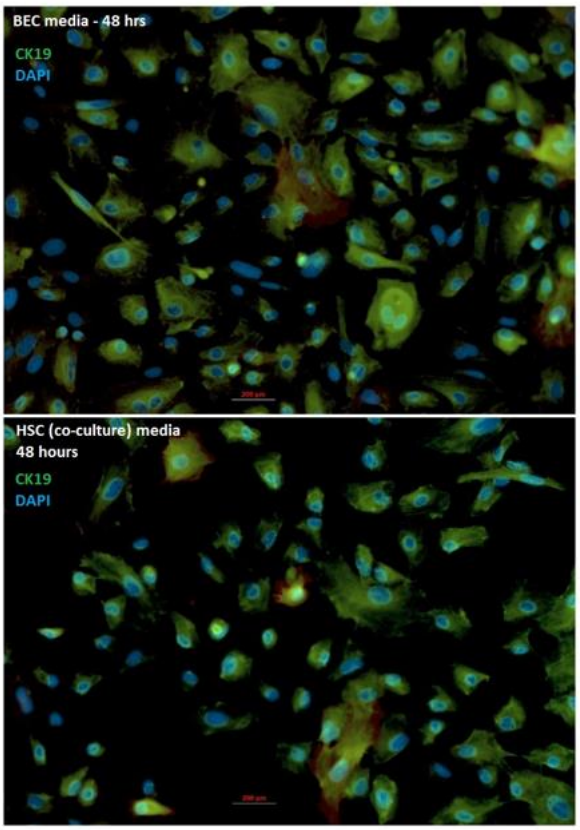

Figure 35: CK19 staining on BEC cultured for 48 hours in "normal" versus HSC cell culture media
BEC were grown for 48 hours in the relevant culture media before being fixed and permeabilised using methanol, as described above. Fluorescent staining was undertaken using a CK19 primary antibody (1:200) with a fluorescent-conjugated secondary antibody (green) and nuclear staining with DAPI (purple). The same fluorescence intensity threshold was used for the two groups, with no staining being detected at this threshold using the IMC control (image not shown).

Co-culture experiments were undertaken using the *Transwell* system described earlier, whereby HSC were cultured with or without the addition of BEC derived from either ArLD or donor livers. Gene expression of αSMA was used to assess changes in HSC activation.

Following co-culture with donor-derived BEC, HSC were less activated as evidenced by downregulation of αSMA gene expression (top panel). However, following co-culture with ArLD-derived BEC, HSC were more activated as evidenced by upregulation of αSMA gene expression (bottom panel).

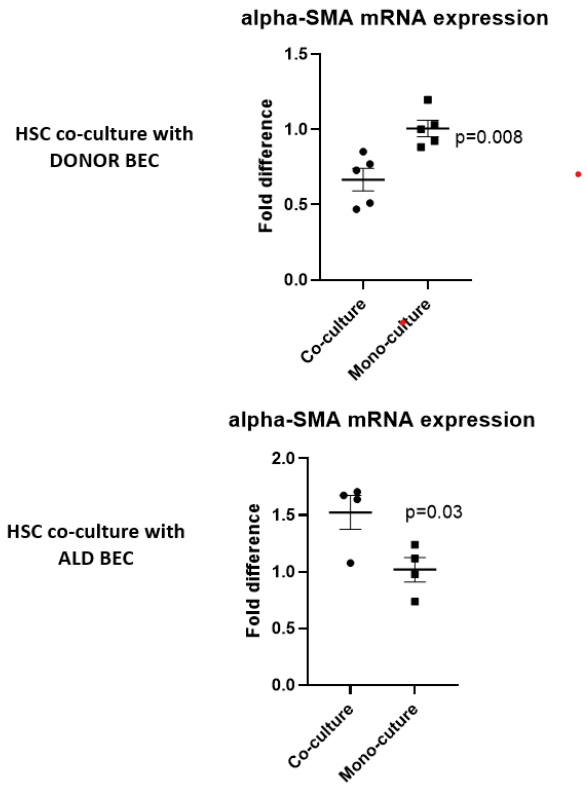

Figure 36: qPCR for αSMA gene expression in HSC co-cultured with BEC compared to HSC in mono-culture
Transwell inserts were seeded with or without BEC derived from ArLD or donor livers and then cultured for 24 hours at 37C before addition of HSC to the other side of the insert and culture for a further 48 hours. After this, BEC and HSC were removed separately from their corresponding side of the *Transwell* insert; cells were subsequently lysed and RNA extraction and reverse transcription were performed. qPCR was used to study the expression of αSMA in the HSC, as a known marker of activation.
HSC from each *Transwell* insert (co-culture with ArLD-derived BEC, co-culture with donor-derived BEC and mono-culture control) were run separately in triplicate with the gene of interest and a housekeeping gene (GAPDH). The average Ct value was taken for each triplicate and ΔCt calculated for the gene of interest vs the housekeeping gene. ΔΔCt was then calculated using the mean ΔCt value for the control group. $2^{\wedge -\Delta\Delta Ct}$ generated the expression fold

difference which is plotted above for each sample per group, with median bar and IQR. A Mann-Whitney-U test was used to compare the groups.

To further investigate this differential activation effect, the expression of HSC-activating ligands PDGFβ and CTGF by donor-derived and ArLD-derived BEC was studied using qPCR. The qPCR data shows that *injured* BEC (derived from ArLD livers) express greater levels of CTGF and PDGFβ mRNA than *non-injured* BEC (derived from donor livers). These ligands have the ability to activate HSC.

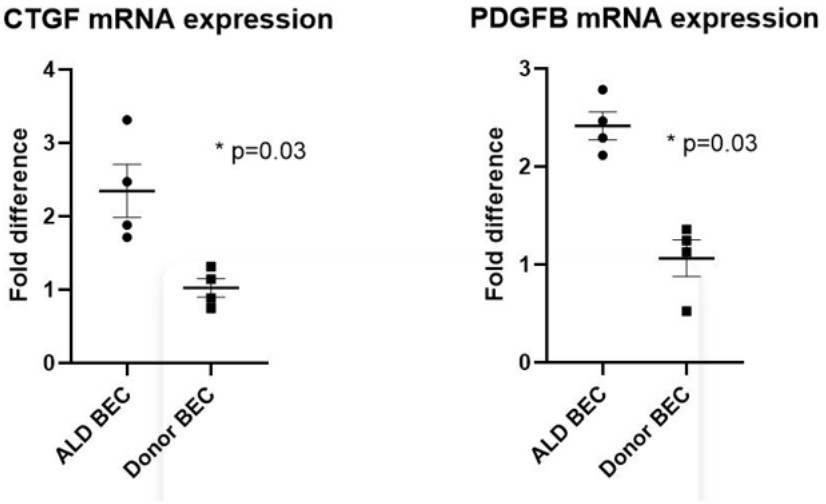

Figure 37: qPCR for CTGF and PDGFβ gene expression in BEC derived from ArLD and donor livers
BEC derived from either ArLD (N=4 wells) or donor (N=4 wells) livers, which had been in mono-culture in HSC media for 48 hours, were lysed and underwent RNA extraction and reverse transcription. qPCR was used to assess the gene expression of CTGF and PDGFβ.
BEC from each well were run separately in triplicate with the gene of interest and a housekeeping gene (GAPDH). The average Ct value was taken for each triplicate and ΔCt calculated for the gene of interest vs the housekeeping gene. ΔΔCt was then calculated using the mean ΔCt value for the control group. $2^{\wedge -\Delta\Delta Ct}$ generated the expression fold difference which is plotted above for each sample per group, with median bar and IQR. A Mann-Whitney-U test was used to compare the groups.

On the assumption that PDGFβ signalling from ArLD-derived BEC could explain the increased activation of HSC seen following co-culture, a PDGFβ blocking antibody was added into the co-culture experiment between ArLD-derived BEC and HSC. This would be expected to abrogate the activating effect of ALD-derived BEC on HSC, if PDGFβ signalling were of functional significance. The qPCR data show that addition of a PDGFβ-blocking antibody did not abrogate the activating effect of co-culture with ArLD-derived BEC on HSC, as shown in the previous experiment. In fact, the activating effect seen in the previous experiment was not recapitulated.

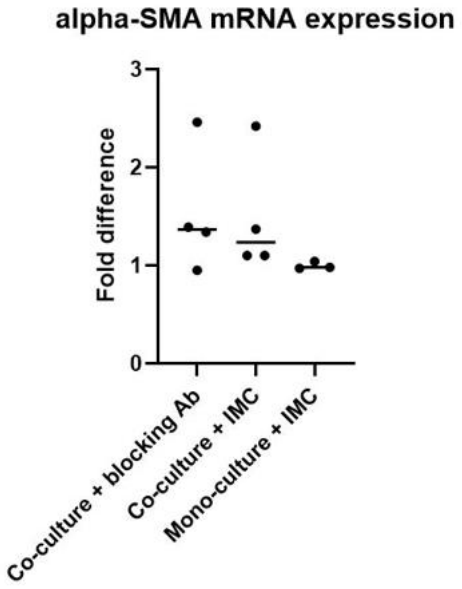

Figure 38: qPCR data for αSMA expression in HSC cultured alone or in co-culture with ArLD-derived BEC, with or without the addition of a PDGF blocking antibody/IMC

Transwell inserts were seeded with or without BEC derived from ArLD livers and then cultured for 24 hours at 37C before addition of HSC to the other side of the insert with either IMC or a PDGFβ blocking antibody, and culture for a further 48 hours. After this, BEC and HSC were removed separately from their corresponding side of the *Transwell* insert; cells were subsequently lysed and RNA extraction and reverse transcription were performed. qPCR was used to study the expression of αSMA in the HSC, as a known marker of activation.

HSC from each *Transwell* insert (co-culture with ArLD-derived BEC and blocking antibody, co-culture with ArLD-derived BEC and IMC and mono-culture with IMC control) were run separately in triplicate with the gene of interest and a

housekeeping gene (GAPDH). The average Ct value was taken for each triplicate and ΔCt calculated for the gene of interest vs the housekeeping gene. ΔΔCt was then calculated using the mean ΔCt value for the control group. $2^{-\Delta\Delta Ct}$ generated the expression fold difference which is plotted above for each sample per group, with median bar and IQR. A Mann-Whitney-U test was used to compare the groups.

3.4. Developing a protocol to perform bulk RNA sequencing on freshly isolated biliary/DR cells from human NASH and donor liver

3.4.1 Introduction

To directly investigate signalling pathways which may be relevant in DR cells in human NASH *in vivo,* it was decided to develop and optimise a protocol to freshly isolate biliary/DR cells using the same EpCAM+ panel as that used in the murine work (Live/CD45-/CD31-/EpCAM+). Given access only to donor livers and explants, the two groups chosen for comparison were NASH cirrhosis and normal donor (n=3 vs 3).

An initial protocol with a long digest time did not result in a sufficiently large proportion of EpCAM+ cells to enable sorting in a short enough time period: therefore several optimisation steps were needed. As the proportion of dead cells and CD45+ cells appeared to be a problem, the utility of adding MACS steps after the digest and prior to the sort was investigated.

3.4.2 Aims

1. Optimise a protocol to isolate EpCAM+ cells from human NASH cirrhosis and donor liver, specifically to enable the sorting of >25,000 cells in 30 minutes.
2. Assess the utility of adding MACS steps prior to cell sorting, using counting beads to assess the number/proportion of target EpCAM+ cells and using the same NASH explant liver for all the comparators.

3. Perform bulk RNA sequencing on freshly isolated EpCAM+ cells from NASH cirrhosis and donor human liver

3.4.3 Results

A quick liver digest protocol, adapted from a laboratory-wide protocol used to isolate cells for previous single-cell RNA sequencing work, resulted in a low yield of the target EpCAM+ cells and thus greatly excessive sort times.

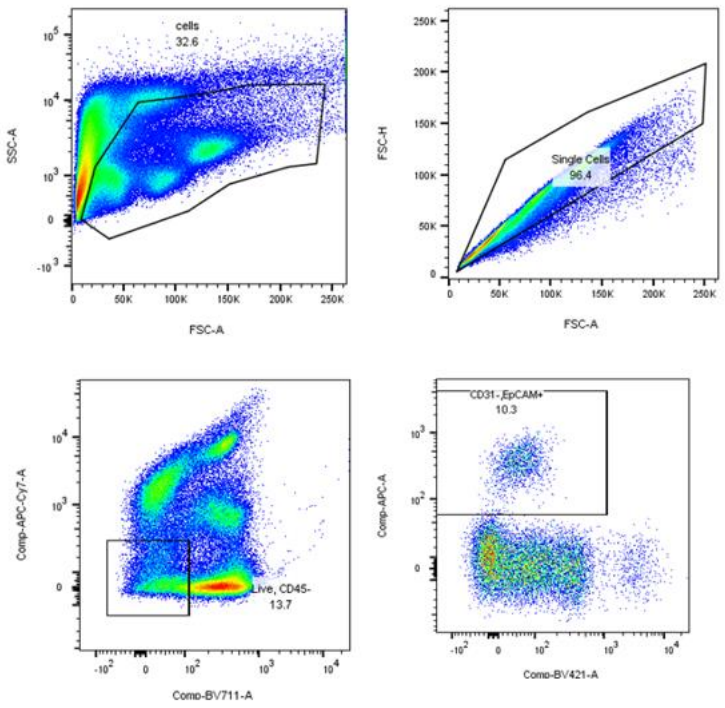

Figure 39: illustration of the gating protocol used for the isolation of EpCAM+ cells, following a quick liver digest
The cell suspension was stained with the determined FACS antibody panel (Live/Dead, CD45, CD31, EpCAM) and the target EpCAM+ population was identified using the gating strategy illustrated above. Scatter was used to identify the cell (top left panel) and then single cell (top right panel) population. The live, CD45- fraction (bottom left panel) was subsequently gated with CD31- and EpCAM+ to show the target population outlined by the box (bottom right panel). The target cell population is shown here to be ~1.4% of single cells (=13.7%x10.3%).

It was decided to incorporate MACS steps into the protocol, to try to increase the prevalence of the EpCAM+ population and thus decrease sort times. Given the results above the three steps chosen to be investigated were: a) EpCAM enrichment, b) EpCAM enrichment with dead cell depletion, c) EpCAM enrichment with dead cell depletion and CD45+ cell depletion. Although the addition of each MACS step results in the inadvertent loss of some of the target cells, it was recognised that increasing the proportion of EpCAM+ cells as a proportion of single cells was the most important factor in decreasing the sort times to become viable to enable RNA sequencing.

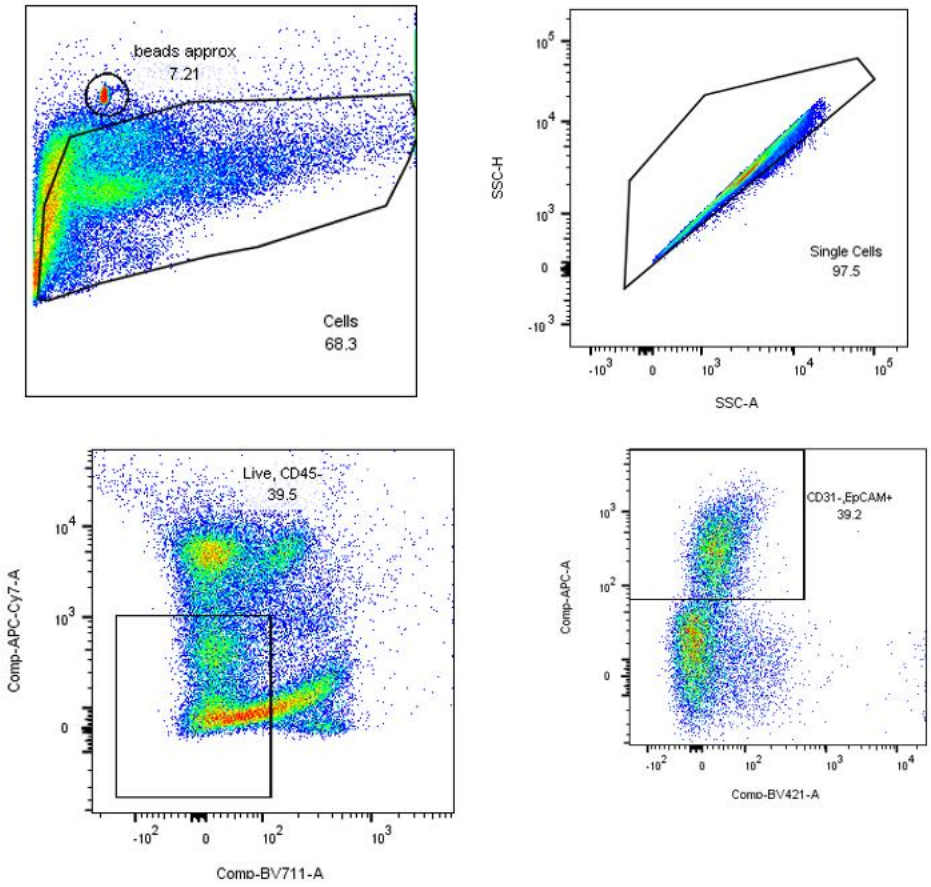

Figure 40: proportion of target EpCAM+ cells following addition of EpCAM enrichment MACS step to quick liver digest protocol

Following a quick liver digest, an EpCAM enrichment step (via MACS) was undertaken prior to staining with the determined FACS antibody panel (Live/Dead, CD45, CD31, EpCAM) This increased the population of EpCAM+ cells to

15% of single cells (fifteen-fold increase in comparison to digest alone), as shown in the illustrative gating analysis above.

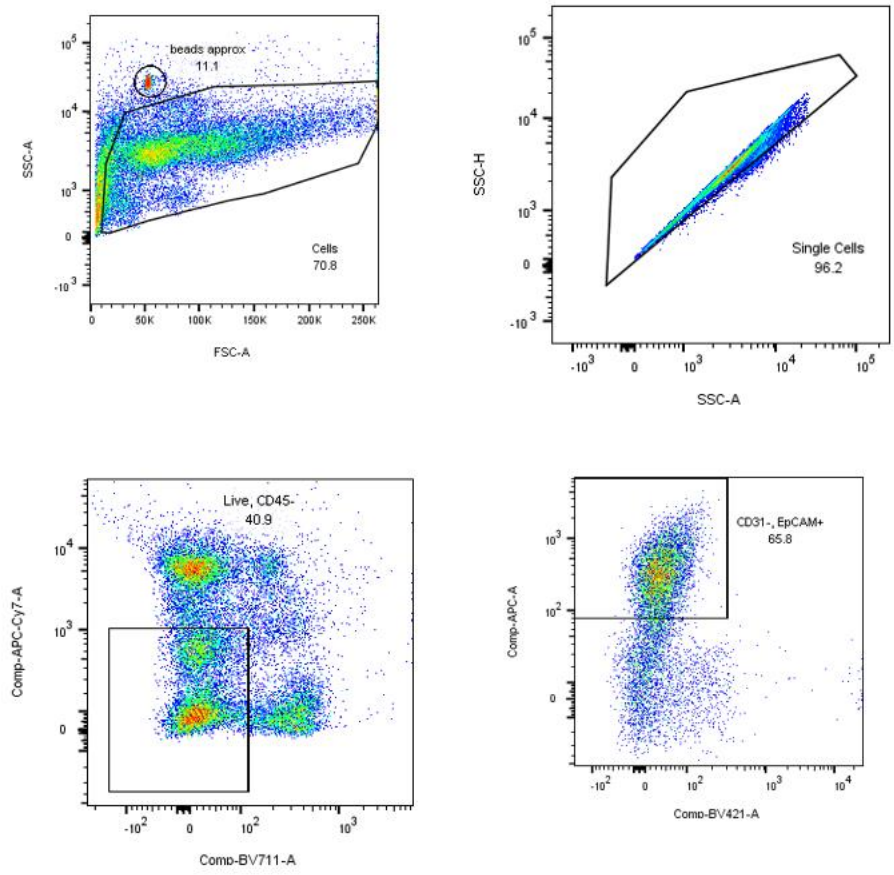

Figure 41: proportion of target EpCAM+ cells following addition of EpCAM enrichment and dead cell depletion MACS steps to quick liver digest protocol

Following a quick liver digest, an EpCAM enrichment and dead cell depletion step (via MACS) was undertaken prior to staining with the determined FACS antibody panel (Live/Dead, CD45, CD31, EpCAM). This increased the population of EpCAM+ cells to 27% of single cells (twenty seven-fold increase in comparison to digest alone), as shown in the illustrative gating analysis above.

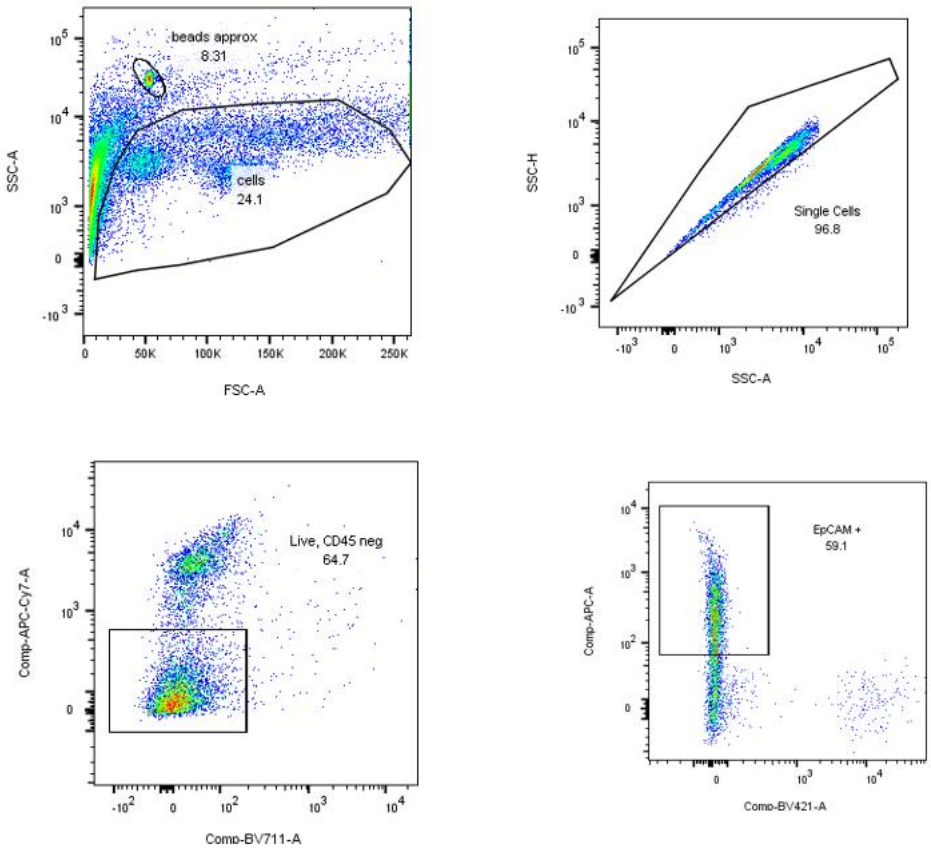

Figure 42: proportion of target EpCAM+ cells following addition of EpCAM enrichment, dead cell depletion and CD45 depletion MACS steps to quick liver digest protocol

Following a quick liver digest, an EpCAM enrichment, dead cell depletion and CD45 depletion step (via MACS) was undertaken prior to staining with the determined FACS antibody panel (Live/Dead, CD45, CD31, EpCAM). This increased the population of EpCAM+ cells to 38% of single cells (thirty eight-fold increase in comparison to digest alone).

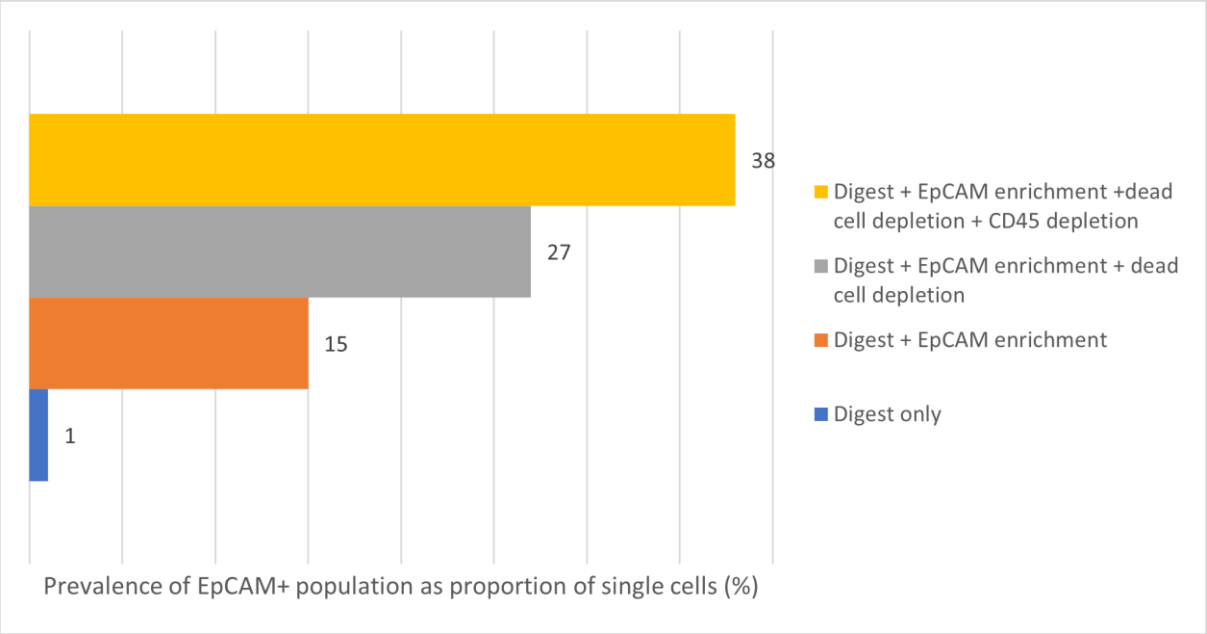

Figure 43: graph showing the prevalence of the EpCAM+ population (as percentage of single cells) with the addition of different MACS steps to the liver digest protocol

Given the maximally improved sort time resulted from the combination of the three MACS steps above, without inadvertent loss of cells to reduce yield to below target, this approach was chosen for the RNA sequencing work. In each case, at least 25,000 EpCAM+ cells were sorted directly into ice-cold PBS, spun down and re-suspended in RLT buffer. Samples were sent directly to Lexogen for their internal quality control (QC) and bulk RNA sequencing.

All six samples (NASH cirrhosis (N=3) and non-fatty donor (N=3)) passed the internal QC at Lexogen and were subjected to transcriptomic analysis. To construct RNA libraries, the QuantSeq 3' mRNA-Seq Library Prep Kit (Lexogen, Inc., Austria) was used according to the manufacturer's instructions.

The Lexogen QuantSeq FWD Data Analysis Pipelines were performed as follows. In brief, the pipelines process the FASTQ files through Trimming, Read Alignment, and Quality Control steps The output includes read QC reports, alignment statistics and .bam files, and read count files. The read count files are used as input for the Differential Expression Pipeline, where specific read count files

can be selected for the desired pair-wise comparisons. The Differential Expression Pipeline outputs the lists of differentially expressed genes, as well as a variety of graphical analyses of the results.

Using the differentially expressed genes data, a principal component analysis was generated plotting the six samples, demonstrating both inter and intra group variability. Principal component 1 accounts for 25% of the variance, and Principal component 2 accounts for an additional 23%.

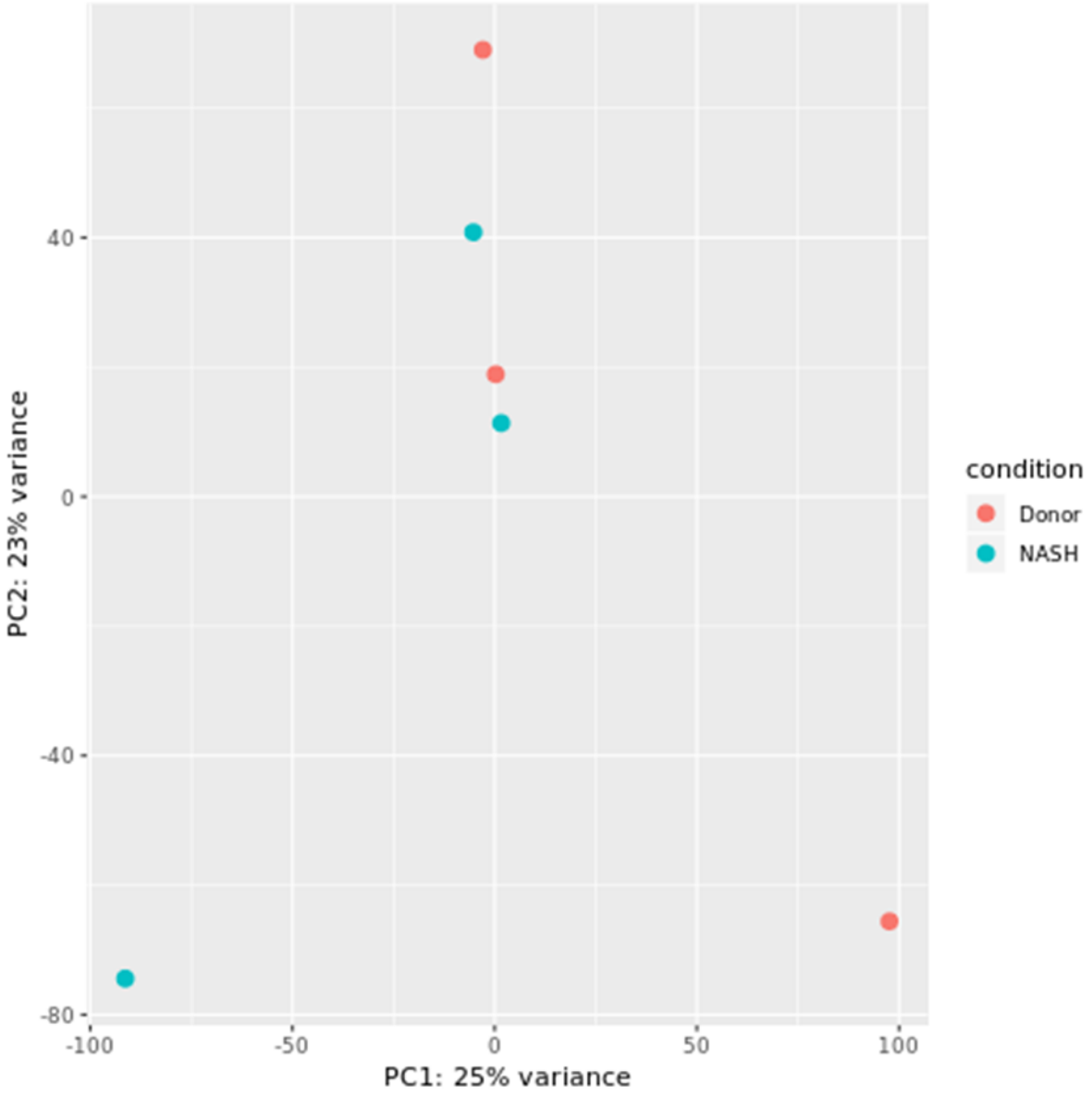

Figure 44: Principal component analysis using differentially expressed genes from DR/biliary cells isolated from Donor and NASH livers.
Plot displaying all 6 samples along Principal Component 1 and Principal Component 2, which describe 25% and 23% of the variability, respectively. PC = principal component.

The *Rosalind* software (https://rosalind.onramp.bio/) was used to generate a Volcano plot, mapping log(2) fold change in gene expression against statistical significance (-log(10) p-value). Statistically significant upregulated genes in biliary/DR cells from Donor livers are plotted in green; statistically significant downregulated genes in biliary/DR cells from Donor livers are plotted in blue. Statistically non-significant changes in differential gene expression are plotted in black.

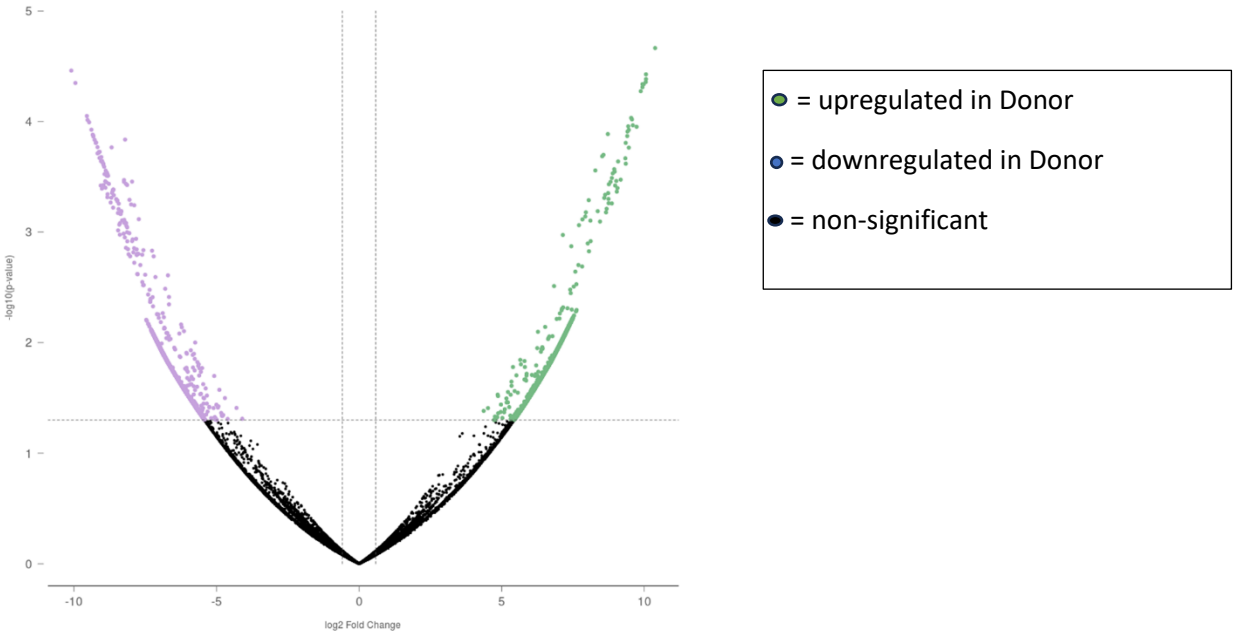

Figure 45: Volcano plot depicting the fold difference and statistical significance of differential gene expression in biliary/DR cells from Donor vs NASH livers.
Coloured points in blue refer to downregulated genes and green for upregulated genes in biliary/DR cells from Donor livers according to their fold change. Statistical significance was defined at p=0.05 (-log(10) p-value >1.30). x-axis plots log(2) fold change and y-axis plots -log(10) p-value.

The *Rosalind* software was used to generate a Heatmap of differentially expressed genes, using a log(2) fold change (0.5) cut-off and p=0.05 statistical significance level. A two colour setup was achieved via mean subtracted normalised $\log_2$ expression values. This confirmed the presence of

1586 upregulated genes and 1550 downregulated genes in biliary/DR cells from Donor vs NASH livers.

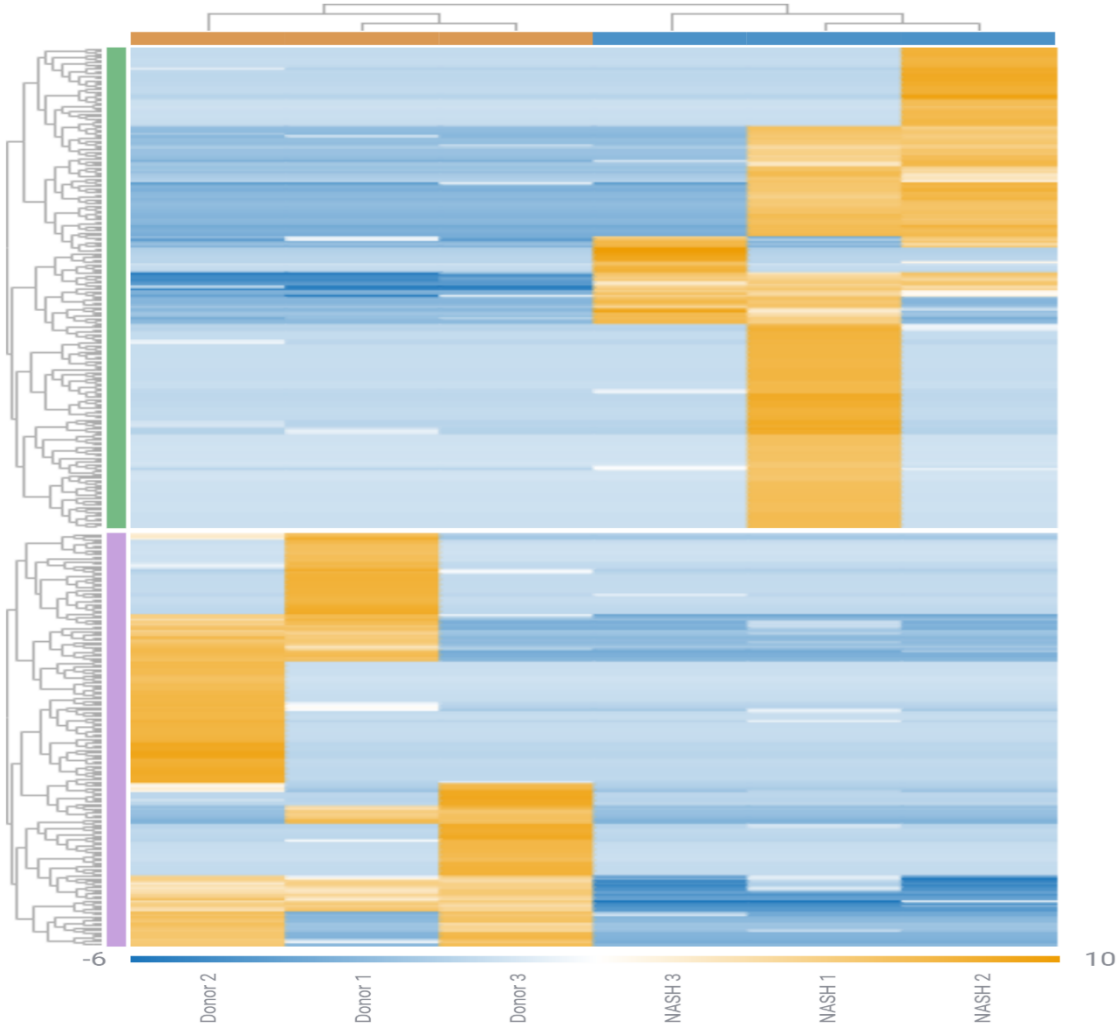

Figure 46: Heatmap illustrating differentially expressed genes in biliary/DR cells from Donor versus NASH livers. A two colour setup was achieved via mean subtracted normalised log(2) expression values. Orange represents gene upregulation, blue represents gene downregulation.

The ten most upregulated and downregulated genes between the Donor and NASH groups were assessed using the differential expression data, and are tabulated below.

Gene ID	Gene Name	baseMean	log2FoldChange	padj
ENSG00000132693	CRP	644.0	10.14	2.6e-02
ENSG00000126391	FRMD8	555.4	9.99	2.6e-02
ENSG00000122176	FMOD	376.2	9.59	2.6e-02
ENSG00000226742	HSBP1L1	372.6	9.58	2.6e-02
ENSG00000100342	APOL1	372.2	9.56	2.6e-02
ENSG00000135452	TSPAN31	350.6	9.51	2.6e-02
ENSG00000074071	MRPS34	329.7	9.43	2.6e-02
ENSG00000179364	PACS2	330.9	9.41	2.6e-02
ENSG00000135637	CCDC142	314.8	9.37	2.6e-02
ENSG00000197157	SND1	312.3	9.36	2.6e-02

Table 5: ten most upregulated genes in biliary/DR cells from Donor vs NASH livers.
CRP = C reactive protein. FRMD8 = FERM domain containing 8. FMOD = fibromodulin. HSBP1L1 = heat shock factor binding protein 1. APOL1 = Apolipoprotein L1. TSPAN31 = tetraspanin 31. MRPS34 = mitochondrial ribosomal protein S34. PACS2 = phosphofurin acidic cluster sorting protein 2. CCDC142 = coiled-coil domain containing 142. SND1 = secondary wall-associated NAC domain protein 1.

Gene ID	Gene Name	baseMean	log2FoldChange	padj
ENSG00000107338	SHB	625.6	-10.47	2.6e-02
ENSG00000166592	RRAD	590.2	-10.19	2.6e-02
ENSG00000072274	TFRC	458.8	-10.12	2.6e-02
ENSG00000135999	EPC2	415.1	-10.06	2.6e-02
ENSG00000166833	NAV2	423.1	-10.05	2.6e-02
ENSG00000154153	RETREG1	441.6	-10.04	2.6e-02
ENSG00000252835	SCARNA21	445.2	-10.02	2.6e-02
ENSG00000173064	HECTD4	394.3	-9.97	2.6e-02
ENSG00000101544	ADNP2	376.6	-9.91	2.6e-02
ENSG00000183520	UTP11	351.0	-9.85	2.6e-02

Table 6: ten most downregulated genes in biliary/DR cells from Donor vs NASH livers.
SHB = SH2 domain containing adaptor protein B. RRAD = Ras Related Glycolysis Inhibitor And Calcium Channel Regulator. TRFC = transferrin receptor. EPC2 = enhancer of polycomb homolog 2. NAV2 = neuron navigator 2. RETREG1 = Reticulophagy Regulator 1. SCARNA21 = Small Cajal Body-Specific RNA 21. HECTD4 = HECT domain E3 ubiquitin protein ligase 4. ADNP2 = ADNP homeobox 2. UTP11 = UTP11 Small Subunit Processome Component.

The *Rosalind* software was used to generate a geneset enrichment plot. This uses a panel of genes known to be implicated within a particular pathway/process, and, in brief, looks for differences in expression at a panel-wide level (enrichment) between different experimental groups. This showed that pathways pertaining to TNFα signalling, epithelial mesenchymal transition and inflammatory response were differentially expressed between the Donor and NASH livers.

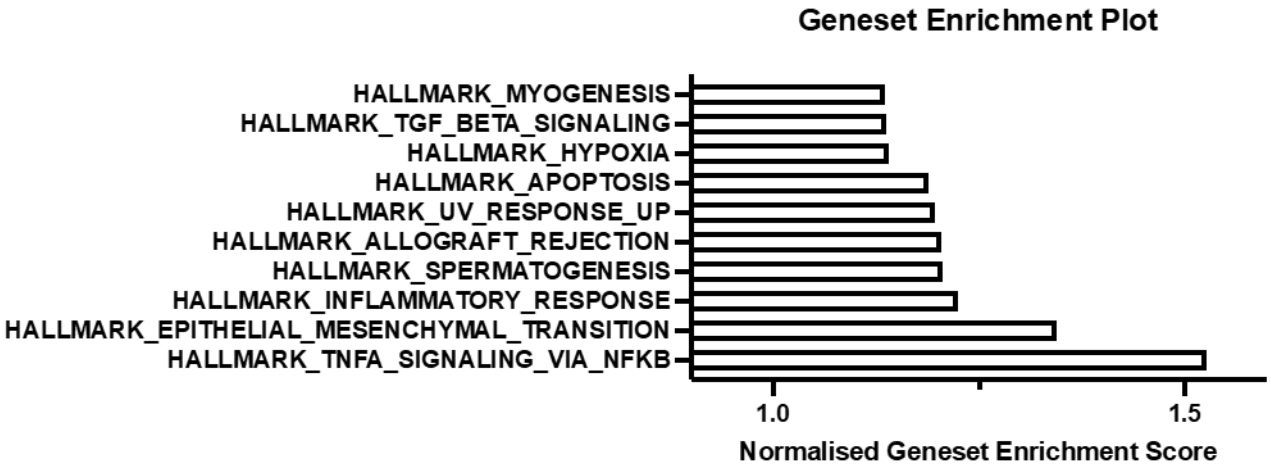

Figure 47: geneset enrichment plot showing the differential expression (enrichment) of gene panels pertaining to discrete pathways, between biliary/DR cells from Donor vs NASH livers. Normalised enrichment score plotted on x-axis = enrichment score corrected for differences in geneset sizes.

Given that CTGF had been implicated in DR cell signalling in the murine MCD model and human *in vitro* work, the *STRING* software (https://string-db.org) was used to generate a protein interaction network, graphically illustrating important upstream and downstream mediators. Target mediators identified from this network, and other proteins known to be of importance in CTGF signalling, were interrogated using the RNA sequencing differential expression data. The *Rosalind* software was used to generate a Heatmap, showing separation between biliary/DR cells from Donor and NASH livers with regard to differentially expressed genes involved in CTGF signalling.

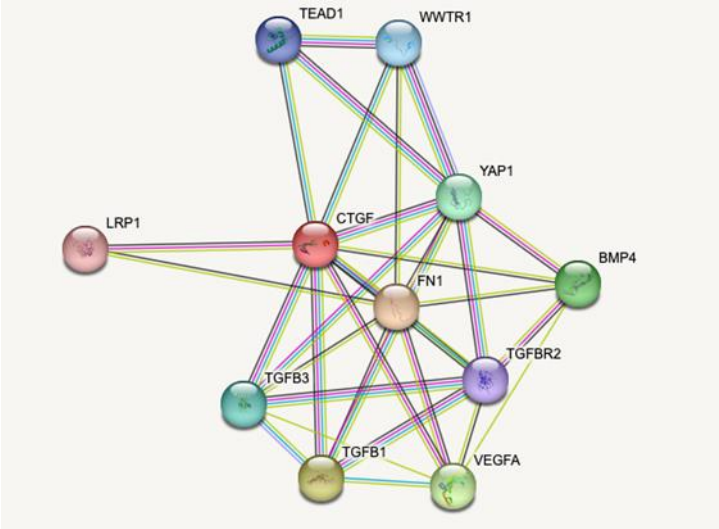

Figure 48: CTGF protein interaction network, generated using the STRING software.

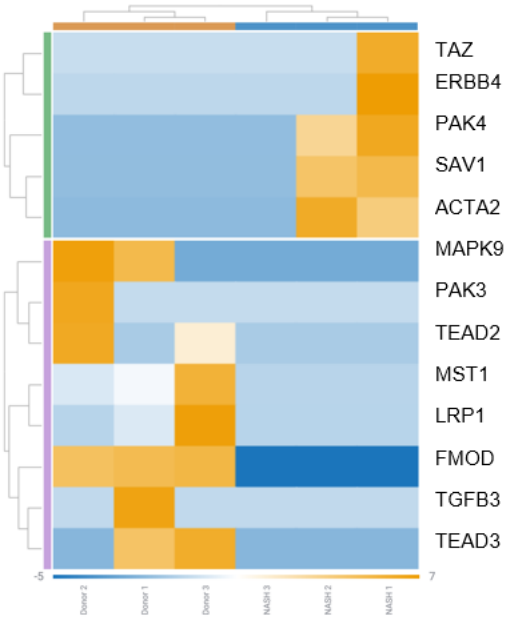

Figure 49: Heatmap showing differential expression of genes involved in CTGF signalling in biliary/DR cells from Donor vs NASH livers.
A two colour setup was achieved via mean subtracted normalised log_2 expression values. Orange represents upregulation, blue represents downregulation.

4. DISCUSSION

4.1 Comparison of DR, fibrosis and HSC activation in two murine models of MASLD

It is known that a DR accompanies liver injury from almost any cause, including fatty liver disease[109]. Moreover, there is known to be a clear positive correlation between the severity of chronic liver injury, usually exhibited by the amount of fibrosis, and the magnitude of the DR[111]. It is less clear whether this association is causal – for example the DR directly drives portal fibrogenesis – or whether both are driven by progressive injury. The former has been shown to be the case in murine models of cholestatic liver injury[124,125], but the relationship is less clear for other mechanisms of liver injury including fatty liver disease.

To investigate the link between DR and fibrosis in MASLD, it was decided to first determine which murine model would most resemble human NASH: ideally this model would recapitulate steatosis and steatohepatitis, whilst also leading to both a DR and some fibrosis during the time of the model. It was shown that both the MCD and CDAA models led rapidly to steatosis (Figure 2), and some features of steatohepatitis as judged by an expert Pathologist (ballooning and inflammation (Figures 3-4)). Both models did induce a mild DR (Figure 5). However, the absence of significant fibrosis in both models was notable: there was only mild threads of fibrosis by week six of the CDAA model, and there was no discernible fibrosis in the MCD model (Figure 8). Whilst it is possible to run these models for longer, welfare concerns and licensing details in our Unit constrain their use to the timescales utilised in this work. Indeed, most work running these models for longer emanates from outside of the UK.

The presence of weight loss during both MCD and to a much lesser extent the CDAA model (>20% of bodyweight in the late MCD cohort (Figure 1)) highlights a crucial way in which murine NASH models differ from human disease, which is strongly associated with excess weight. Although a more human-like phenotype of NASH can be invoked by feeding mice a high fat diet, such models need to be undertaken for many months which limits their utility as a research tool. A model that would deserve investigation in future work, particularly with regard to its ability to induce a DR, is the choline-deficient, L-amino acid-defined, high-fat diet (CDAHFD)[62]. This has been shown to induce weight gain, steatohepatitis and indeed significant fibrosis by six weeks, the same late timepoint used in this work for the CDAA model. If the CDAHFD model did also induce a robust DR, this would represent an ideal model on which to base future murine experiments examining the DR/fibrosis axis in fatty liver disease.

Although the MCD and CDAA diet are established and well-published models of fatty liver disease, and are shown in this work to also recapitulate a DR, the un-physiological nature of the models is a general limitation and thus any mechanistic conclusions derived from these models need to be applied to human disease with caution. Indeed, a crucial difference between these models and human disease is the absence of significant fibrosis, the development of which is a cornerstone in the progression of MASLD, denoting a poorer prognosis and what many would consider to be "clinically significant" disease. However, it should be noted that MASLD in humans is a slowly progressive disease, with the accumulation of fibrosis over many years. Therefore, trying to recapitulate these slow changes in short-term murine models is extremely challenging.

Taking into account the significant limitations above, the more weight-neutral nature of the CDAA model, paired with its greater (albeit mild) DR and fibrosis, was deemed to constitute a better

murine model on which to base further experiments. Specifically, transgenic murine experiments using the CDAA model were planned to try to gain further clarity on the relationship between the DR and fibrosis: unfortunately, these experiments did not prove possible within the constraints of this project.

One key aim of this work was to understand potential cellular interactions between DR cells and neighbouring cells within the DR niche, particularly HSC and fibroblasts, which play a key role in the development of fibrosis[4]. To examine the transcriptional profile of DR cells directly, FACS was utilised to isolate biliary/DR cells from injured and healthy murine liver tissue. EpCAM was chosen as the DR marker for cell sorting experiments given its status as a surface antigen and specificity to the biliary epithelium in the liver, whereas CK19 (which had been used for IHC staining experiments), is an intracellular antigen. EpCAM is well-recognised as a cholangiocyte/DR marker in the published literature[134]. It should be highlighted that in injured liver, EpCAM sorting will select both DR cells – i.e. those invading into the lobule histologically – and normal biliary cells. By contrast, in uninjured liver, EpCAM sorting would solely be expected to sort normal biliary cells given the absence of a DR. One limitation that directly follows from this observation is that potential differences between these two phenotypes of EpCAM+ cell cannot be elucidated. Using a maker to solely select the more “activated” EpCAM+ cells forming the DR would be optimal, however no reliable marker for these cells is known. Single-cell RNA sequencing might constitute a tool in future work to understand these differences by defining subsets within the total EpCAM+ population, based on the transcriptomic profile of the individual cells. However, identifying subsets according to transcriptomic signature would still require significant further work to determine the function and roles of cholangiocyte subpopulations, particularly with regard to development/sustainment of the DR and indeed disease progression.

qPCR was used to show that EpCAM+ cells from injured MCD and CDAA livers express greater levels of Ctgf and Pdgfβ mRNA respectively, in comparison to uninjured livers (Figure 12). Both of these ligands are known to be pro-inflammatory and fibrogenic, with roles in HSC activation[69,72]. Whilst both ligands have been shown to be produced by biliary cells in rodent models of biliary injury[125,126], this has not hitherto been shown within the sphere of fatty liver disease. PDGFβ has a receptor which is well studied, and is a known marker of activated HSC/fibroblasts[4]. Thus, staining for PDGFRβ was undertaken with dual immunofluorescence showing co-localisation between DR cells and PDGFRβ+ positive cells in MCD liver. Unfortunately, due to the Covid pandemic it was not possible to get frozen slides from the CDAA mice to complete this experiment. The co-localisation seen in MCD liver suggests that DR cells may have a functional interaction with HSC, which could be mediated by PDGFβ. Such a finding has been previously described in murine models of biliary injury[125], but not within the realm of fatty liver disease.

A general limitation of this work is that qPCR reflects the gene expression of a particular protein, which does not necessarily correlate with intracellular levels of that protein or the degree of activity of the relevant signalling pathway to that protein. Staining for the ligands themselves (PDGFβ and CTGF) and downstream targets such as low-density lipoprotein receptor-related protein-1 was attempted - however it was unhelpful given a large amount of background staining which could not be ameliorated despite many attempts at protocol optimisation.

4.2 Characterisation of human MASLD with regard to DR, HSC activation and fibrosis

Work on human liver tissue was then undertaken to understand and demonstrate differences with the murine models, and to assess the relevance of findings resulting from the murine work, for

example whether the PDGFβ and CTGF pathways are also of relevance within the human disease sphere.

Staining for the DR and fibrosis confirmed the well-described positive correlation between the two across the spectrum of human MASLD, specifically incorporating normal liver, steatotic liver without fibrosis, NASH with advanced (F3) fibrosis and NASH cirrhosis (Figures 16,18). The latter two stages are well-accepted among the Hepatology community as being clinically significant. As discussed above, the extent of fibrosis and DR observed in the clinically significant groups is notable and proves near impossible to recapitulate in short-term murine models. αSMA staining demonstrated the presence of activated HSC/fibroblasts in the clinically significant groups, with staining mirroring the collagen deposition within the fibrosis/scar (Figure 20). As PDGFβ had been found to be potentially significant in the murine work, staining for PDGFRβ showed a similar pattern to αSMA with increased expression in the clinically significant groups (Figure 23).

Dual-immunofluorescence was utilised to show areas of co-localisation between DR (CK19 positive) and both αSMA and PDGFRβ positive cells in the NASH with advanced fibrosis and cirrhosis groups (Figures 25,26). As both αSMA and PDGFRβ are known markers for activated HSC and fibroblasts, this is supportive evidence for potential interactions between these cells and DR cells. Furthermore, as Pdgfβ gene expression by DR cells had been shown to be significantly increased in two murine models of NASH, one potential mechanism of interaction would be via PDGFβ signalling. However, spatial co-localisation does not necessarily mean significant cellular interaction, and it is possible that HSC could be activated by different pathways or even different cells and still show positivity for PDGFRβ as a marker of activation *per se* rather than upregulation of the receptor in response to PDGFβ signalling specifically by DR cells.

To try to understand more fully what signalling pathways may be relevant in DR cells in human NASH, a key focus for later work became to perform bulk RNA sequencing of human DR cells.

4.3 Assessing the interactions between DR cells and HSC *in vitro*

In vitro work was used to try to shed further light on interactions between DR cells and HSC. It was decided to use BEC as a surrogate for DR cells, given BEC are readily available in our laboratories, can be isolated from livers with different pathologies (including NASH cirrhosis and normal donors to permit comparison) and are shown to express CK19 (the DR marker used for IHC staining for this project) in culture. Directly isolating and culturing DR cells using EpCAM sorting via FACS would have been an optimal strategy, however this was beyond the scope of this project. In order to co-culture with HSC, BEC were switched to a generic "simple" culture medium (DMEM with 10% FCS) without loss of CK19 expression after 48 hours (Figure 27). Although switching culture medium could be proposed to change the phenotype of BEC, the same phenotypic switch should happen to BEC derived from any liver type, and therefore differences in interactions with HSC should be a true effect.

Due to time constraints caused by the Covid-19 pandemic, it was not possible to use NASH-derived BEC for these co-culture experiments. Instead, BEC derived from end-stage cirrhotic livers with ArLD were used. As another cause of fatty liver disease and steatohepatitis, ArLD closely resembles NASH and histologically it can be very challenging to tell the two conditions apart. As all cirrhotic livers used by the laboratory were explanted organs at the time of transplantation, patients with ArLD would have been abstinent from alcohol for at least six months and probably significantly longer. As such, the changes of "burnt-out" ArLD (scarring with some steatosis) would

be expected to closely resemble the changes of NASH seen in end-stage cirrhotic livers. Therefore, it was considered reasonable to use the ArLD-derived BEC for these experiments, albeit with this caveat.

Supporting previous hypotheses that DR cells from injured liver exhibit an inflammatory/fibrogenic phenotype, ALD-derived BEC were shown to activate HSC after co-culture, as evidenced by increased gene expression of αSMA compared to HSC cultured alone. Conversely, donor-derived BEC were shown to reduce gene expression of αSMA by HSC after co-culture. To interrogate the potential mechanism for this difference, qPCR showed increased gene expression of PDGFβ and CTGF in the ALD-derived BEC, reflecting the earlier results from the FACS-sorted DR cells in the murine models.

To attempt to modulate the PDGFβ signalling pathway, and see if this abrogated the activating effect of ArLD-derived BEC on HSC, a PDGFβ blocking antibody was added into the co-culture experiment. This did not have any significant effect, and indeed the activating-effect on HSC of co-culture with ALD-derived BEC even without the blocking antibody was lost. It is not clear if this were due to anomalous results, or a true finding particularly reflecting batch effects of the BEC, and unfortunately it was not possible to repeat this experiment due to time constraints as a result of the Covid pandemic.

It was also attempted to demonstrate increased PDGFβ protein in the supernatant of ALD-derived BEC in comparison to donor BEC, but the ELISA result did not support this (graph not shown in results as no PDGFβ detected in supernatant despite successful creation of the standard curve). This could reflect inadequate cell numbers, or perhaps insufficient secretion of PDGFβ into the culture media.

Further work would be to repeat the co-culture experiments with and without PDGFβ blocking antibodies to see if the initial differential effect of ALD and donor-derived BEC on HSC were true, and to see if the antibody can modulate the effect. Such modulation would give strong support to PDGFβ signalling from DR cells to HSC being of functional significance. As with all *in vitro* work, limitations are the extent to which effects seen do or do not play out *in vivo.* In particular, whether BEC do or do not constitute a reliable DR-cell surrogate is a concern. However, it is notable that even directly sorting cells using EpCAM via FACS, would still result in the presence of "normal" biliary cells in culture, in addition to "activated" DR cells. It would be of interest to carry out RNA sequencing on cultured BEC at different passage, and compare to freshly sorted EpCAM+ cells via FACS.

The HSC used for the co-culture experiments were isolated from human cells and were originally supplied frozen at *passage* one. For these experiments, they were all used at *passage* four or five. Using these cells was deemed superior to using an immortalised stellate-cell line such as LX2 cells which had been done in preparatory work for this project.

4.4. Developing a protocol to perform bulk RNA sequencing on freshly isolated biliary/DR cells from human NASH and donor liver

To more fully understand the pathways which may be of significance in DR cells in human NASH, bulk RNA sequencing was undertaken using freshly sorted EpCAM+ cells from NASH and donor human liver. Difficulties initially in sorting sufficient cells led to a period of optimisation in the digest and sorting protocol. Using the same NASH cirrhosis liver, it was shown that a quicker digest was equally effective as a longer one, and the proportion of EpCAM+ cells was greatly increased

(from 1% to 38% of single cells) via the addition of three magnetic cell-sorting steps prior to FACS (EpCAM enrichment, dead cell depletion and CD45+ cell depletion), speeding up the sort-time to become viable without reducing yield deleteriously.

Bulk RNA sequencing was thus performed using EpCAM+ cells from NASH (n=3) and donor (n=3) livers. Among the ten most upregulated and downregulated genes between the two groups, one gene (fibromodulin: upregulated in donor cf. NASH) stands out due to its link with fibrosis.

Fibromodulin is an extracellular matrix small leucine-rich proteoglycan, with important roles in extracellular matrix organisation[135]. The finding of upregulation in the donor livers is noteworthy and perhaps unexpected, as fibromodulin has been found to be increased at both mRNA and protein level in human cirrhotic livers, and furthermore three murine injury models (bile duct ligation, thioacetamide and CCl4) increased levels of fibromodulin as assessed both by IHC and Western blot from isolated HSC, endothelial cells and hepatocytes.[136] This study by Mormone *et al* went on to show that recombinant fibromodulin was able to activate HSC *in vitro*, as assessed by levels of collagen-1 and αSMA mRNA. In addition, the authors developed a transgenic model using Fibromodulin knockout (-/-) mice, which showed that Fibromodulin -/- mice developed less fibrosis and DR than wild type animals in response to bile duct ligation.

Although the fact that fibromodulin gene expression was upregulated in the donor livers is perhaps opposite to the suspected direction of change, a search of the literature has not found any work directly examining the expression of fibromodulin by biliary or specifically DR cells from human tissue. Interesting further work would be to confirm that fibromodulin gene expression is upregulated in the NASH livers used for the RNAseq work at the “whole liver” level, and to assess

the gene expression of fibromodulin in both cultured BEC and isolated EpCAM+ cells from livers with different disease aetiologies.

Geneset enrichment data utilises pre-defined sets of genes to see whether two groups demonstrate changes in expression at a set or "pathway" level. The geneset enrichment data for the NASH and donor biliary/DR samples show that pathways including TNFα signalling via NFKβ, epithelial mesenchymal transition and inflammatory response were significantly different at gene expression level.

NFKβ is a nuclear transcription factor and an important mediator of the inflammatory response in multiple systems[137]. Within the liver, NFKβ has been shown to protect hepatocytes from apoptosis during TNFα mediated liver injury[138]. In murine models, cholangiocytes have been found to produce NFKβ-inducing kinase which activates the NFKβ2 pathway: furthermore, cholangiocyte specific deletion of NFKβ-inducing kinase using a transgenic animal was shown to abrogate the DR and fibrosis in response to liver injury via three models of cholestasis[139]. Staining for activated HSC using αSMA was reduced in these mice suggesting that the NFKβ pathway may be implicated in paracrine signalling from cholangiocytes to HSC, resulting in activation.

Assuming that a similar mechanism may play out in human disease, the differential gene expression of a NFKβ pathway between NASH and donor biliary/DR cells lends support to the hypothesis of signalling between DR cells and neighbouring HSC. It is interesting that NFKβ has been implicated in protecting hepatocytes from apoptosis, with activation of this pathway potentially having beneficial effects on cell survival at the same time as effects on HSC activation and DR development, the latter two phenomena being viewed by some as deleterious.

The murine experiments in this project suggested that CTGF, a known HSC-activating pro-fibrotic ligand, may be produced by DR cells in response to fatty liver injury, mirroring previous results from the literature within the sphere of biliary injury. The RNA sequencing results from EpCAM+ cells in NASH and donor liver show that there is clear separation between the two groups with regard to the CTGF interactome. One finding is that TGFβ-receptor signalling, an upstream mediator of the CTGF response, is upregulated at pathway level in the NASH livers as shown by the geneset enrichment score. The differential expression data show that the expression of *CTGF per se* is also upregulated in NASH livers albeit non-significantly (log_2 fold change donor cf. NASH -1.30, p=0.51).

These results give tentative support to the hypothesis that DR cells in NASH liver comprise an inflammatory and potentially fibrogenic phenotype, as evidenced by the increased expression of genes pertaining to inflammatory response and TGFB receptor signalling. However, there was no significantly increased expression of the protein PDGFβ in NASH DR cells (log_2 fold change donor cf. NASH 0.44), a known potent HSC activator which has been shown to be of relevance in murine biliary models of liver injury and the murine qPCR data in this project.

To provide context, a search of the literature was undertaken to find studies reporting transcriptomic analysis of human DR cells:

Aguilar-Bravo *et al* utilised laser-capture microdissection to perform RNA sequencing on CK7 positive cells from human patients with alcoholic hepatitis with varying degrees of fibrosis[116]. They found that DR cells displayed a pro-inflammatory profile, with upregulation of genes pathways including NFKB and inflammatory response, mirroring the results of this project. Importantly, the comparator in this study was CK7 *negative* areas captured by microdissection from the same liver,

quoted as comprising “hepatocytes and areas of fibrosis”. Thus, the control group was fundamentally different in not containing biliary cells, whereas in this project biliary cells (EpCAM+) from healthy donor liver were the comparator.

Ceulemans *et al* performed transcriptomic analysis of DR cells also isolated from human patients with alcoholic hepatitis[115]. Mirroring the results of this project, they found upregulation of pathways including TNFα and TGFB signalling, although their finding of upregulation of the IL-17 pathways was not recapitulated here. Importantly, their comparator was *whole liver* transcriptomic analysis, and thus crucially different from this project.

Govaere *et al* utilised laser capture microdissection to provide transcriptomic analysis of DR cells from human patients with PSC and chronic Hepatitis C and interestingly compared the two disease aetiologies[140]. They found upregulated expression of extracellular matrix related genes (collagens and fibronectin) in the PSC livers and upregulated expression of “pro-invasive” genes such as PDGFRα in the Hepatitis C livers. Pathways pertaining to inflammation and immune cell recruitment were upregulated in both groups when compared to adjacent hepatocytes.

One explanation for the lack of a definitive inflammatory/fibrogenic signature of DR cells in NASH liver in this project is the fact that cirrhotic explants, by definition, represent end-stage disease in which the steatohepatitic aspect of NASH is often “burnt out”. It is possible that DR cells earlier in the disease spectrum, for example in bridging F3 or F2 fibrosis, may play more of a role in HSC activation and fibrosis given the dynamic and often ongoing accumulation of liver damage in this setting. Further work to explore the transcriptomic profile of DR cells in NASH with lesser levels of fibrosis, perhaps using laser capture microdissection from liver biopsy specimens, would be very interesting but beyond the scope of this project.

It is notable also that the control group in this project, EpCAM+ cells from healthy donor livers, is different to that reported in the three RNA sequencing papers above which used neighbouring hepatocytes or whole liver transcriptomic analysis as the control. This was done to try to explore whether the development of a DR is associated with a change in the transcriptomic profile of the biliary (EpCAM+) cells, and thus a comparator of biliary cells without a DR was deemed the most robust.

The most pressing limitation for the RNA sequencing data in this project stems from using EpCAM as the marker on which to sort cells. Whilst EpCAM is an established biliary cell (and DR) marker, in the NASH livers this will lead to both non-activated biliary cells lining bile ducts and "activated" DR cells invading the lobule being sorted at the same time. However, there is no single established DR marker to reliably sort DR cells from non-activated biliary cells. The consequence is that it is impossible to know the proportion of "activated" DR cells which were sorted in the NASH livers, and thus the true transcriptomic signature of activated DR cells cannot be reliably elucidated.

Single-cell RNA sequencing offers the opportunity to define subsets of DR cells, and if used with localisation modalities could discern the transcriptomic profile of DR cells in different regions e.g. invading into the lobule versus close to the biliary tree. Such work would be very helpful in clarifying the clearly complex ways in which DR cells communicate with their cellular niche including HSC and fibroblasts, and would lead to further light being shone on the DR/fibrosis axis. Single-cell RNA sequencing of DR cells has been carried out in mice, but no studies specifically targeting human patients have been found.

4.5 Conclusions

The exact nature of the relationship between the DR and liver fibrosis is not certain. Whilst there is a strong positive correlation between the two, including in human MASLD, it is not definitively known whether the DR drives fibrosis, and even if it does whether it constitutes a maladaptive or an adaptive response.

Although the work in this project has no conclusive answer for this longstanding and important question, it has shown that EpCAM+ cells in both murine and human NASH disease produce factors and upregulate gene pathways associated with the development of fibrosis. Moreover, the data are supportive of a functional interaction between DR cells and neighbouring HSC/fibroblasts, a finding which has been reported in murine models of biliary injury but not within the realm of fatty liver disease. The establishment of a protocol to isolate fresh biliary/DR cells from clinical samples streamlined the logistics and future work required in performing single cell RNA sequencing analysis of the liver epithelium.

Key further experiments would be to perform transcriptomic analysis of DR cells from human NASH patients with lesser levels of fibrosis, using historic liver biopsy specimens, and to pursue spatially discriminated single-cell RNA sequencing to look for DR subtypes. It would be perhaps expected to show that geographically distinct DR cells interact differently with neighbouring cells including HSC, a finding which would add more complexity to the fascinating relationship between the DR and liver fibrosis.

APPENDIX

1. Representative image of IMC staining performed on donor human liver for PDGFRβ, αSMA and pan-cytokeratin primary antibodies (all rabbit IgG host with 1:200 dilution of primary antibody)

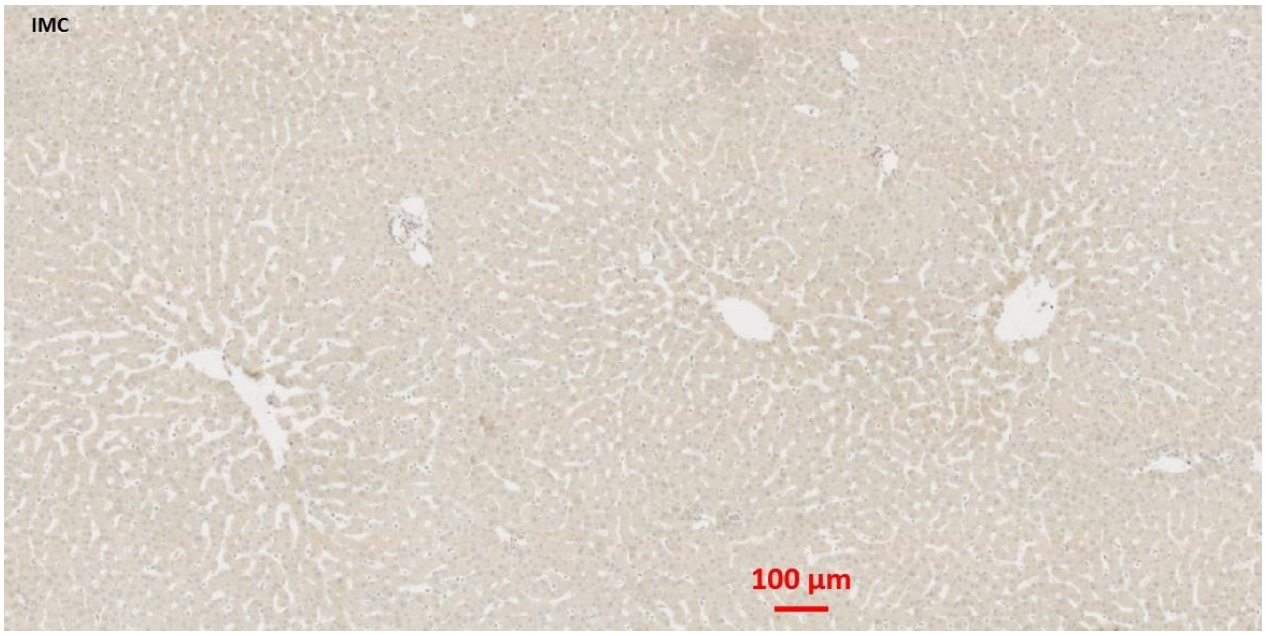

2. Representative images of IMC staining performed on NASH with fibrosis liver for the dual immunofluorescent panels: A = rabbit IgG with anti-rabbit AF 488 secondary (pan-cytokeratin IMC), mouse IgG-1 with anti-mouse AF 555 secondary (αSMA IMC), DAPI. B = rabbit IgG with anti-rabbit 488 secondary (pan-cytokeratin IMC), mouse IgG-2a with anti-mouse AF 555 secondary (PDGFRβ IMC), DAPI.

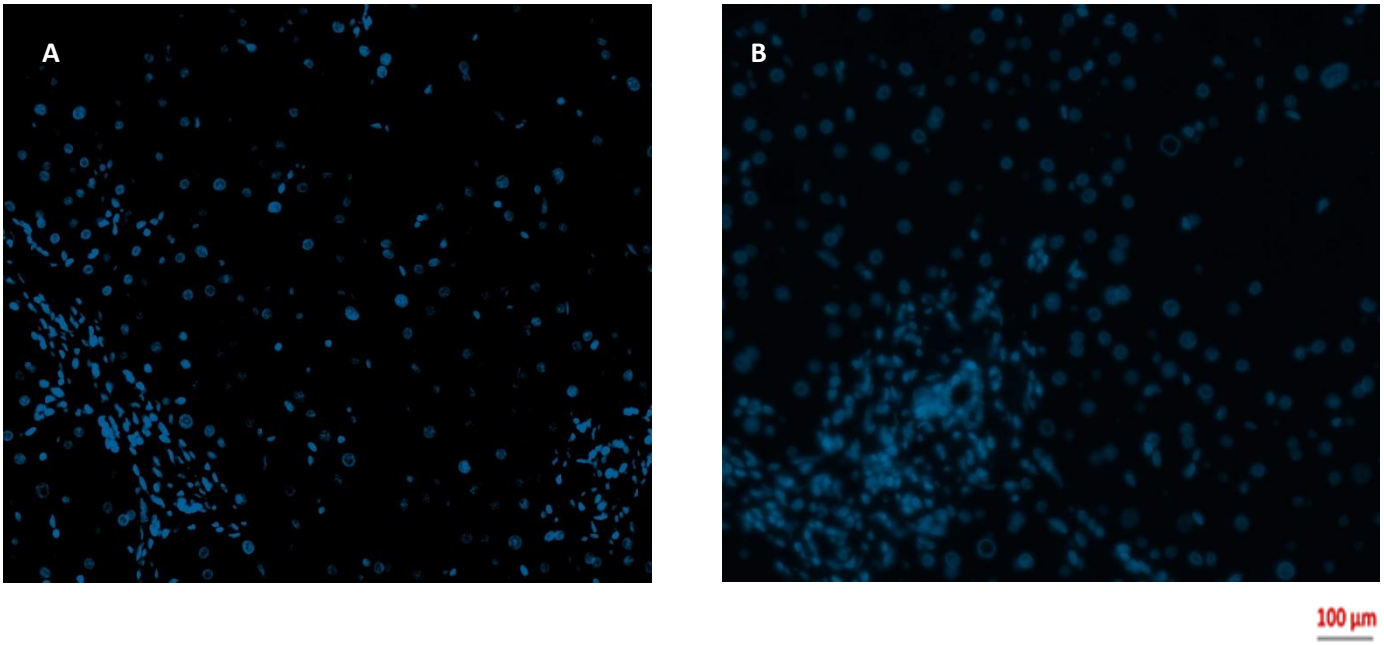

3. Representative image of IMC staining performed on MCD liver as part of mouse dual immunofluorescent panel. Rat IgG2a with anti-rat AF 488 secondary antibody (CK19 IMC), rabbit IgG with anti-rabbit AF 555 secondary antibody (PDGFRβ IMC), DAPI.

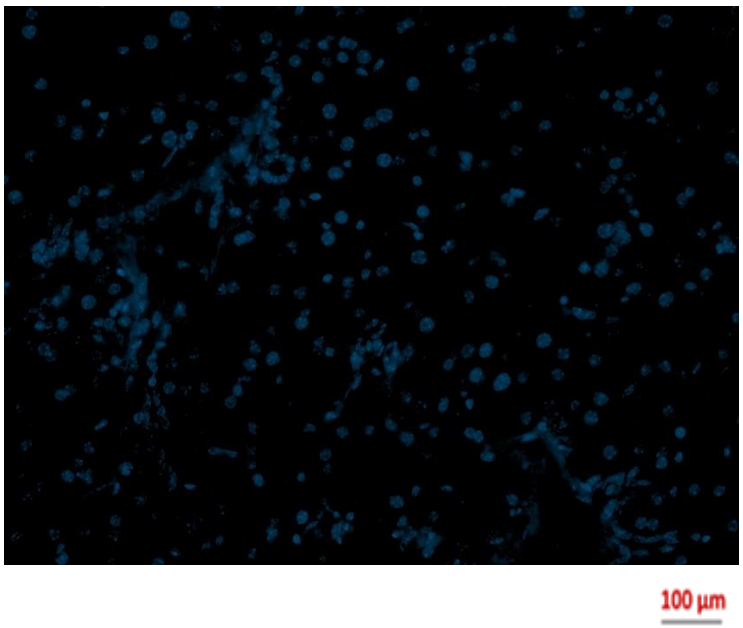

REFERENCES

1. Ellis H, Mahadevan V. *Clinical anatomy : applied anatomy for students and junior doctors*. 12th ed. ed. Wiley-Blackwell; 2010.
2. Joshi Da, Keane MGa, Brind Aa. *Hepatology at a glance*.
3. Torbenson MSa. *Biopsy interpretation of the liver*.
4. Friedman SL. Hepatic stellate cells: protean, multifunctional, and enigmatic cells of the liver. *Physiol Rev*. Jan 2008;88(1):125-72. doi:10.1152/physrev.00013.2007
5. Kietzmann T. Metabolic zonation of the liver: The oxygen gradient revisited. *Redox Biol*. 04 2017;11:622-630. doi:10.1016/j.redox.2017.01.012
6. Hinson JA, Roberts DW, James LP. Mechanisms of acetaminophen-induced liver necrosis. *Handb Exp Pharmacol*. 2010;(196):369-405. doi:10.1007/978-3-642-00663-0_12
7. Clark ML, Kumar PJ. *Kumar & Clark clinical medicine*. 6th ed. ed. Elsevier Saunders; 2005.
8. McDonnell AM, Dang CH. Basic review of the cytochrome p450 system. *J Adv Pract Oncol*. Jul 2013;4(4):263-8. doi:10.6004/jadpro.2013.4.4.7
9. Williams R, Aspinall R, Bellis M, et al. Addressing liver disease in the UK: a blueprint for attaining excellence in health care and reducing premature mortality from lifestyle issues of excess consumption of alcohol, obesity, and viral hepatitis. *Lancet*. Nov 2014;384(9958):1953-97. doi:10.1016/S0140-6736(14)61838-9
10. Trust BL. The alarming impact of liver disease in the UK.
11. Wendon, J., Cordoba J, Dhawan A, et al. EASL Clinical Practical Guidelines on the management of acute (fulminant) liver failure. *J Hepatol*. 05 2017;66(5):1047-1081. doi:10.1016/j.jhep.2016.12.003
12. Education OM. Chronic liver disease - compensated.
13. easloffice@easloffice.eu EAftSotLEa, Liver EAftSot. EASL Clinical Practice Guidelines for the management of patients with decompensated cirrhosis. *J Hepatol*. 08 2018;69(2):406-460. doi:10.1016/j.jhep.2018.03.024
14. Neuberger J, Trotter P, Stratton R. Organ transplantation rates in the UK. *BMJ*. 11 2017;359:j5218. doi:10.1136/bmj.j5218
15. Neuberger J. Liver transplantation in the United Kingdom. *Liver Transpl*. 08 2016;22(8):1129-35. doi:10.1002/lt.24462
16. Hansel MC, Gramignoli R, Skvorak KJ, et al. The history and use of human hepatocytes for the treatment of liver diseases: the first 100 patients. *Curr Protoc Toxicol*. Nov 2014;62:14.12.1-23. doi:10.1002/0471140856.tx1412s62
17. Forbes SJ, Gupta S, Dhawan A. Cell therapy for liver disease: From liver transplantation to cell factory. *J Hepatol*. Apr 2015;62(1 Suppl):S157-69. doi:10.1016/j.jhep.2015.02.040
18. Lindner U, Kramer J, Rohwedel J, Schlenke P. Mesenchymal Stem or Stromal Cells: Toward a Better Understanding of Their Biology? *Transfus Med Hemother*. Apr 2010;37(2):75-83. doi:10.1159/000290897
19. Newsome PN, Fox R, King AL, et al. Granulocyte colony-stimulating factor and autologous CD133-positive stem-cell therapy in liver cirrhosis (REALISTIC): an open-label, randomised, controlled phase 2 trial. *Lancet Gastroenterol Hepatol*. 01 2018;3(1):25-36. doi:10.1016/S2468-1253(17)30326-6
20. Le Blanc K, Mougiakakos D. Multipotent mesenchymal stromal cells and the innate immune system. *Nat Rev Immunol*. Apr 2012;12(5):383-96. doi:10.1038/nri3209
21. Zhao L, Chen S, Shi X, Cao H, Li L. A pooled analysis of mesenchymal stem cell-based therapy for liver disease. *Stem Cell Res Ther*. 03 2018;9(1):72. doi:10.1186/s13287-018-0816-2
22. Tolosa L, Caron J, Hannoun Z, et al. Transplantation of hESC-derived hepatocytes protects mice from liver injury. *Stem Cell Res Ther*. Dec 2015;6:246. doi:10.1186/s13287-015-0227-6

23. Asgari S, Moslem M, Bagheri-Lankarani K, Pournasr B, Miryounesi M, Baharvand H. Differentiation and transplantation of human induced pluripotent stem cell-derived hepatocyte-like cells. *Stem Cell Rev Rep*. Aug 2013;9(4):493-504. doi:10.1007/s12015-011-9330-y
24. Yu Y, Liu H, Ikeda Y, et al. Hepatocyte-like cells differentiated from human induced pluripotent stem cells: relevance to cellular therapies. *Stem Cell Res*. Nov 2012;9(3):196-207. doi:10.1016/j.scr.2012.06.004
25. Younossi Z, Anstee QM, Marietti M, et al. Global burden of NAFLD and NASH: trends, predictions, risk factors and prevention. *Nat Rev Gastroenterol Hepatol*. Jan 2018;15(1):11-20. doi:10.1038/nrgastro.2017.109
26. Hruby A, Hu FB. The Epidemiology of Obesity: A Big Picture. *Pharmacoeconomics*. Jul 2015;33(7):673-89. doi:10.1007/s40273-014-0243-x
27. Glen J, Floros L, Day C, Pryke R, Group GD. Non-alcoholic fatty liver disease (NAFLD): summary of NICE guidance. *BMJ*. Sep 2016;354:i4428. doi:10.1136/bmj.i4428
28. (EASL) EAftSotL, (EASD) EAftSoD, (EASO) EAftSoO. EASL-EASD-EASO Clinical Practice Guidelines for the management of non-alcoholic fatty liver disease. *J Hepatol*. 06 2016;64(6):1388-402. doi:10.1016/j.jhep.2015.11.004
29. Puri P, Sanyal AJ. Nonalcoholic fatty liver disease: Definitions, risk factors, and workup. *Clin Liver Dis (Hoboken)*. Sep 2012;1(4):99-103. doi:10.1002/cld.81
30. Dyson JK, Anstee QM, McPherson S. Non-alcoholic fatty liver disease: a practical approach to diagnosis and staging. *Frontline Gastroenterol*. Jul 2014;5(3):211-218. doi:10.1136/flgastro-2013-100403
31. Tana C, Ballestri S, Ricci F, et al. Cardiovascular Risk in Non-Alcoholic Fatty Liver Disease: Mechanisms and Therapeutic Implications. *Int J Environ Res Public Health*. 08 2019;16(17)doi:10.3390/ijerph16173104
32. Calzadilla Bertot L, Adams LA. The Natural Course of Non-Alcoholic Fatty Liver Disease. *Int J Mol Sci*. May 2016;17(5)doi:10.3390/ijms17050774
33. Singh S, Allen AM, Wang Z, Prokop LJ, Murad MH, Loomba R. Fibrosis progression in nonalcoholic fatty liver vs nonalcoholic steatohepatitis: a systematic review and meta-analysis of paired-biopsy studies. *Clin Gastroenterol Hepatol*. Apr 2015;13(4):643-54.e1-9; quiz e39-40. doi:10.1016/j.cgh.2014.04.014
34. Angulo P, Hui JM, Marchesini G, et al. The NAFLD fibrosis score: a noninvasive system that identifies liver fibrosis in patients with NAFLD. *Hepatology*. Apr 2007;45(4):846-54. doi:10.1002/hep.21496
35. Srivastava A, Jong S, Gola A, et al. Cost-comparison analysis of FIB-4, ELF and fibroscan in community pathways for non-alcoholic fatty liver disease. *BMC Gastroenterol*. Jul 2019;19(1):122. doi:10.1186/s12876-019-1039-4
36. Dulai PS, Singh S, Patel J, et al. Increased risk of mortality by fibrosis stage in nonalcoholic fatty liver disease: Systematic review and meta-analysis. *Hepatology*. May 2017;65(5):1557-1565. doi:10.1002/hep.29085
37. Kleiner DE, Makhlouf HR. Histology of Nonalcoholic Fatty Liver Disease and Nonalcoholic Steatohepatitis in Adults and Children. *Clin Liver Dis*. May 2016;20(2):293-312. doi:10.1016/j.cld.2015.10.011
38. Dowman JK, Tomlinson JW, Newsome PN. Pathogenesis of non-alcoholic fatty liver disease. *QJM*. Feb 2010;103(2):71-83. doi:10.1093/qjmed/hcp158
39. Sanders FW, Griffin JL. De novo lipogenesis in the liver in health and disease: more than just a shunting yard for glucose. *Biol Rev Camb Philos Soc*. May 2016;91(2):452-68. doi:10.1111/brv.12178
40. Lewis GF, Carpentier A, Adeli K, Giacca A. Disordered fat storage and mobilization in the pathogenesis of insulin resistance and type 2 diabetes. *Endocr Rev*. Apr 2002;23(2):201-29. doi:10.1210/edrv.23.2.0461
41. Stefan N, Kantartzis K, Häring HU. Causes and metabolic consequences of Fatty liver. *Endocr Rev*. Dec 2008;29(7):939-60. doi:10.1210/er.2008-0009
42. Postic C, Girard J. Contribution of de novo fatty acid synthesis to hepatic steatosis and insulin resistance: lessons from genetically engineered mice. *J Clin Invest*. Mar 2008;118(3):829-38. doi:10.1172/JCI34275

43. Zatloukal K, French SW, Stumptner C, et al. From Mallory to Mallory-Denk bodies: what, how and why? *Exp Cell Res*. Jun 2007;313(10):2033-49. doi:10.1016/j.yexcr.2007.04.024
44. Cai D, Yuan M, Frantz DF, et al. Local and systemic insulin resistance resulting from hepatic activation of IKK-beta and NF-kappaB. *Nat Med*. Feb 2005;11(2):183-90. doi:10.1038/nm1166
45. Sanyal AJ, Campbell-Sargent C, Mirshahi F, et al. Nonalcoholic steatohepatitis: association of insulin resistance and mitochondrial abnormalities. *Gastroenterology*. Apr 2001;120(5):1183-92. doi:10.1053/gast.2001.23256
46. Wigg AJ, Roberts-Thomson IC, Dymock RB, McCarthy PJ, Grose RH, Cummins AG. The role of small intestinal bacterial overgrowth, intestinal permeability, endotoxaemia, and tumour necrosis factor alpha in the pathogenesis of non-alcoholic steatohepatitis. *Gut*. Feb 2001;48(2):206-11. doi:10.1136/gut.48.2.206
47. Miele L, Valenza V, La Torre G, et al. Increased intestinal permeability and tight junction alterations in nonalcoholic fatty liver disease. *Hepatology*. Jun 2009;49(6):1877-87. doi:10.1002/hep.22848
48. Solga SF, Diehl AM. Non-alcoholic fatty liver disease: lumen-liver interactions and possible role for probiotics. *J Hepatol*. May 2003;38(5):681-7. doi:10.1016/s0168-8278(03)00097-7
49. Vilar-Gomez E, Friedman SL, Romero-Gomez M. Reply: To PMID 25865049. *Gastroenterology*. Dec 2015;149(7):1988-9. doi:10.1053/j.gastro.2015.10.040
50. Townsend SA, Newsome PN. Non-alcoholic fatty liver disease in 2016. *Br Med Bull*. 09 2016;119(1):143-56. doi:10.1093/bmb/ldw031
51. Castracane VD, Henson MC. *Leptin*. Springer; 2006.
52. Van Herck MA, Vonghia L, Francque SM. Animal Models of Nonalcoholic Fatty Liver Disease-A Starter's Guide. *Nutrients*. Sep 2017;9(10)doi:10.3390/nu9101072
53. Wei G, An P, Vaid KA, et al. Comparison of murine steatohepatitis models identifies a dietary intervention with robust fibrosis, ductular reaction, and rapid progression to cirrhosis and cancer. *Am J Physiol Gastrointest Liver Physiol*. Jan 2020;318(1):G174-G188. doi:10.1152/ajpgi.00041.2019
54. Gauthier MS, Favier R, Lavoie JM. Time course of the development of non-alcoholic hepatic steatosis in response to high-fat diet-induced obesity in rats. *Br J Nutr*. Feb 2006;95(2):273-81. doi:10.1079/bjn20051635
55. Sanches SC, Ramalho LN, Augusto MJ, da Silva DM, Ramalho FS. Nonalcoholic Steatohepatitis: A Search for Factual Animal Models. *Biomed Res Int*. 2015;2015:574832. doi:10.1155/2015/574832
56. Velázquez KT, Enos RT, Bader JE, et al. Prolonged high-fat-diet feeding promotes non-alcoholic fatty liver disease and alters gut microbiota in mice. *World J Hepatol*. Aug 2019;11(8):619-637. doi:10.4254/wjh.v11.i8.619
57. Ito M, Suzuki J, Tsujioka S, et al. Longitudinal analysis of murine steatohepatitis model induced by chronic exposure to high-fat diet. *Hepatol Res*. Jan 2007;37(1):50-7. doi:10.1111/j.1872-034X.2007.00008.x
58. Yao ZM, Vance DE. Reduction in VLDL, but not HDL, in plasma of rats deficient in choline. *Biochem Cell Biol*. Feb 1990;68(2):552-8. doi:10.1139/o90-079
59. Dela Peña A, Leclercq I, Field J, George J, Jones B, Farrell G. NF-kappaB activation, rather than TNF, mediates hepatic inflammation in a murine dietary model of steatohepatitis. *Gastroenterology*. Nov 2005;129(5):1663-74. doi:10.1053/j.gastro.2005.09.004
60. Rinella ME, Green RM. The methionine-choline deficient dietary model of steatohepatitis does not exhibit insulin resistance. *J Hepatol*. Jan 2004;40(1):47-51. doi:10.1016/j.jhep.2003.09.020
61. Ibrahim SH, Hirsova P, Malhi H, Gores GJ. Animal Models of Nonalcoholic Steatohepatitis: Eat, Delete, and Inflame. *Dig Dis Sci*. May 2016;61(5):1325-36. doi:10.1007/s10620-015-3977-1
62. Matsumoto M, Hada N, Sakamaki Y, et al. An improved mouse model that rapidly develops fibrosis in non-alcoholic steatohepatitis. *Int J Exp Pathol*. Apr 2013;94(2):93-103. doi:10.1111/iep.12008
63. Santhekadur PK, Kumar DP, Sanyal AJ. Preclinical models of non-alcoholic fatty liver disease. *J Hepatol*. 02 2018;68(2):230-237. doi:10.1016/j.jhep.2017.10.031
64. Wake K. "Sternzellen" in the liver: perisinusoidal cells with special reference to storage of vitamin A. *Am J Anat*. Dec 1971;132(4):429-62. doi:10.1002/aja.1001320404

65. Giampieri MP, Jezequel AM, Orlandi F. The lipocytes in normal human liver. A quantitative study. *Digestion*. 1981;22(4):165-9. doi:10.1159/000198640
66. Dobie R, Wilson-Kanamori JR, Henderson BEP, et al. Single-Cell Transcriptomics Uncovers Zonation of Function in the Mesenchyme during Liver Fibrosis. *Cell Rep*. 11 2019;29(7):1832-1847.e8. doi:10.1016/j.celrep.2019.10.024
67. Win KM, Charlotte F, Mallat A, et al. Mitogenic effect of transforming growth factor-beta 1 on human Ito cells in culture: evidence for mediation by endogenous platelet-derived growth factor. *Hepatology*. Jul 1993;18(1):137-45.
68. Mullhaupt B, Feren A, Fodor E, Jones A. Liver expression of epidermal growth factor RNA. Rapid increases in immediate-early phase of liver regeneration. *J Biol Chem*. Aug 1994;269(31):19667-70.
69. Yoshida S, Ikenaga N, Liu SB, et al. Extrahepatic platelet-derived growth factor-β, delivered by platelets, promotes activation of hepatic stellate cells and biliary fibrosis in mice. *Gastroenterology*. Dec 2014;147(6):1378-92. doi:10.1053/j.gastro.2014.08.038
70. Liu C, Li J, Xiang X, et al. PDGF receptor-α promotes TGF-β signaling in hepatic stellate cells via transcriptional and posttranscriptional regulation of TGF-β receptors. *Am J Physiol Gastrointest Liver Physiol*. Oct 2014;307(7):G749-59. doi:10.1152/ajpgi.00138.2014
71. Gressner AM. Cytokines and cellular crosstalk involved in the activation of fat-storing cells. *J Hepatol*. 1995;22(2 Suppl):28-36.
72. Paradis V, Dargere D, Bonvoust F, Vidaud M, Segarini P, Bedossa P. Effects and regulation of connective tissue growth factor on hepatic stellate cells. *Lab Invest*. Jun 2002;82(6):767-74. doi:10.1097/01.lab.0000017365.18894.d3
73. Marra F, Valente AJ, Pinzani M, Abboud HE. Cultured human liver fat-storing cells produce monocyte chemotactic protein-1. Regulation by proinflammatory cytokines. *J Clin Invest*. Oct 1993;92(4):1674-80. doi:10.1172/JCI116753
74. Pinzani M, Carloni V, Marra F, Riccardi D, Laffi G, Gentilini P. Biosynthesis of platelet-activating factor and its 1O-acyl analogue by liver fat-storing cells. *Gastroenterology*. May 1994;106(5):1301-11. doi:10.1016/0016-5085(94)90023-x
75. Tiggelman AM, Boers W, Linthorst C, Brand HS, Sala M, Chamuleau RA. Interleukin-6 production by human liver (myo)fibroblasts in culture. Evidence for a regulatory role of LPS, IL-1 beta and TNF alpha. *J Hepatol*. Sep 1995;23(3):295-306.
76. Lee UE, Friedman SL. Mechanisms of hepatic fibrogenesis. *Best Pract Res Clin Gastroenterol*. Apr 2011;25(2):195-206. doi:10.1016/j.bpg.2011.02.005
77. Breitkopf K, Godoy P, Ciuclan L, Singer MV, Dooley S. TGF-beta/Smad signaling in the injured liver. *Z Gastroenterol*. Jan 2006;44(1):57-66. doi:10.1055/s-2005-858989
78. Carloni V, Defranco RM, Caligiuri A, et al. Cell adhesion regulates platelet-derived growth factor-induced MAP kinase and PI-3 kinase activation in stellate cells. *Hepatology*. Sep 2002;36(3):582-91. doi:10.1053/jhep.2002.35277
79. Pinzani M, Failli P, Ruocco C, et al. Fat-storing cells as liver-specific pericytes. Spatial dynamics of agonist-stimulated intracellular calcium transients. *J Clin Invest*. Aug 1992;90(2):642-6. doi:10.1172/JCI115905
80. Ramadori G, Veit T, Schwögler S, et al. Expression of the gene of the alpha-smooth muscle-actin isoform in rat liver and in rat fat-storing (ITO) cells. *Virchows Arch B Cell Pathol Incl Mol Pathol*. 1990;59(6):349-57. doi:10.1007/bf02899424
81. Ikeda K, Wakahara T, Wang YQ, Kadoya H, Kawada N, Kaneda K. In vitro migratory potential of rat quiescent hepatic stellate cells and its augmentation by cell activation. *Hepatology*. Jun 1999;29(6):1760-7. doi:10.1002/hep.510290640
82. Marra F, Romanelli RG, Giannini C, et al. Monocyte chemotactic protein-1 as a chemoattractant for human hepatic stellate cells. *Hepatology*. Jan 1999;29(1):140-8. doi:10.1002/hep.510290107
83. Iredale JP. Hepatic stellate cell behavior during resolution of liver injury. *Semin Liver Dis*. Aug 2001;21(3):427-36. doi:10.1055/s-2001-17557

84. Xu L, Hui AY, Albanis E, et al. Human hepatic stellate cell lines, LX-1 and LX-2: new tools for analysis of hepatic fibrosis. *Gut*. Jan 2005;54(1):142-51. doi:10.1136/gut.2004.042127
85. Barron L, Wynn TA. Fibrosis is regulated by Th2 and Th17 responses and by dynamic interactions between fibroblasts and macrophages. *Am J Physiol Gastrointest Liver Physiol*. May 2011;300(5):G723-8. doi:10.1152/ajpgi.00414.2010
86. Bourbonnais E, Raymond VA, Ethier C, et al. Liver fibrosis protects mice from acute hepatocellular injury. *Gastroenterology*. Jan 2012;142(1):130-139.e4. doi:10.1053/j.gastro.2011.09.033
87. Duarte S, Baber J, Fujii T, Coito AJ. Matrix metalloproteinases in liver injury, repair and fibrosis. *Matrix Biol*. 2015 May-Jul 2015;44-46:147-56. doi:10.1016/j.matbio.2015.01.004
88. Park SA, Kim MJ, Park SY, et al. TIMP-1 mediates TGF-β-dependent crosstalk between hepatic stellate and cancer cells via FAK signaling. *Sci Rep*. Nov 2015;5:16492. doi:10.1038/srep16492
89. Tacke F, Zimmermann HW. Macrophage heterogeneity in liver injury and fibrosis. *J Hepatol*. May 2014;60(5):1090-6. doi:10.1016/j.jhep.2013.12.025
90. Junying Yu JT. Embryonic Stem Cells. National Institutes of Health, U.S. Department of Health and Human Services. //stemcells.nih.gov/info/Regenerative_Medicine/2006Chapter1.htm
91. Schaub JR, Malato Y, Gormond C, Willenbring H. Evidence against a stem cell origin of new hepatocytes in a common mouse model of chronic liver injury. *Cell Rep*. Aug 21 2014;8(4):933-9. doi:10.1016/j.celrep.2014.07.003
92. Deng X, Zhang X, Li W, et al. Chronic Liver Injury Induces Conversion of Biliary Epithelial Cells into Hepatocytes. *Cell stem cell*. Jul 5 2018;23(1):114-122 e3. doi:10.1016/j.stem.2018.05.022
93. Yanger K, Knigin D, Zong Y, et al. Adult hepatocytes are generated by self-duplication rather than stem cell differentiation. *Cell Stem Cell*. Sep 4 2014;15(3):340-349. doi:10.1016/j.stem.2014.06.003
94. Sell S. Is there a liver stem cell? *Cancer Res*. Jul 1 1990;50(13):3811-5.
95. Robey PG. Stem cells near the century mark. *J Clin Invest*. Jun 2000;105(11):1489-91. doi:10.1172/JCI10256
96. Duncan AW, Dorrell C, Grompe M. Stem cells and liver regeneration. *Gastroenterology*. Aug 2009;137(2):466-81. doi:10.1053/j.gastro.2009.05.044
97. Michalopoulos GK. Liver regeneration. *Journal of cellular physiology*. Nov 2007;213(2):286-300. doi:10.1002/jcp.21172
98. Evarts RP, Nagy P, Nakatsukasa H, Marsden E, Thorgeirsson SS. In vivo differentiation of rat liver oval cells into hepatocytes. *Cancer research*. Mar 15 1989;49(6):1541-7.
99. Newsome PN, Hussain MA, Theise ND. Hepatic oval cells: helping redefine a paradigm in stem cell biology. *Current topics in developmental biology*. 2004;61:1-28. doi:10.1016/S0070-2153(04)61001-5
100. Espanol-Suner R, Carpentier R, Van Hul N, et al. Liver progenitor cells yield functional hepatocytes in response to chronic liver injury in mice. *Gastroenterology*. Dec 2012;143(6):1564-1575 e7. doi:10.1053/j.gastro.2012.08.024
101. Roskams T, Desmet V. Ductular reaction and its diagnostic significance. *Semin Diagn Pathol*. Nov 1998;15(4):259-69.
102. Yoon SM, Gerasimidou D, Kuwahara R, et al. Epithelial cell adhesion molecule (EpCAM) marks hepatocytes newly derived from stem/progenitor cells in humans. *Hepatology*. Mar 2011;53(3):964-73. doi:10.1002/hep.24122
103. Lin WR, Lim SN, McDonald SA, et al. The histogenesis of regenerative nodules in human liver cirrhosis. *Hepatology*. Mar 2010;51(3):1017-26. doi:10.1002/hep.23483
104. Yanger K, Stanger BZ. Facultative stem cells in liver and pancreas: fact and fancy. *Dev Dyn*. Mar 2011;240(3):521-9. doi:10.1002/dvdy.22561
105. Chen Y, Wong PP, Sjeklocha L, Steer CJ, Sahin MB. Mature hepatocytes exhibit unexpected plasticity by direct dedifferentiation into liver progenitor cells in culture. *Hepatology*. Feb 2012;55(2):563-74. doi:10.1002/hep.24712

106. Oh SH, Witek RP, Bae SH, et al. Bone marrow-derived hepatic oval cells differentiate into hepatocytes in 2-acetylaminofluorene/partial hepatectomy-induced liver regeneration. *Gastroenterology*. Mar 2007;132(3):1077-87. doi:10.1053/j.gastro.2007.01.001
107. Wang X, Foster M, Al-Dhalimy M, Lagasse E, Finegold M, Grompe M. The origin and liver repopulating capacity of murine oval cells. *Proc Natl Acad Sci U S A*. Sep 30 2003;100 Suppl 1:11881-8. doi:10.1073/pnas.1734199100
108. Yanger K, Zong Y, Maggs LR, et al. Robust cellular reprogramming occurs spontaneously during liver regeneration. *Genes Dev*. Apr 01 2013;27(7):719-24. doi:10.1101/gad.207803.112
109. Sato K, Marzioni M, Meng F, Francis H, Glaser S, Alpini G. Ductular Reaction in Liver Diseases: Pathological Mechanisms and Translational Significances. *Hepatology*. Jan 2019;69(1):420-430. doi:10.1002/hep.30150
110. Gouw AS, Clouston AD, Theise ND. Ductular reactions in human liver: diversity at the interface. *Hepatology*. Nov 2011;54(5):1853-63. doi:10.1002/hep.24613
111. Williams MJ, Clouston AD, Forbes SJ. Links between hepatic fibrosis, ductular reaction, and progenitor cell expansion. *Gastroenterology*. Feb 2014;146(2):349-56. doi:10.1053/j.gastro.2013.11.034
112. Theise ND, Saxena R, Portmann BC, et al. The canals of Hering and hepatic stem cells in humans. *Hepatology*. Dec 1999;30(6):1425-33. doi:10.1002/hep.510300614
113. Sell S. Comparison of liver progenitor cells in human atypical ductular reactions with those seen in experimental models of liver injury. *Hepatology*. Feb 1998;27(2):317-31. doi:10.1002/hep.510270202
114. Zhou H, Rogler LE, Teperman L, Morgan G, Rogler CE. Identification of hepatocytic and bile ductular cell lineages and candidate stem cells in bipolar ductular reactions in cirrhotic human liver. *Hepatology*. Mar 2007;45(3):716-24. doi:10.1002/hep.21557
115. Ceulemans A, Verhulst S, Van Haele M, et al. RNA-sequencing-based comparative analysis of human hepatic progenitor cells and their niche from alcoholic steatohepatitis livers. *Cell Death Dis*. 11 2017;8(11):e3164. doi:10.1038/cddis.2017.543
116. Aguilar-Bravo B, Rodrigo-Torres D, Ariño S, et al. Ductular Reaction Cells Display an Inflammatory Profile and Recruit Neutrophils in Alcoholic Hepatitis. *Hepatology*. May 2019;69(5):2180-2195. doi:10.1002/hep.30472
117. Okada H, Yamada M, Kamimoto K, et al. The transcription factor Klf5 is essential for intrahepatic biliary epithelial tissue remodeling after cholestatic liver injury. *J Biol Chem*. 04 2018;293(17):6214-6229. doi:10.1074/jbc.RA118.002372
118. Sackett SD, Li Z, Hurtt R, et al. Foxl1 is a marker of bipotential hepatic progenitor cells in mice. *Hepatology*. Mar 2009;49(3):920-9. doi:10.1002/hep.22705
119. Clerbaux LA, Manco R, Van Hul N, et al. Invasive Ductular Reaction Operates Hepatobiliary Junctions upon Hepatocellular Injury in Rodents and Humans. *Am J Pathol*. Aug 2019;189(8):1569-1581. doi:10.1016/j.ajpath.2019.04.011
120. Clouston AD, Powell EE, Walsh MJ, Richardson MM, Demetris AJ, Jonsson JR. Fibrosis correlates with a ductular reaction in hepatitis C: roles of impaired replication, progenitor cells and steatosis. *Hepatology*. Apr 2005;41(4):809-18. doi:10.1002/hep.20650
121. Van Hul NK, Abarca-Quinones J, Sempoux C, Horsmans Y, Leclercq IA. Relation between liver progenitor cell expansion and extracellular matrix deposition in a CDE-induced murine model of chronic liver injury. *Hepatology*. May 2009;49(5):1625-35. doi:10.1002/hep.22820
122. Kallis YN, Robson AJ, Fallowfield JA, et al. Remodelling of extracellular matrix is a requirement for the hepatic progenitor cell response. *Gut*. Apr 2011;60(4):525-33. doi:10.1136/gut.2010.224436
123. Lorenzini S, Bird TG, Boulter L, et al. Characterisation of a stereotypical cellular and extracellular adult liver progenitor cell niche in rodents and diseased human liver. *Gut*. May 2010;59(5):645-54. doi:10.1136/gut.2009.182345
124. Pinzani M. PDGF and signal transduction in hepatic stellate cells. *Frontiers in bioscience : a journal and virtual library*. Aug 1 2002;7:d1720-6.

125. Kinnman N, Hultcrantz R, Barbu V, et al. PDGF-mediated chemoattraction of hepatic stellate cells by bile duct segments in cholestatic liver injury. *Lab Invest*. May 2000;80(5):697-707. doi:10.1038/labinvest.3780073
126. Sedlaczek N, Jia JD, Bauer M, et al. Proliferating bile duct epithelial cells are a major source of connective tissue growth factor in rat biliary fibrosis. *The American journal of pathology*. Apr 2001;158(4):1239-44. doi:10.1016/S0002-9440(10)64074-6
127. Dai Z, Song G, Balakrishnan A, et al. Growth differentiation factor 11 attenuates liver fibrosis via expansion of liver progenitor cells. *Gut*. Nov 2019;doi:10.1136/gutjnl-2019-318812
128. Boulter L, Govaere O, Bird TG, et al. Macrophage-derived Wnt opposes Notch signaling to specify hepatic progenitor cell fate in chronic liver disease. *Nat Med*. Mar 2012;18(4):572-9. doi:10.1038/nm.2667
129. Ramachandran P, Dobie R, Wilson-Kanamori JR, et al. Resolving the fibrotic niche of human liver cirrhosis at single-cell level. *Nature*. Oct 2019;doi:10.1038/s41586-019-1631-3
130. Knight B, Akhurst B, Matthews VB, et al. Attenuated liver progenitor (oval) cell and fibrogenic responses to the choline deficient, ethionine supplemented diet in the BALB/c inbred strain of mice. *J Hepatol*. Jan 2007;46(1):134-41. doi:10.1016/j.jhep.2006.08.015
131. Ferreira-Gonzalez S, Lu WY, Raven A, et al. Paracrine cellular senescence exacerbates biliary injury and impairs regeneration. *Nat Commun*. 03 2018;9(1):1020. doi:10.1038/s41467-018-03299-5
132. Fiorotto R, Raizner A, Morell CM, et al. Notch signaling regulates tubular morphogenesis during repair from biliary damage in mice. *J Hepatol*. Jul 2013;59(1):124-30. doi:10.1016/j.jhep.2013.02.025
133. Kuramitsu K, Sverdlov DY, Liu SB, et al. Failure of fibrotic liver regeneration in mice is linked to a severe fibrogenic response driven by hepatic progenitor cell activation. *Am J Pathol*. Jul 2013;183(1):182-94. doi:10.1016/j.ajpath.2013.03.018
134. Dollé L, Theise ND, Schmelzer E, Boulter L, Gires O, van Grunsven LA. EpCAM and the biology of hepatic stem/progenitor cells. *Am J Physiol Gastrointest Liver Physiol*. Feb 15 2015;308(4):G233-50. doi:10.1152/ajpgi.00069.2014
135. Pourhanifeh MH, Mohammadi R, Noruzi S, et al. The role of fibromodulin in cancer pathogenesis: implications for diagnosis and therapy. *Cancer Cell Int*. 2019;19:157. doi:10.1186/s12935-019-0870-6
136. Mormone E, Lu Y, Ge X, Fiel MI, Nieto N. Fibromodulin, an oxidative stress-sensitive proteoglycan, regulates the fibrogenic response to liver injury in mice. *Gastroenterology*. Mar 2012;142(3):612-621.e5. doi:10.1053/j.gastro.2011.11.029
137. Schütze S, Wiegmann K, Machleidt T, Krönke M. TNF-induced activation of NF-kappa B. *Immunobiology*. Jul 1995;193(2-4):193-203. doi:10.1016/s0171-2985(11)80543-7
138. Papa S, Bubici C, Zazzeroni F, Franzoso G. Mechanisms of liver disease: cross-talk between the NF-kappaB and JNK pathways. *Biol Chem*. Oct 2009;390(10):965-76. doi:10.1515/BC.2009.111
139. Zhang Z, Zhong X, Shen H, et al. Biliary NIK promotes ductular reaction and liver injury and fibrosis in mice. *Nat Commun*. Aug 30 2022;13(1):5111. doi:10.1038/s41467-022-32575-8
140. Govaere O, Cockell S, Van Haele M, et al. High-throughput sequencing identifies aetiology-dependent differences in ductular reaction in human chronic liver disease. *J Pathol*. May 2019;248(1):66-76. doi:10.1002/path.5228